이 학 박 사 학 위 논 문

Critical Behavior in Multifurcation Phenomena and Invariant Circles in Area-Preserving Maps

서 울 대 학 교 대 학 원

물 리 학 과

김 상 윤

Critical Behavior in Multifurcation Phenomena and Invariant Circles in Area-Preserving Maps

지도교수 이 구 철

이 논문을 이학박사학위 논문으로 제출함.

1986년 10월16일

서울대학교 대학원

물리학과

김 상 윤

김 상윤의 박사학위 논문을 인준함.

1986년 12월22일

위 원 장 _____

부위원장 _____

위 원 _____

위 원 _____

위 원 _____

Critical Behavior in Multifurcation Phenomena and Invariant Circles in Area-Preserving Maps

Sang-Yoon Kim

Advisor : Professor Koo-Chul Lee

A Dissertation

Presented to the

Faculty of Seoul National University

in Candidacy for the Degree

of Doctor of Philosophy

October, 1986

Recommended for Acceptance by the

Department of Physics

December, 1986

Critical Behavior in Multifurcation Phenomena and Invariant Circles in Area-Preserving Maps

Sang-Yoon Kim

Abstract: In the phase spase of generic area-preserving maps periodic, quasi-periodic and stochastic orbits coexist and interact . We study two phenomena related to periodic and quasi-periodic orbits among the three kinds of orbits.

The first phenomenon is the infinitely nested structure of islands which play the role of 'trap'. We show that at the accumulation point islands of all classes exist and they have a self-similar structure asymptotically for 1/n-bifurcation, with n=3 to 6. It is also observed that the pattern of periodic orbits repeats itself asymptotically from one bifurcation to the next one for even n and to every other one for odd n. Indeed, even more limiting self-similar behavior exists near the accumulation point. When we rescale not only dynamical variables but also the parameter with appropriate rescaling facctors , the pattern of periodic orbits also exhibits the limiting self-similar behavior.

We also study the asymptotically self-similar structure by a simple approximate renormalization method. By the method, we obtained the accumulation point, the bifurcation ratio, the scaling factors and the universal

residue values. These values agree well with the values obtained by following multifurcation-sequences. Furthermore, we obtained an approximate universal map of 1/n-bifurcation, with n=3 to 6. In this way , we show approximately that the limiting self-similar behavior is universal.

The second phenomenon we studied is the break-up of invariant circles which play the role of 'dam' under a rough perturbtion . We show numerically that a noble invariant circle persists below a critical parameter value in a C^2-map. Therefore, the invariant circle plays the role of complete barrier to the transport of stochastic orbits below the critical parameter value. Furthermore, we also observed that the critical behavior of the invariant circle is the same as that in analytic maps within numerical accuracy. Therefore, they seem to be in the same universality class .

Acknowledgement

I would like to express my gratitude to my advisor Professor Koo-Chul Lee for his support and guidance during my graduate years .

I would also like to thank Professor Duk-In Choi for his interest in my work and guidance .

There are many other people to whom I would like to express my gratitude . Firstly , I thank my roommates Mr. Jong-Uk Kwon and Mr. Young-Rok Chang for their great help for various things . I would also like to thank my fellow graduate students , particularily Mr. Chang-Ho Cho, Mr. In-Duk Hwang, Mr. Byung-Yoon Park, Mr. Jai-Chul Um, Mr. An-Sung Choi, Mr. Joo-Ha Min, Mr. Jong-Gul Yoon , Mr. Dong-Soo kim, Mr. Seung-Chang Lee and Mr. Jong-Won Kim , for serious conversations about the life in this graduate school. The comments on my writings of Mr. Do-Young Kim and Mr. Hyeong-Chai Jeong were helpful to me , and thus I also thank them . Miss Kyung-Hoon Kwon typed the manuscript in part , which was also helpful to me. So, I thank her for her kindness .

Finally , I would like to express my deep gratitude to my family , especially my parents , for their selfless support through my graduate years .

Table of Contents

Figures and Tables

Introduction

The phase space of generic 1-parameter families of area-preserving maps is divided into regular components and stochastic components, each measure of which depends on the parameter. In this way, the phase space has a very intricate structure : periodic , quasi-periodic and stochastic orbits coexist and interact. Therefore, in order to study the long-time behavior of orbits, one should study the whole phase space, for a given parameter value. On the other hand, in dissipative systems , only studying attractors and their basins in the phase space suffices, for a given parameter value. In this thesis, I consider conservative systems.

To see the roles of orbits in the phase space,as an example, let us consider a periodic area-preserving radial twist map T_ϵ with zero net flux , e.g. a simplified Fermi accleration map (Liebermann and Lichtenberg,1972), the separatrix map and the standard map (Chirikov,1979) :

$$T_\epsilon : \begin{cases} I_{n+1} = I_n + \epsilon \cdot f(\theta_n) \\ \theta_{n+1} = \theta_n + 2\pi \cdot \nu'(I_{n+1}) \end{cases} \quad . \qquad (1)$$

Here θ is an angle variable, f a periodic function in θ with zero average over θ, $\nu'(I) \neq 0$, ϵ a parameter which denotes the strength of perturbtion . The meaning of I depends on the system. I sketch a typical phase flow of the separatrix map in the figure 1 (to see in some details, refer to § 1.4). This separatrix map describes the motion near a broken separatrix. It is also worth while to note that generically a separatrix in an integrable system is broken by arbitrarily

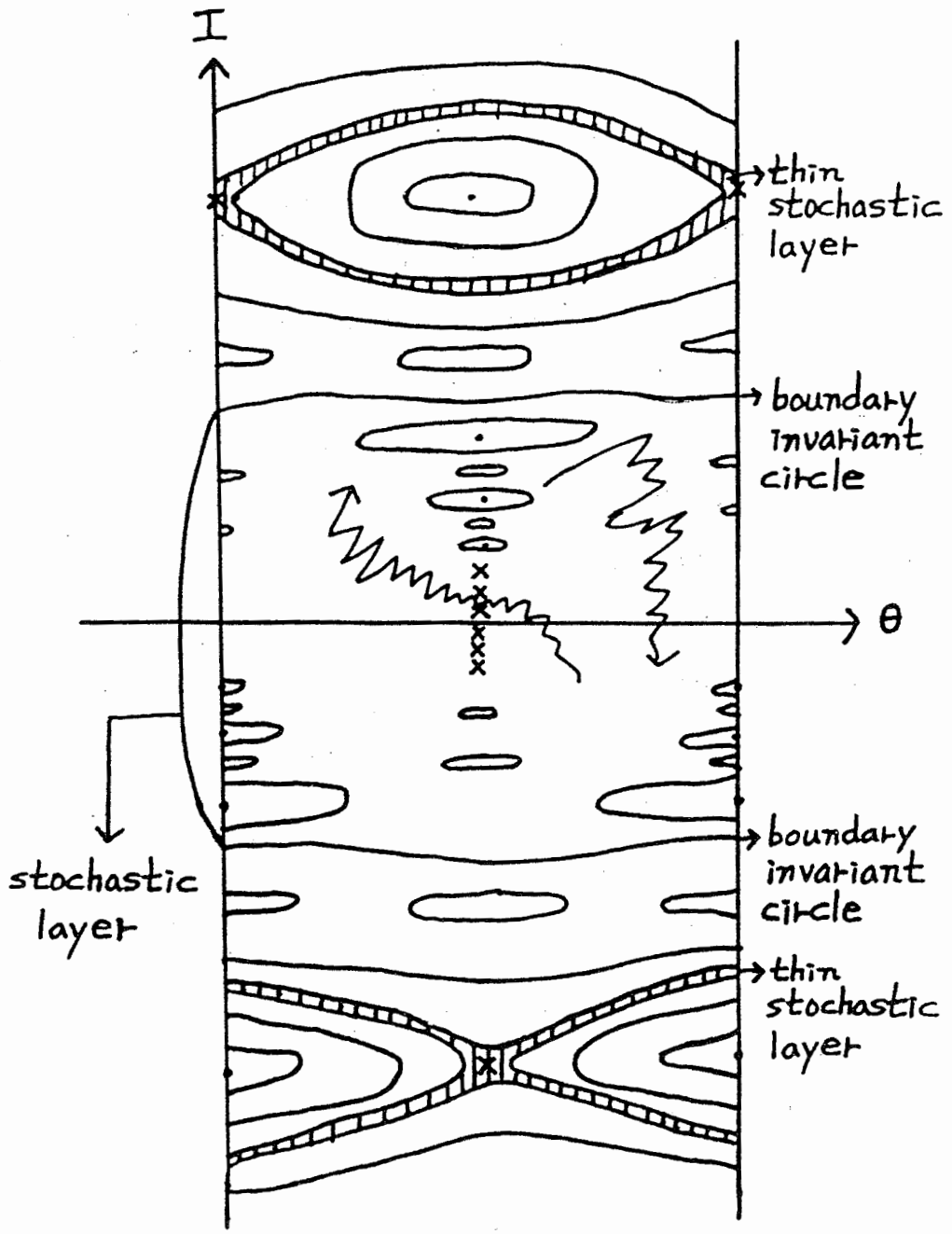

Figure 1 : A typical phase flow in the separatrix map

small perturbations (Robinson,1970, Arnold,197σ). In the separatrix map, the dynamical variable I denotes the degree of relative deviation from the unperturbed separatrix (I=0). That is, as the magnitude of I increases, the degree of relative deviation increases. Here, the region in which I>0 is the rotational one and the region in which I<0 the vibrational one. As shown in the figure 1, near the broken separatrix, a stochastic layer with two boundary invariant circles is formed. Inside the stochastic layer, no rotational invariant circles exist. On the other hand, outside the stochastic layer, invariant circles and islands are interleaved, and thin stochastic layers are formed near unstable orbits.

For the sake of convenience, let us restrict our attention to the stochastic layer near the broken separatrix, since it is sufficient to do so because our present aim is to see the roles of orbits. The stochastic layer consists of two parts. The central part has no islands, and in this part many unstable periodic orbits denoted by x in the figure 1 are embedded in this part. On the other hand, the peripheral part near the boundary circles has large islands. Inside this stochastic layer , apparently area-filling stochastic orbits denoted by wavy arrows wander about. In this way, the stochastic layer bounded by two boundary circles consists of islands, unstable periodic orbits and stochastic orbits.

Now, let us see the roles of orbits which coexist and interact in the stochastic layer. Near the central part, many unstable orbits are embedded and they play the role of

'scatter'. Therefore, a stochastic orbit has an exponentially decaying short-term correlation in this region (Chirikov,1979, Rechester and White, 1980). Sometime, the stochastic orbit approaches the region near the boundary circle in which large islands exist. In this region, the stochastic orbit has a long-time correlation, since islands play the role of ' trap ' (Channon and Lebowitz,1980, Karney,1983, Chrikov and Shepelyansky,1984). Also, one should notice that the stochastic orbit can not penetrate the boundary circles. Therefore, the invariant circle play the role of 'dam'.

In the manner described above, periodic,quasi-periodic and stochastic orbits coexist and interact. In this thesis we study two phenomena related to periodic and quasi- periodic orbits among the three kinds of orbits.

The first phenomenon is the infinitely nested structure of islands which play the role of ' trap '. To study the phase flow near an island in a generalized area-preserving map T, it is generally sufficient to study the phase flow in a quadratic map obtained by keeping the terms to the second order in Taylor-expansion of T about the stable periodic point (Henon,1969, Helleman,1983, Karney,1982). In this case, the quadratic map exhibits nearly the same phase flow near an island as that in the original map, and since the quadratic map is the nontrivial simplest map we can save computing time in numerical study and reduce numerical error. Many authors (Henon,1969, DeVogelaere,1958, Helleman,1980, Karney,1983) studied various quadratic maps. However, general quadratic

maps can be related one another by appropriate coordinate changes (Henon,1969, Lee,1983). Therefore, we can choose a quadratic map without loss of generality. In this thesis, we choose the DeVogelaere quadratic map, since the map is represented in terms of symmetry coordinate (see (1.1.3.4)). Thus, in § 2.3 and § 2.4, we study the infinitely nested structure of islands which make a stochastic orbit have a long-time correlation in the DeVogelaere quadratic map.

The second phenomenon we studied is the break-up of invariant circles which play the role of 'dam' under rough perturbations . The persistence of an invariant circle depends on the quality and strength of perturbtion and the robustness of the invariant circle. In fact, Moser(1973) shows that a sufficiently robust invariant circle persists under a sufficiently small and smooth perturbtion. The sufficient smoothness is now C^r($r>3$). In § 2.5, we study the persistence of an invariant circle whose rotation number is Golden-Mean under a C^2-perturbtion. The Golden-Mean invariant circle is expected to be the most robust in some sense (Greene,1979). But, since the smoothness of perturbation is C^2, the persistence of the invariant circle is not guaranteed by Moser's twist theorem. In this case, following Greene's residue criterion (1979) and Mather's criterion(Mackay et al, 1984), we study the persistence of the Golden-Mean circle in a generalized standard map of class-C^2. Generalized standard maps can be obtained in the following way. We first locate the fixed points of a generalized radial twist map T_ϵ (1) in which

ν is a nonliner function of I. Secondly, keep the linear term in I in Taylor-expansion of T_ϵ in I about a fixed point $(\hat{I},\hat{\theta})$. Then, we can obtain a generalized standard map T(K):

$$T(K):\begin{cases} J_{n+1} = J_n + K(\epsilon,\hat{I})\cdot f(\theta) \\ \theta_{n+1} = \theta_n + J_{n+1} \end{cases} \qquad (2)$$

This generalized standard map exhibits nearlly the same phase flow as that in the original map near an fixed point in the I-direction. Therefore, studying the generalized standard map T(K) alone, we can see the phase flow near fixed points in a generalized radial twist map T_ϵ. In this sense, T(K) may be called the generalized standard map. Therefore, instead of studying the generalized radial twist map T_ϵ, we study in § 2.5 the persistence of the Golden-Mean invariant circle in a generalized standard map (2) with some $f(\theta)$ of class-C^2.

This thesis consists of three chapters . CHAPTER 1 is devoted to an introduction to area-preserving maps and a review of the background which is relevant to this thesis . In § 1.1, we describe how an area-preserving map can be obtained from a conservative flow, and introduce area-preserving maps and reversible maps. In the remaining sections (i.e., from § 1.2 to § 1.4), We devote a section to each of periodic, quasi-periodic and stochastic orbits which coexist and interact in area-preserving maps. CHAPTER 2 contains the major part of this thesis . § 2.1 is the introduction to two phenomena we studied. In § 2.2, we describe generic bifurca-

tions in reversible area- preserving maps in some details. This is because the relation between symmetric periodic orbits and symmetry half-lines is very important in understanding the critical behavior in multifurcation phenomena and invariant circles. In § 2.3 and § 2.4, we show that near the accumulation point, the infinitely nested islands have a universally self-similar structure, empirically and by some approximate renormalization method in each section respectively. In § 2.5, we show that the Golden-Mean invariant circle in a C^2-map persists below a critical parameter value and it has the same critical behavior as that in analytic maps. Finally, in the CHAPTER 3, we summarize and discuss our work .

CHAPTER 1: Introduction to area-preserving maps

A dynamical system is simply a time evolution defined by an ordinary differential equation :

$dx/dt = f(x)$, where x and f are n-vectors.

Such dynamical systems can be used to model many systems in physics, chemistry, biology and other areas (Lichtenberg and Liebermann, 1982).

In this thesis, I consider only coservative systems in which volumes are preserved under evolution:

$$\nabla \cdot \underset{\sim}{f} = 0 \ .$$

Then orbits in conservative systems cannot be asymptotically stable, and thus the limit set under evolution , for a conservative system, is the whole space. On the other hand, in dissipative (or volume-contracting) systems there is attration, and thus the long-time behaviors of all orbits in its basin are reduced to those of the orbits on the attractor.

Long-time behavior in conservative systems is of particular importance for questions of stability and confinement, on the one hand , and instability and transport on the other hand. Historically, the interest in long -time behavior in conservative systems began with the question of the stability of the solar system. The problem of stability for long times is now one of considerable practical significance in the design of intersecting storage rings and magnetic fusion device, where charged particles are required to remain trapped

for many millions of revolutions. On the other hand, instability and transport is also of considerable importance to many applications, including calculations of particle loss from accelerators and plasmas and wave heating rates in plasmas, and the fundamental problems in statistical physics.

Physically, the most important class of conservative systems is the class of Hamiltonian systems. The simplest nontrivial Hamiltonian systems are all autonomous Hamiltonian systems with 2 degrees of freedom, and equivalently all periodically time-dependent Hamiltonian systems with 1 degree of freedom which are called systems with 1½ degrees of freedom, since all autonomous Hamiltonian systems with 1 degree of freedom are integrable. These simplest nontrivial Hamiltonian systems exhibit many of the features of Hamiltonian systems with higher degrees of freedom, though there are some phenomena only possible in systems with higher degrees of freedom, such as Arnold diffusion and the Krein crunch. So, I will devote my attention to Hamiltonian systems with 1½ or 2 degrees of freedom.

The study of continuous time systems can often be reduced to that of discrete time systems (or maps) by considering the return map on a surface of section. In the case of a Hamiltonian system with 1½ or 2 degrees of freedom, the return map is a two dimensional area-preserving map. In § 1.1, how a Hamiltonian flow can be reduced to an area-preserving map on a surface of section is described, and area-preserving maps and reversible maps are introduced. There are three

important types of orbits in area-preserving maps. They are periodic orbits, quasiperiodic orbits which densely fill an invariant circle or a Cantor set, and stochastic orbits which are very sensitive to initial conditions and appear to be area-filling. In the remaning sections, we devote a section to each of the three kinds of orbits.

§ 1.1 Maps

In § 1.1.1, I review how a Hamiltonian system with 1½ or 2 degrees of freedom can be reduced to a two dimensional area-preserving map. In the next two subsections, I introduce two important class of maps, area-preserving twist maps and reversible maps.

§ 1.1.1 Area-preserving maps

Let us consider a two degree of freedom system with Hamiltonian $H(q_1, p_1, q_2, p_2)$. The Hamilton's equations are:

$$\dot{q}_1 = \frac{\partial H}{\partial p_1} \quad , \quad \dot{p}_1 = - \frac{\partial H}{\partial q_1} \quad ,$$
$$\dot{q}_2 = \frac{\partial H}{\partial p_2} \quad , \quad \dot{p}_2 = - \frac{\partial H}{\partial q_2} \quad . \qquad (1.1.1.1)$$

Since this system is autonomous, H is a constant of motion:

$$H(q_1,p_1,q_2,p_2) = E = \text{const.} \qquad (1.1.1.2)$$

So, for a given total energy E, the flow is essentially three dimensional. This enables us to construct a global or local surface of section and an associated return map which is often called Poincare's map.

Suppose that two of the variables, say q_2 and p_2, can be expessed as action-angle coordinates (I,θ):

$$I = I(q_2,p_2) \quad , \qquad \theta = \theta(q_2,p_2) \quad ,$$

$$q_2 = Q_2(\theta,I) \quad , \qquad p_2 = P_2(\theta,I) \quad ,$$

where Q_2 and P_2 are 2π periodic in θ.
Then the Hamiltonian $H(q_1,p_1,q_2,p_2)$ becomes:

$$H(q_1,p_1,Q_2(\theta,I),P_2(\theta,I)) = H(q,p,\theta,I) = E \quad , \qquad (1.1.1.3)$$

where we drop the subscripts on q_1 and p_1.
Suppose that $\partial H/\partial I \neq 0$ in some region D of phase space.
Then (1.1.1.3) can be inverted in D to solve for I in terms of q,p,θ and E:

$$I = L(q,p,\theta;E) \quad . \qquad (1.1.1.4)$$

We write $q' = dq/d\theta$, $p' = dp/d\theta$, so that

$$q' = \dot{q}/\dot{\theta} = \frac{\partial H}{\partial p} \Big/ \frac{\partial H}{\partial I} \quad , \quad p' = \dot{p}/\dot{\theta} = -\frac{\partial H}{\partial q} \Big/ \frac{\partial H}{\partial I} \quad . \qquad (1.1.1.5)$$

Differentiating (1.1.1.2) implictly, using (1.1.1.4), gives

$$\frac{\partial H}{\partial q} + \frac{\partial H}{\partial I}\cdot\frac{\partial L}{\partial q} = 0 \quad , \quad \frac{\partial H}{\partial p} + \frac{\partial H}{\partial I}\cdot\frac{\partial L}{\partial q} = 0 \quad , \qquad (1.1.1.6)$$

and thus, using (1.1.1.6), (1.1.1.5) becomes:

$$q' = -\frac{\partial L(q,p,\theta;E)}{\partial p}$$

$$p' = \frac{\partial L(q,p,\theta;E)}{\partial q} \qquad ; (q,p,\theta)\in D \times S^1 \quad . \qquad (1.1.1.7$$

We call the 2π-periodic 1-degree of freedom system (1.1.1.7) the reduced Hamiltonian system. Such a system exists on each energy surface H=E, and in each region D of phase space, in which our assumption $\partial H/\partial I \neq 0$ is valid. The reduced Hamiltonian system (1.1.1.7) is essentially equivalent to a periodically time-dependent system with 1 degree of freedom. So, it is sufficient to consider only the reduced Hamiltonian.

We take a surface of section:

$$\Sigma(E_o,\theta_o) = \{(q,p,\theta)\in D \times S^1 \mid \theta=\theta_o \in S^1 \; ; \; E=E_o \} \quad .$$

Then the flow (1.1.1.7) induces a map associated with this surface of section, called the return map or Poincare's map, defined by following the flow until the return to the surface of section. That is, the Poincare map $P: \Sigma \longrightarrow \Sigma$ is given by

$$P(x_o)=x(x_o,\theta_o+2\pi) \; ,$$

where we write $x=(q,p)$ and $x(x_o,\theta)$ is the flow with an initial condition (x_o, θ_o). Thus we obtain a two dimensional map P.

Given a solution $(\hat{q}(\theta),\hat{p}(\theta))$, let us linearize the equation of motion (1.1.1.7) about $(\hat{q}(\theta),\hat{p}(\theta))$:

$$q = \hat{q} + \delta q \quad , \qquad p = \hat{p} + \delta p$$

Then the linearized equations are:

$$\frac{d}{d\theta}\begin{bmatrix} \delta q \\ \delta p \end{bmatrix} = A(\theta)\begin{bmatrix} \delta q \\ \delta p \end{bmatrix} \quad , \tag{1.1.1.8}$$

$$A(\theta) = \begin{bmatrix} -\frac{\partial^2 L}{\partial q \partial p} & -\frac{\partial^2 L}{\partial p^2} \\ \frac{\partial^2 L}{\partial q^2} & \frac{\partial^2 L}{\partial p \partial q} \end{bmatrix}_{(\hat{q},\hat{p})}$$

The general solution of the linearized equations are:

$$\begin{bmatrix} \delta q(\theta) \\ \delta q(\theta) \end{bmatrix} = c_1 x_1(\theta) + c_2 x_2(\theta) \quad , \tag{1.1.1.9}$$

where x_1 and x_2 are two linearly independent solutions and

$$x_i(\theta) = \begin{bmatrix} u_i(\theta) \\ v_i(\theta) \end{bmatrix} \quad .$$

We write $X(\theta) = (x_1(\theta), x_2(\theta))$. Then (1.1.1.9) becomes:

$$\begin{bmatrix} \delta q(\theta) \\ \delta p(\theta) \end{bmatrix} = X(\theta)\begin{bmatrix} c_1 \\ c_2 \end{bmatrix} = X(\theta)X^{-1}(0)\begin{bmatrix} \delta q(0) \\ \delta p(0) \end{bmatrix} \quad .$$

Without loss of generality, one can choose an independent pair of solutions $x_1(\theta)$ and $x_2(\theta)$, such that

$$x_1(0) = \begin{bmatrix} 1 \\ 0 \end{bmatrix} \quad , \qquad x_2(0) = \begin{bmatrix} 0 \\ 1 \end{bmatrix} \quad .$$

Then,

$$\begin{bmatrix} \delta q(\theta) \\ \delta p(\theta) \end{bmatrix} = X(\theta) \cdot \begin{bmatrix} \delta q(0) \\ \delta p(0) \end{bmatrix} . \qquad (1.1.1.10)$$

The linearized Poincare map DP is:

$$\begin{bmatrix} \delta q(2\pi) \\ \delta q(2\pi) \end{bmatrix} = DP \cdot \begin{bmatrix} \delta q(0) \\ \delta p(0) \end{bmatrix} .$$

Then, by (1.1.1.10),

$$DP = X(2\pi) = \begin{bmatrix} u_1(2\pi) & u_2(2\pi) \\ v_1(2\pi) & v_2(2\pi) \end{bmatrix} ,$$

where $\begin{bmatrix} u_1(0) \\ v_1(0) \end{bmatrix} = \begin{bmatrix} 1 \\ 0 \end{bmatrix}$ and $\begin{bmatrix} u_2(0) \\ v_2(0) \end{bmatrix} = \begin{bmatrix} 0 \\ 1 \end{bmatrix}$.

The Wronskian determinant of two solutions x_1 and x_2 of (1.1.1.8) is given by

$$W(\theta) = \begin{vmatrix} u_1(\theta) & u_2(\theta) \\ v_1(\theta) & v_2(\theta) \end{vmatrix}$$

Since $dW/d\theta = \mathrm{Tr}\ A(\theta)\cdot W$,

$$W(\theta) = W(0)\cdot\exp\left(\int_0 \mathrm{Tr}\ A(\theta)\cdot d\theta\right) \quad .$$

By (1.1.1.8), $\mathrm{Tr}A(\theta) = 0$ for all θ. Thus $W(\theta)=w(0)=1$. Therefore, det DP = $W(2\pi) = 1$. Since det DP=1, the Poincare map is area-preserving.

I illustrate the Poincare map for a periodically kicked rotator governed by a Hamiltonian H:

$$H= H_0(I) + \epsilon V(\theta)\cdot\sum_{\ell=-\infty}^{\infty} \delta(t-\ell)$$

$$= H_0(I) + \epsilon \sum_{\ell=-\infty}^{\infty} \sum_{m=1}^{\infty} V_m \cos 2\pi(m\theta-\ell t) \quad ,$$

$$V(\theta) = V(-\theta) \quad , \quad V(\theta) = V(\theta+1) \quad .$$

The perturbation represents a 'kick' per unit time. By constructing a surface of section at t=0 (mod 1) in the (I, θ, t)-space, the Poincare time-1 map T can be obtained:

$$T : \begin{bmatrix} I_n \\ \theta_n \end{bmatrix} \rightarrow \begin{bmatrix} I_{n+1} = I_n + \epsilon F(\theta_n) \\ \theta_{n+1} = \theta_n + \omega(I_{n+1}) \end{bmatrix} \quad , \qquad (1.1.1.11)$$

$F(\theta) = -V'(\theta)$ and $\omega = H_0'(I)$.

§ 1.1.2. Twist maps

A particularly important class of area-preserving maps is the class of area-preserving twist maps. An area-preserving twist map T is an area-preserving map that has rotational shear: there exist coordinates (θ, I), θ an angle variable such that

$$\left.\frac{\partial\theta'}{\partial I}\right|_{\theta} \text{ has constant sign ,} \qquad (1.1.2.1)$$

where $(\theta', I') = T(\theta, I)$ and $\det(DT)=1$ in these coordinates. Since θ is an angle variable, the map T is a periodic amp in the plane:

$$(\theta', I') = T(\theta, I) \longrightarrow (\theta'+2\pi,\ I') = T(\theta+2\pi, I) .$$

Then T can be represented on a cylinder. For example, near an elliptic fixed point a map typically has twist.

It turns out that any area-preserving twist map can be expressed as a generating function, and conversely (Mackay et al, 1984). If an area-preserving map $(x', p') = T(x,p)$ satisfies the twist condition :

$$\frac{\partial x'}{\partial p} \neq 0 \quad \text{for all } (x,p) , \qquad (1.1.2.2)$$

then there exist a generating function $L(x,x')$ such that

$$p = -\partial L(x,x')/\partial x \qquad p' = \partial L(x,x')/\partial x' \,. \qquad (1.1.2.3)$$

Note from (1.1.2.2) and (1.1.2.3) that

$$\partial^2 L/\partial x \partial x' \neq 0 \,. \qquad (1.1.2.4)$$

Conversely, if the generating function $L(x,x')$ satisfies the condition (1.1.2.4), then the relations (1.1.2.3) can be inverted to generate a map $T: (x,p) \rightarrow (x',p')$.

The Jacobian matrix for the map T is :

$$DT = \begin{bmatrix} -\dfrac{L_{11}}{L_{12}} & -\dfrac{1}{L_{12}} \\ L_{12} - \dfrac{L_{22}\cdot L_{11}}{L_{12}} & -\dfrac{L_{22}}{L_{12}} \end{bmatrix} , \qquad (1.1.2.5)$$

where the subscript i denote the derivative with respect to the ith argument. Since det DT=1, T is an area-preserving map. However, T is not necessarily periodic. Therefore the twist condition (1.1.2.2) is the generalization of (1.1.2.1) to non-periodic maps.

In this thesis, I devote my attention to area-preserving twist maps that satisfy the twist condition (1.1.2.2), and if the maps are periodic maps, I restrict my attention to maps with zero calabi invariant. To explain calabi invariants, firstly, it is necessary to define the flux across a closed curve . The flux across a closed curve C in the plane is the area occupied by all the phase points mapped from the interior R of C to the exterior in one iteration of a map T (Mackay et al, 1984). Let $C'=T(C)$ and $R'=T(R)$ be the image of C and R, so that R' is the interior of C'. Then ,

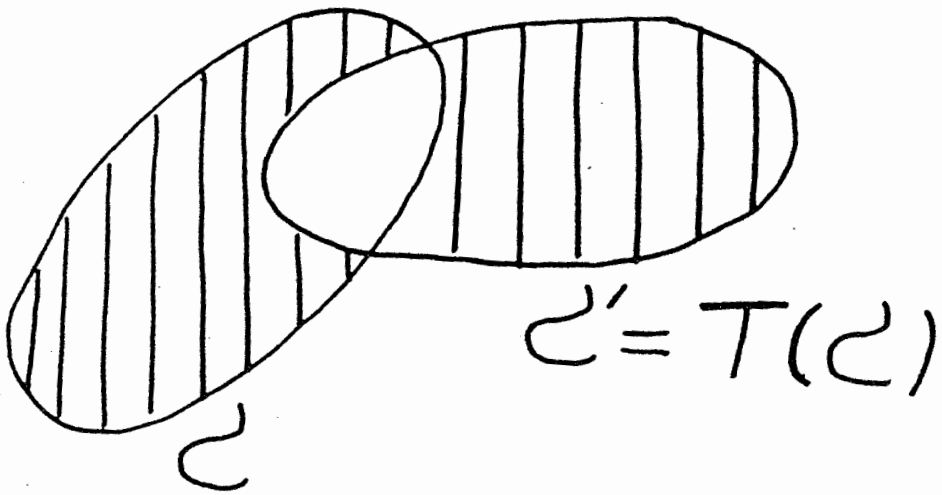

Figure 1.1.2.1 : The flux across a closed curve $\mathcal{C}$

flux across C = $Ar(R'-R) = Ar(R-R')$, where $Ar(U)$ represents an area of U, and $R'-R$ and $R-R'$ are shaded regions in the figure 1.1.2.1. If a map T is a periodic map in the plane, then the map can be represented on a cylinder. On the cylinder, each rotational circle C divides the cylindrical phase space into two infinite parts. Let R be the region below the circle C and R' the region below the circle $C'=T(C)$. Since the regions are infinite, in general

$$Ar(R'-R)-Ar(R-R') \neq 0 \ .$$

Therefore, generally the upward and downward fluxes are not the same and thus the net flux is not zero , in general. By considering the area of the finite region between any two rotational circles, it is easy to see that the net flux is independent of C. This net flux is known as the Calabi invariant. So, a periodic map T with zero Calabi invariant is a map with zero net flux. If $L(x,x')$ generates a periodic area-preserving twist map, then $L(x+1, x'+1)$ generates the same map, where $2\pi x$ is an angle variable. So, they can differ only by a constant. In fact the constant is just the net flux. To see this, let us take any curve C joining (x,x') to $(x+1,x'+1)$. Then, it defines a rotational circle $p(x)$ and its image $p'(x')$ on the cylinder by the relations (1.1.2.3). Then the net flux is the difference in areas under $p(x)$ and $p'(x')$:

$$\text{net flux} = \int p'(x')dx' - \int p(x)\,dx$$
$$= \int \partial L(x,x')/\partial x'\, dx' + \partial L(x,x')/\partial x\, dx$$
$$= \int_C dL(x,x')$$
$$= L(x+1,x'+1)-L(x,x'). \qquad (1.1.2.6)$$

For example, the generating function $L(\theta,\theta')$ for the periodic area-preserving twist map T of the periodically kicked rotator(1.1.1.11) in which $H_0(I)=I^2/2$ and $V(\theta)= \cos 2\pi\theta$ is:

$$L(\theta,\theta')=1/2(\theta-\theta')^2-\epsilon V(\theta)\ , \qquad (1.1.2.7)$$

where the map T is called the standard map or Taylor-Chirikov map.

Orbits in an area-preserving twist map T can be obtained by a stationary action principle. If x,x',x'' are three successive points of x on an orbit, then

$$\frac{\partial}{\partial x'}\,[L(x,x')+L(x',x'')]= p' - p' \qquad (1.1.2.8)$$
$$= 0\ , \quad \text{from (1.1.2.3)}$$

and conversely. Let A(x) be L(x,x). Then the stationary points of A(x) are the fixed point of the map T. For integer r and s with $r+1 < s$ let $(x_t(r\leq t\leq s))$ be an arbitrary sequence of real values of x subject to fixed initial x_r and final x_s. From(1.1.2.8), this sequence defines an orbit segment if and only if the action

$$A_{rs} = \sum_{t=r}^{s-1} L(x_t,x_{t+1})$$

is stationary with respect to arbitrary variations of the intermediate x_t , holding the initial x_r and final x_s fixed. An infinite sequence defines an orbit if and only if every finite segment has stationary action.

Aubry(1983) has some example in solid-state physics corresponding to the standard map(1.1.2.7). He studied the discrete Frenkel-Kontorova model. The model consists of a one-dimensional chain of elastically coupled atoms i at abscissa u_i which is subject to a periodic potential with period 2a and amplitude λ. Its energy is:

$$\varphi(\{u_i\}) = \sum_i [\frac{1}{2}(u_{i+1}-u_i)^2 + \frac{\lambda}{2}(1-\cos\frac{\pi u_i}{a})]. \qquad (1.1.2.9)$$

He studied the absolute minimum of the energy when the atomic mean distance :

$$\Lambda = \lim_{N-N'\to\infty} \frac{u_N - u_{N'}}{N-N'}$$

is fixed by boundary conditions.

The ground-state $\{u_i\}$ necessarily satisfies

$$\partial\varphi/\partial u_i = 2u_i - u_{i+1} - u_{i-1} + \frac{\lambda\pi}{2a}\sin\frac{\pi u_i}{a} = 0 , \qquad (1.1.2.10)$$

which corresponds to the map of a dynamical system with the discrete time i. So, the energy φ plays the role of the action in a dynamical system and orbits in the dynamical system correspond to stationary configurations of atoms.

By defining the conjugate variable of u_i

$$I_i = u_i - u_{i-1} \quad \text{and} \quad \theta_i = u_i \pmod{2a}$$

(1.1.2.10) becomes :

$$I_{i+1} = I_i + \frac{\lambda\pi}{2a} \sin \frac{\pi\theta_i}{a} , \qquad \theta_{i+1} = \theta_i + I_{i+1} \quad .$$

This is just the standard map (1.1.2.7).

§ 1.1.3 Reversible maps

A dynamical system is reversible if it is conjugate to its time-reverse by a coordinate change whose square is the identity(called an involution)(Moser,1973).

Let us consider a first order system:

$$\dot{x} = f(x) , \qquad (1.1.3.1)$$

where x and f are n-vectors. Then the system is reversible if there exists a coordinate change S of R^n , such that

$$S^2 = I(\text{identity})$$
$$\text{and} \qquad (1.1.3.2)$$
$$-f(x)=S\cdot f(S\cdot x).$$

So, if $x_1(t)$is a solution of (1.1.3.1), then $x_2(t)=S\cdot x_1(-t)$ is also a solution of (1.1.3.1). For example, reversing all the velocities of a potential systme:

$$\dot{x} = v \quad , \quad \dot{v} = - \nabla\cdot U(x)$$

reverses the flow.

A map T is said to have symmetry S if S is an orientation-reversing involution :

$$\mathrm{Det}(DS) = -1 \ ,$$

$$S^2 = (T \cdot S)^2 = I(\text{identity}) \ , \qquad (1.1.3.3)$$

where DS is the Jacobian matrix of S.

Then $T^{-1} = STS$ is the inverse of T, and thus T is conjugate to its inverse by an orientation-reversing involution S. That is, if $((x_i, y_i), i \in Z)$ is an orbit of T, then $(S(x_i, y_i), i \in Z)$ is an orbit of T^{-1}. So, possession of a symmetry S is equivalent to reverservility in continuous systems(1.1.3.2). If S is a symmetry for T, then so are T^ms, $m \in Z$, since $T^m \cdot S \cdot T^m = S$. In particular, TS is called a complementary symmetry, since T can be factorized into the product $(TS) \cdot S$ of two involutions.

The set of the fixed points of symmetries is used to locate symmetric orbits as will be seen later. Usually, the notation Fix(S) is used to denote the fixed points of the symmetry S, and hereafter I use this notation. A fixed point of an orientation-reversing involution S has a neighborhood in which there exist coordinates(X,Y), called the symmetry coordinates, such that

$$S(X,Y) = (X,-Y) \ . \qquad (1.1.3.4)$$

Therefore, the fixed points form a curve called the symmetry line. This was shown by Finn(1974.) If x is a fixed point of S, then $T^n(x)$ is the fixed point of $T^{2n}S$:

$$S \cdot x = x \ \Rightarrow \ T^{2n} S(T^n \cdot x) = T^n \cdot x \ .$$

So, $\mathrm{Fix}(T^{2n}S) = T^n \cdot \mathrm{Fix}(S)$. Similarly, $\mathrm{Fix}(T^{2n+1} \cdot S) = T^n \cdot \mathrm{Fix}(T$

Therefore, a family of symmetries $\{T^m S,\ m\in Z\}$ separates into two half-families $\{T^{2n}S\}$ and $\{T^{2n+1}S\}$.

I give some examples of reversible maps which are also area-preserving twist maps. They are given below.

The general DeVogelaere map T(1958):

$$T:\begin{bmatrix} X \\ Y \end{bmatrix} \rightarrow \begin{bmatrix} X' = -Y + f(X) \\ Y' = X - f(X') \end{bmatrix} \qquad (1.1.3.5)$$

can be factorized into the product (TS)•S of two involutions:

$$S:\begin{bmatrix} X \\ Y \end{bmatrix} \rightarrow \begin{bmatrix} X' = X \\ Y' = -Y \end{bmatrix}$$

$$TS:\begin{bmatrix} X \\ Y \end{bmatrix} \rightarrow \begin{bmatrix} X' = Y + f(X) \\ Y' = X - f(X') \end{bmatrix} \qquad (1.1.3.6)$$

For this map, coordinates (X,Y) are symmetry coordinates for S- symmetry and symmetry lines Fix(S) and Fix(TS) are:

$$\text{Fix(S): } Y=0,\ \text{Fix(TS): } Y= X-f(X) \quad . \qquad (1.1.3.7)$$

Since det DT=1 and $\partial X'/\partial Y=-1$ for all (X,Y), T is an area-preserving twist map. The generating function $L(X,X')$ for the map T is:

$$L(X,X') = X\cdot X' - F(X) - F(X') \ , \qquad (1.1.3.8)$$

where $F'(X) = f(X)$.

Particularly, the quadratic Devogelaere map in which $f(X)= p\cdot X-(1-p)X^2$ has been extensively studied by Greene et al (1981

The McMillan map T(1971):

$$T:\begin{bmatrix} x \\ y \end{bmatrix}\longrightarrow\begin{bmatrix} x' = -y + 2f(x) \\ y' = x \end{bmatrix} \qquad (1.1.3.9)$$

is also a reversible map, since it can be factorized into the product (TS)·S of two involutions:

$$S:\begin{bmatrix} x \\ y \end{bmatrix}\longrightarrow\begin{bmatrix} x' = x \\ y' = -y + 2f(x) \end{bmatrix} ,$$

$$TS:\begin{bmatrix} x \\ y \end{bmatrix}\longrightarrow\begin{bmatrix} x' = y \\ y' = x \end{bmatrix} . \qquad (1.1.3.10)$$

So, two symmetry lines Fix(S) and Fix(TS) are:

$$\text{Fix(S): } y = f(x),\ \text{Fix(TS): } y = x \ . \qquad (1.1.3.11)$$

Since det DT = 1 and $\partial x'/\partial y = -1$ for all (x,y), the McMillan map T is an area-preserving twist map. The generating function L(x,x′) for this map T is:

$$L(x,x') = x\cdot x' - x\circ F(x) \qquad (1.1.3.12)$$

where $F'(x) = f(x)$.

When $f(x)= \frac{1}{2}\cdot(1-ax^2)$, T is called Henon's guadratic map (1969), and when $f(x)=cx + x^2$, T is called Helleman's standard guadratic map(1980). In fact, the McMillan map is equivalent to the DeVogelaere map by an area-preserving coordinate change:

$$x = X$$
$$y = Y + f(Y) \ . \qquad (1.1.3.13)$$

The standard or Taylor - Chirikov map T (Chirikov, 1979) is:

$$T:\begin{bmatrix} y \\ x \end{bmatrix} \rightarrow \begin{bmatrix} y' = y + f(x) \\ x' = x + y' \end{bmatrix} , \qquad (1.1.3.14)$$

$$f(x) = -k \sin x.$$

The standard map T is doubly reversible, since it has two independent symmetries S_1 and S_2:

$$S_1:\begin{bmatrix} y' = y + f(x) \\ x' = -x \end{bmatrix} , \qquad TS_1:\begin{bmatrix} y'=y \\ x'= -x + y \end{bmatrix} ,$$

$$S_2:\begin{bmatrix} y' = -y - f(x) \\ x' = x \end{bmatrix} , \qquad TS_2:\begin{bmatrix} y'= -y \\ x'= x - y \end{bmatrix} . \qquad (1.1.3.15)$$

Since the standard map is doubly periodic in x and y, one can regard the map as acting on the torus.
Then the symmetry lines are:

$$\begin{aligned} &Fix(S_1): x = 0 , \pi , \qquad Fix(TS_1): x= y/2, y/2+\pi, \\ &Fix(S_2): y= -f(x)/2 , -f(x)/2 + \pi, \qquad (1.1.3.16) \\ &Fix(TS_2): y = 0 . \end{aligned}$$

Note that the standard map can also be put into the generalized DeVogelaere form (1.1.3.5) by an area-preserving coordinate change:

$$\begin{bmatrix} X = x \\ Y = -y + x - f(x) \end{bmatrix} . \qquad (1.1.3.17)$$

§ 1.2 Periodic orbits

In this section, I discuss periodic orbits in reversible area-preserving twist maps with zero net flux.

In § 1.2.1, I discuss the linear stability and the Poincare index of fixed points in area-preserving maps. In § 1.2.2, for area-preserving twist maps with zero net flux, periodic orbits are definrd in the action representationn and their stability are considered in the action representation. Then I discuss the Poincare - Birkhoff theorem which proves the existence of many periodic orbits which are called Birkhoff orbits. In § 1.2.3. symmetric periodic orbits are defined in reversible maps. I describe their connection with symmetry lines and the dominant symmetry for Birkhoff orbits. In the final subsection(§ 1.2.4), I discuss bifurcation of periodic orbits in reversible area-preserving maps, which means the branching of periodic orbits as a parameter is varied.

§ 1.2.1 Stability of periodic orbits

A point x is said to be a fixed point of a map T if $T \cdot x = x$. A point x is said to be periodic if it is a fixed point of some iterate of T. The smallest positive integer n such that $T^n x = x$ is called its period, and its orbit is called a periodic orbit of period n. Periodic orbits are important because they govern the behavior in a neighborhood. The type of the nearby behavior is given almost completely

by the eigenvalues of the linearization of a map T^n about the periodic orbit. Since a periodic point of period n of a map T can be considered as a fixed point of T^n, I will consider only fixed points without loss of generality.

A fixed point x of a map T is said to be Liapunov stable if every neighborhood U has a subneighborhood, such that

$$T^k(V) \subset U \quad , \quad \forall\, k \in Z^+ \, , \qquad (1.2.1.1)$$

where Z^+ is the non-negative integers.
Also, a fixed point x of a map T is said to be asymptotically stable if it has a neighborhood U, such that

$$T(U) \subset U \, , \qquad \bigcap_{k \geq 0} T^k(U) = (x) \quad . \qquad (1.2.1.2)$$

If x is asymptotically stable, then it is called an attractor with its basin U. An attracting fixed point is Liapunov stable, but not necessarily vice versa. A fixed point is said to be unstable if it is not Liapunov stable.

The linear stability analysis of a fixed point is to examine the stability of the linearization of a map T (i.e. the derivative map DT, also called the Jacobian matrix) at the fixed point. Its stability is called the linear stability of the fixed point. This is given by the eigenvalues of DT, which are called the multipliers of the fixed point.

The Jacobian matrix DT can be put into its Jordan normal form by a similarity transformation (Nering, 1963):

$$\begin{bmatrix} B_1 & & & & \\ & B_2 & & & \\ & & B_3 & & \\ & & & \ddots & \\ & & & & \ddots \end{bmatrix}, \qquad (1.2.1.3)$$

where the B_j are Jordan blocks of the form:

$$B_j = \begin{bmatrix} \lambda_j & 1 & & & \\ & \lambda_j & 1 & & \\ & & \ddots & \ddots & \\ & & & \ddots & 1 \\ & & & & \lambda_j \end{bmatrix}, \qquad (1.2.1.4)$$

where λ_j is an eigenvalue of the Jacobian matrix DT. If all the multipliers of the fixed point are inside the unit circle, then the fixed point is asymptotically stable under DT. Only if there is some multipliers outside the unit circle, it is unstable under DT. In fact, in these two cases, the fixed point always has the same stability under T as that under DT. Thus, in these two cases, the multipliers are sufficient to determine the stability under T. In the remaining cases, there are some multipliers on the unit circle and the others inside the unit circles. If DT has a nontrivial Jordan block (i.e. of order greater than 1) with eigenvalue on the unit circle, then the fixed point is unstable under DT, and always, unstable under T. If all the eigenvalues on the unit circle have diagonal Jordan blocks (i.e. of order 1), then the fixed point is stable under DT. But the stability under T is not given by multipliers. So, in this case, nonlinear analysis is required to determine the stability under T.

I restrict my attention to the stability of fixed points in two-dimensional area-preserving maps. In these maps, the fixed points cannot be asymptotically stable, since the area is preserved under evolution.

The Jacobian matric M of a periodic orbit of period n (i.e. the derivative map DT^n) in a 2-dim. area-preserving map T is:

$$M = \prod_{i=0}^{n-1} DT\,(\hat{x}_i,\ \hat{y}_i) \qquad (1.2.1.5)$$

where $\{\ (\hat{x}_i,\hat{y}_i),\ i = 0,\ldots,\ n-1\}$ is a periodic orbit of period n, and DT is the derivative map of a map T. The multipliers λ are the roots of :

$$\lambda^2 - \mathrm{Tr}\ M\cdot\lambda + \mathrm{Det}\ M = 0 \quad , \qquad (1.2.1.6)$$

where Det M = 1.

Area-preservation implies that Det M=1, and thus the product of the multipliers of a periodic orbit must be 1. Together with reality of M, this restricts them to be a reciprocal pair of reals, or a complex conjugate pair on the unit circle. The multipliers are:

$$\lambda = \frac{\mathrm{Tr}\ M}{2} \pm ((\mathrm{Tr}M)^2/4 - 1)^{1/2} \quad . \qquad (1.2.1.7)$$

Thus, the linear stability of a periodic orbit is determined by the trace of the Jacobian matrix(i.e. TrM) or some derived quantity called the residue(Greene, 1979) defined by:

$$R = (2-\mathrm{Tr}M)/4 \quad . \qquad (1.2.1.8)$$

If TrM>2 or R<0, then the multipliers are a reciprocal pair of positive reals with one multiplier greater than 1. In this case, the periodic orbit is linearly unstable, and also unstable under T. If | TrM | <2 or 0 <R <1, then the multipliers are a complex conjugate pair on the unit circle. In this case, the periodic orbit is linearly stable. In fact, this periodic orbit is typically stable, apart from the cases R=3/4, 1/2 corresponding to 1/3- , 1/4- resonance. The case of 1/3-resonance is unstable, and the case of 1/4-resonance can be stable or unstable. These follow from a normal form analysis and Moser's twist theorem (Moser, 1973),and I will discuss these in § 1.2.4. If TrM <-2 or R>1 , then the multipliers are a reciprocal pair of negative reals with one multiplier less than -1. In this case, the periodic orbit is linearly unstable, and also unstable. In the remaining cases, TrM is 2 or -2, and R is 0 or 1. In these cases, the periodic orbit is linearly stable or unstable according as its jordan normal form is diagonal or not, and when it is linearly unstable, it is also unstable. In fact, even when the Jordan normal form is diagonal the periodic orbit is typically unstable (Mackay, 1982).

The quadratic form:

$$w = -Cx^2 + (A-D)xy + By^2 \qquad (1.2.1.9)$$

is invariant under the Jacobian matrix M of a periodic orbit (Greene, 1968):

$$M = \begin{bmatrix} A & B \\ C & D \end{bmatrix}, \qquad \det M = 1 \quad .$$

The quadratic invariant curve is an ellipse or hyperbola according as Δ is positive or negative:

$$\Delta = 1 - (TrM/2)^2 = 4R(1-R) \ . \qquad (1.2.1.10)$$

If $0 < R < 1$, then the invariant curve is an ellipse. In this case, the multipliers λ can be written as $\exp(\pm i\alpha)$ and the residue R is $\sin^2(\alpha/2)$. Then, tangent orbits on the invariant ellipse rotate about the periodic orbit with the average angle α per period. So, the periodic orbit is called an elliptic orbit. The orientation θ for the invariant ellipse is given by :

$$\tan 2\theta = (D-A)/(B+C) \ . \qquad (1.2.1.11)$$

The ratio of the major, ρ_+, to the minor, ρ_-, semiaxes can be also obtained by :

$$\left[\frac{2(\rho_-/\rho_+)}{1+(\rho_-/\rho_+)^2} \right]^2 = 16 \cdot \frac{R(1-R)}{(B-C)^2} \ . \qquad (1.2.1.12)$$

If $R<0$ or $R>1$, then the invariant curve is an hyperbola. Then tangent orbits on the invariant hyperbola diverge exponentially from the periodic orbits. When $R<0$ the multipliers are positive, and thus the periodic orbit is called an ordinary (or regular) hyperbolic orbit, while when $R > 1$ the periodic orbit is called an inversion hyperbolic orbit (or a hyperbolic orbit with reflection) because the multipliers are negative. The angle γ between the asymptotes of this invariant hyperbola is given by:

$$\tan^2 \gamma = 16 \cdot R \cdot (R-1)/(B-C)^2 . \qquad (1.2.1.13)$$

If Δ defined in (1.2.1.10) is zero, then R is 0 or 1. In this case A=D, and B or C is zero. If one of B and C is not zero, then the invariant curves are a set of parallel lines:

y=constant or x=constant .

In this case, there is a line of fixed points or period-2 orbits of M according as R is 0 or 1 :

$$y = 0 \quad \text{or} \quad x = 0$$

Except the line of fixed points or period-2 orbits of M , tangent orbits on an invariant straight line diverge linearly from the periodic orbit. If both B and C are zero, all the points in the tangent space are the fixed points or period-2 points of M according as R is 0 or 1. In this case the periodic orbit is linearly stable. When R=0 the multipliers are a pair at 1 and the periodic orbit is called an ordinary (or regular)parabolic orbit, while when R=1 the periodic orbit is called an inversion parabolic orbit (or a parabolic orbit with reflection) because the multipliers are a pair at -1. All the cases are sketched in figure 1.2.1.1 for a linear area-preserving map.

If a fixed point has no multipliers equal to +1,then the fixed point is isolated;it has a neighborhood in which there are no other fixed points(Mackay,1982). Similarly, periodic orbits with no multipliers equal to +1 are isolated from periodic orbits of the same period, or a submultiple.

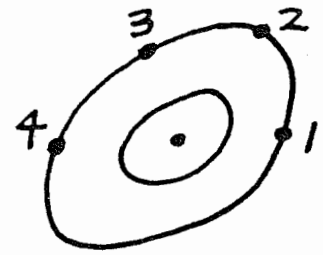

elliptic

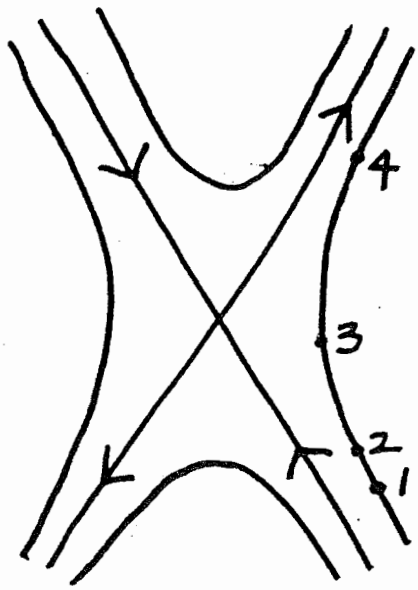

ordinary hyperbolic

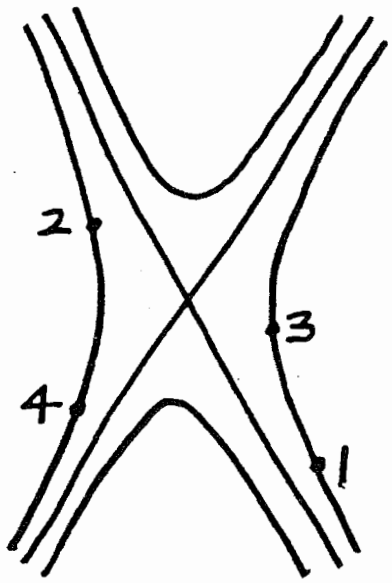

inversion hyperboli

Figure 1.2.1.1 : Orbits in linear area-preserving maps

Therefore, a periodic orbit which is not ordinary parabolic is an isolated periodic orbit. For an isolated fixed point, a topological index of a fixed point, called the Poincare index, can be defined (Arnold and Avez, 1968). For a map T on a plane, consider a vector field v such that the field vector v(x) at x is the vector connecting x with its image T(x):

$$v(x) = T(x) - x \quad . \qquad (1.2.1.14)$$

A point at which the field vector vanishes is called a singular point of the vector field. A fixed point x of a map T is a singular point of the vector field defined by (1.2.1.14). Note that the components of the field have no singularities at a singular point. The term 'singular point' stems from the fact that the directions of the field vectors change near such a singular point, ingeneral, discontinuously.

The index of a closed curve C which does not go through any singular points of the field is defined as the number of times that the field vector at x encircles 0 as x traverses C , and the sign of the index is positive or negative according as the encirclement and traversal are in the same or opposite direction. The index of a closed curve does not change under continuous transformation of the closed curve, as long as the curve does not pass through any singular points. The direction of the field vector changes continuously away from the singular points. Therefore the number of encirclements also depends continuously on the curve, and must be constant, being an

integer. So, the index of a closed curve containing no fixed points is zero, provided that the closed curve can be shrunk to a point. This is because it can be shrunk to a curve small enough that the directions of field vectors are restricted to some angle, so that no encirclements are possible. Similarly, the index of a curve does not change under continuous transformation of the vector field or the map, as long as there are no fixed points of the map on the curve. The index of an isolated fixed point is the index of any closed curve surrounding it and no other fixed points. The index of a closed curve is the sum of the index of each fixed point contained in the closed curve. In area-preserving maps, the index of a fixed point is +1 or -1 according as the residue R of the fixed point is greater or less than 0 (Arnod and Avez, 1968).

In an area-preserving map T, the linear stability in one direction of time implies the same stability in the other direction(Arnold, 1978). This can be seen easily as follows . The derivative map DT of T satisfies :

$$(DT)^{t} \cdot J \cdot DT = J \ ,$$

$$J = \begin{bmatrix} 0 & -1 \\ 1 & 0 \end{bmatrix}, \qquad (1.2.1.15)$$

where the superscript t denotes the transpose of a matrix. Then, the characteristic polynomial $p(\lambda)$ of DT is reflexive:

$$p(\lambda) = \mathrm{Det}(DT - \lambda I)$$
$$= \mathrm{Det}(DT^{-1} - \lambda I) \qquad (1.2.1.16)$$
$$= \lambda^2\ \mathrm{Det}(DT - \lambda^{-1}\cdot I) \quad ,$$

where I is the identity matrix.

Thus, if an periodic orbit is stable under T, the periodic orbit is also stable under T^{-1}. Recall that the Liapunov stability is defined only in the case of the forward direction of time (see(1.2.1.1)) .

§ 1.2.2 Periodic orbits in twist maps

In this subsection, I consider an periodic area-preserving twist map T with zero net flux. Then, there exists a generating function $L(x,x')$ for T which satisfies the twist condition(1.1.2.2) or (1.1.2.4)and has zero Calabi invariant

$$\partial^2 L/\partial x\partial x' < 0\ , \quad L(x,x') = L(x+1,\ x'+1) \qquad (1.2.2.1)$$

Here, $2\pi x$ denotes an angle variable.

Consider generalized paths, such that

$$x_{i+q} = x_i + p \quad \text{for some integer } p,q\ . \qquad (1.2.2.2)$$

They are called periodic paths of type(p,q).

Orbits satisfying(1.2.2.2) are called periodic orbits of type (p,q) and are given by the stationary action principle:a path of type(p,q) gives an orbit of type(p,q)if its action

$$A = \sum_{i=0}^{q-1} L(x_i,\ x_{i+1}) \qquad (1.2.2.3)$$

is stationary with respect to variations keeping

$$x_q = x_0 + p \quad .$$

If the generating function L satisfies (1.2.2.1), then the action of periodic paths of type(p,q) is bounded below, and thus there is a minimizing periodic orbit of type (p,q) (Aubry 1983, Mather 1982). There can be more than one minimizing orbit. This can be seen easily as follows. Translating one minimizing orbit by an integer in time or space or both gives another minimizing orbit. Since the net flux is zero, these minimizing orbits have the same action. This implies existence of saddle points with one downward direction of the action (1.2.2.3) between the minima(Aubry 1983, Mather 1982). They are called minimax periodic orbits. Therefore,there are two types of periodic orbit of type(p,q): one is minimizing periodic orbit,and the other is a minimax periodic orbit.

Mackay and Meiss(1983) have examined the stability of periodic orbits in the action representation. By the stationary action principle, an orbit satisfies (1.1.2.8):

$$L_2(x_{i-1}, x_i) + L_1(x_i, x_{i+1}) = 0 \ ,$$

where the subscript i denotes the derivative with respect to ith argument. Then, the tangent orbits (ζ_i) satisfy :

$$\begin{aligned} & L_{21}(x_{i-1}, x_i)\cdot\zeta_{i-1} \\ & + [L_{22}(x_{i-1}, x_i) + L_{11}(x_i, x_{i+1})]\ \zeta_i \ , \qquad (1.2.2.5) \\ & + L_{12}(x_i, x_{i+1})\ \zeta_i \quad = 0 \quad . \end{aligned}$$

If a periodic orbit of period q has the multipliers λ, then there exists a tangent orbit satisfying

$$\zeta_{i+q} = \lambda\, \zeta_i \quad . \qquad (1.2.2.6)$$

Then

$$\zeta_{q+1} = \lambda\, \zeta_1 \quad , \quad \zeta_0 = \lambda^{-1}\, \zeta_q \qquad (1.2.2.7)$$

Combining (1.2.2.7) with (1.2.2.5), a system of equations to solve is:

$$M(\lambda)\cdot\, \zeta = 0 \qquad (1.2.2.8)$$

where ζ is the column vector $\{\zeta_i\}$ and M a q x q matrix $(M_{ij}, 1 \le i,j \le q)$ with entries, such that

for $q > 2$,

$$M_{i,i-1} = L_{21}(x_{i-1},\, x_i) \ ,$$

$$M_{ii} = L_{22}(x_{i-1}, x_i) + L_{11}(x_i,\, x_{i+1}) \ ,$$

$$M_{i,i+1} = L_{12}(x_i,\, x_{i+1}), \quad M_{1q} = \lambda^{-1}\, L_{21}(x_0\ , x_1) \ ,$$

$$M_{q1} = \lambda\, L_{12}(x_q\ ,\, x_{q+1}) \ ,$$

for $q = 2$,

$$M(\lambda) = \begin{bmatrix} L_{22}(0,1) + L_{11}(1,\, 2) & \lambda^{-1}\, L_{21}(0,1) + L_{12}(1,2) \\ L_{21}(1,2) + \lambda\, L_{12}(2,\, 3) & L_{22}(1,2) + L_{11}(2,3) \end{bmatrix} \ ,$$

for $q = 1$,

$$M(\lambda) = L_{22}(0,\, 1) + L_{11}(1,2) + \lambda^{-1}\, L_{21}(0,1) + \lambda\, L_{12}(1.2)$$

To have a non-trivial solution for ζ ,

$$\text{Det } M(\lambda) = 0 \quad , \qquad (1.2.2.9)$$

where for q=1 Det M(λ) means M(λ).

After a expansion of Det M(λ), one finds :

$$\text{Det } M(\lambda)=\text{Det } M(1)-(\lambda + \lambda^{-1} - 2)\cdot \prod_{i=0}^{q-1}(-L_{12}(x_i, x_{i+1})).$$

Since the residue R of the periodic orbit is $(2-\lambda-\lambda^{-1})/4$ defined in (1.2.1.8), the residue R becomes:

$$R = -\frac{1}{4}\cdot\text{Det } M(1)\cdot\left(\prod_{i=0}^{q-1}(-L_{12}(x_i , x_{i+1}))\right)^{-1} \qquad (1.2.2.10)$$

Note that M(1) is the matrix of the second variations of the action in the space of periodic paths of type(p,q). Thus,the multipliers of a periodic orbit of period q are related to the second variations of the action about the periodic orbit. Under the twist condition ($\partial^2 L/\partial x\partial x' < 0$), the denominator of(1.2.2.10) is negative. So,at a minimum of the action all the eigenvalues of M(1) are positive, and thus R < 0. At a minimax with one downward direction, all the eigenvalues except one are positive and thus R>0. So, minimizing periodic orbits have negative residues, while minimaximizing periodic orbits have positive residues.

Birkhoff(1927)showed that every periodic area-preserving map with zero net flux has at least two periodic orbits of type (p,q)for each rational p/q in an appropriate interval which is often called the range of twist and these orbits are called Birkhoff orbits. This is called the Poincare-Birkhoff theorem. For example, a map near an elliptic fixed point with multipliers $e^{\pm i\alpha}$ typically has twist, and the range of twist

is between 0 and $\alpha/2\pi$. So, in this range of twist there exist at least two periodic orbits of type (p,q) for each rational p/q. Arnold and Avez(1968) have proved the Poincare-Birkhoff theorem only for maps close enough to an integrable twist map:

$$T_\epsilon : \begin{bmatrix} I \\ \theta \end{bmatrix} \rightarrow \begin{bmatrix} I' = I + \epsilon f(I,\theta) \\ \theta' = \theta + 2\pi\alpha(I) + \epsilon g(I,\theta) \end{bmatrix} ,$$

where $\alpha'(I) < 0$, Det $(DT_\epsilon) = 1$, f and g are 2π-Periodic in θ, $f(0,0) = 0 = g(0,0)$ and thus (0,0) is the fixed point of T_ϵ. Here θ is an angle variable. Even though their proof is restricted to T_ϵ with sufficiently small ϵ, it is easy to understand, and thus I reproduce it. Consider an invariant circle Γ of T on which $\alpha(I) = m/n$, where T is the integrable twist map when $\epsilon = 0$. Then, every point on Γ is a fixed point of T^n. Also, consider two invariant circles Γ^+ and Γ^- of T between which the invariant circle Γ lies. On Γ^+, $\alpha > m/n$ and on Γ^-, $\alpha < m/n$. Then, under the map T^n, every point on Γ^+ rotates counterclockwise, every point on Γ^- clockwise, and every point on Γ remains unchanged. These relative twists are preserved for T_ϵ^n if ϵ is small enough. So, on each radius θ = constant, there exist a point $I(\theta,\epsilon)$ whose angular coordinat θ is unchanged under T_ϵ^n. These radially mapped points make up a curve Γ_ϵ . Applying T_ϵ^n to Γ_ϵ gives another curve $T_\epsilon^n \cdot \Gamma_\epsilon$. Since T_ϵ^n is area-preserving, and Γ_ϵ and $T_\epsilon^n \cdot \Gamma_\epsilon$ enclose the fixed point (0,0), Γ_ϵ and $T_\epsilon^n \cdot \Gamma_\epsilon$ must intersect each other. Ignoring the degenerate case in which $T_\epsilon^n \cdot \Gamma_\epsilon$ coincides with Γ_ϵ , there must be even number of intersections. It is helpful to see

figure 1.2.2.1. Each intersection point is a fixed point of T_ϵ^n. Examining the nearby flows about a fixed point under T_ϵ^n , one finds that half of all the intersection points are elliptic, the other half ordinary hyperbolic , and elliptic and ordinary hyperbolic points alternate (see figure 1.2.2.1). Consider an elliptic fixed point x : $T_\epsilon^n x = x$. The orbit of x under T_ϵ is $(x, T_\epsilon x, \cdots, T_\epsilon^{n-1} x)$. Then, all points of the orbit of x are fixed points of T_ϵ^n. Hence, the set of elliptic fixed points splits into orbits consisting of distinct n points. Let k be the number of such orbits. Then, there are k·n elliptic fixed points and also there are k·n ordinary hyperbolic points, because the number of ordinary hyperbolic fixed points is the same as that of elliptic fixed points.

Let F be the difference in actions between the minimizing and minimax periodic orbits:

$$F = A_{minimax} - A_{min} \quad . \qquad (1.2.2.11)$$

Then, F can be interpreted as the area that is transported between the minimizing and minimax periodic orbits per iteration (Mackay et al. 1984). This can be seen easily as follows . Join up the gap between two neighboring minimizing points by any curve C passing through the minimax point lying between the two neighboring minimizing point(see Figure 1.2.2.2). Let us describe the chosen curve C by a function $p_0(x_0)$. Then, one can close the image gaps with the image of C . The images $p_t(x_t)$ of C , with t=1 to n, form a partial barrier with one turnstile in the chosen gap. Thus, one can

blame all the transport on the chosen gap (see Figure 1.2.2.2).

The flux through the turnstile is:

$$F = \int_{\ell_n}^{c_n} p_n \, dx_n - \int_{\ell_o}^{c_o} p_0 \, dx_0 \qquad (1.2.2.12)$$

$$= \int \frac{\partial L}{\partial x_n}(x_{n-1}, x_n)\, dx_n + \int \frac{\partial L}{\partial x_0}(x_0, x_1)\, dx_0 \quad .$$

If x_{t-1}, x_t and x_{t+1} are three successive points on an orbit, then

$$\frac{\partial L}{\partial x_t}(x_{t-1}, x_t) + \frac{\partial L}{\partial x_t}(x_t, x_{t+1}) = 0$$

So, $\sum_{t=1}^{n-1} \int dx_t \left(\frac{\partial L}{\partial x_t}(x_{t-1}, x_t) + \frac{\partial L}{\partial x_t}(x_t, x_{t+1})\right) = 0 \quad .$

Add this in (1.2.2.12). Then,

$$F = \int dA \quad , \quad A = \sum_{t=0}^{n-1} L(x_t, x_{t+1}) \qquad (1.2.2.13)$$

$$= A_{\text{minimax}} - A_{\text{min}} \quad .$$

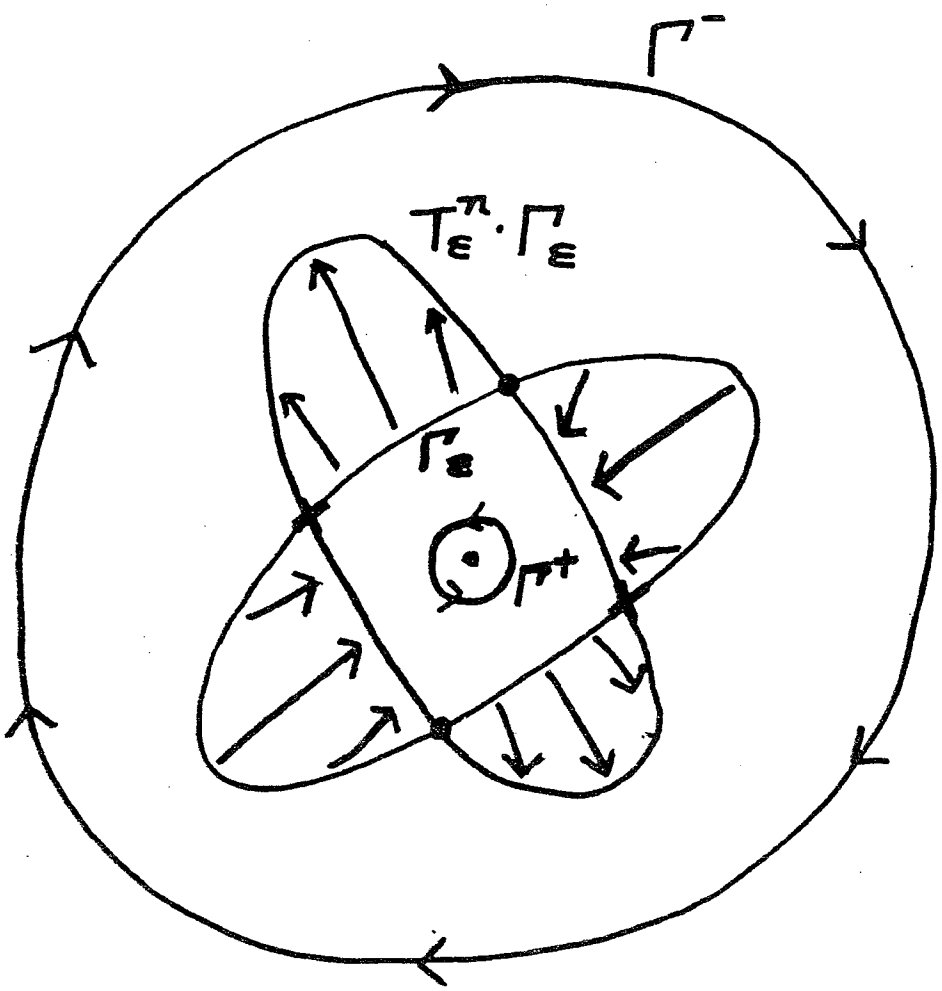

Figure 1.2.2.1 : Birkhoff orbits for an area-preserving twist map T_ε close to an integrable twist map. • denotes an elliptic point and × ordinary hyperbolic point.

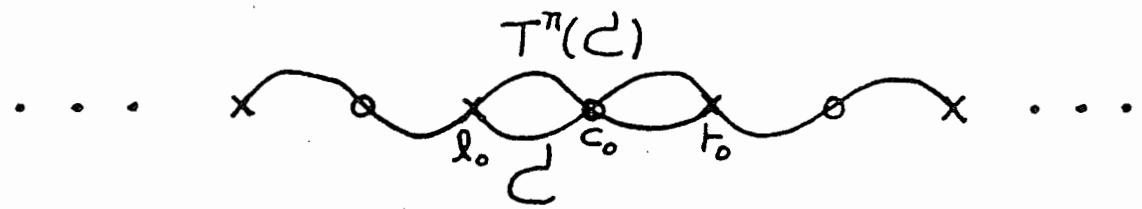

Figure 1.2.2.2 : Formation of a partial barrier with turnstile from periodic orbits.

§ 1.2.3 Symmetric periodic orbits in reversible maps

Reversibility implies that if $((x_i, y_i))$ is an orbit of a reversible map T with symmetry S (see §1.1.3), then the reflection $(s(x_i, y_i))$ of the orbit by S is an orbit of its time reversal T^{-1}. A symmetric orbit is an orbit that is invariant under S : an orbit that is its own time reversal.

Firstly, I discuss the stability of symmetric periodic orbits in a reversible map T. A symmetric fixed point cannot be asymptotically stable, because if U were a neighborhood of the symmetric fixed point x, satisfying (1.2.1.2)(i.e. a basin of attraction), then SU would be a neighborhood of x, hence

$$\exists_{k_o} \quad \text{s.t.} \quad T^k U \subset SU \qquad \text{for } k > k_o \quad , \qquad (1.2.3.1)$$

and applying $T^k S$ to (1.2.3.1),

$$T^k U \subset SU \qquad \text{for } k > k_o \quad , \qquad (1.2.3.2)$$

which is a contradiction to the fact that $T^k U$ contracts asymptotically to (x). Also, like the case in area-preserving maps, the multipliers of the symmetric fixed points come in reciprocal pairs (Devaney, 1976). This can be seen easily as follows. The derivative map DT(x) of a symmetric fixed point x is :

$$DT(x) = DTS(x) \cdot DS(x) \quad , \qquad (1.2.3.3)$$

because $T = (TS) \cdot S$ and $S \cdot x = x$.

Since $S^2 = I = (TS)^2$, $DS(x)$ and $DTS(x)$ are linear involutions. So, for a symmetric fixed point x the derivative map $DT(x)$ is a linear reversible map. Then, the characteristic polynomial of $DT(x)$ is reflexive:

$$\begin{aligned} p(\lambda) &= \mathrm{Det}(DT(x) - \lambda I) \\ &= \mathrm{Det}(DT^{-1}(x) - \lambda I) \\ &= \lambda^2 \, \mathrm{Det}(DT(x) - \lambda^{-1} I)/\mathrm{Det}(DT(x)). \end{aligned} \tag{1.2.3.4}$$

Therefore, if λ is an eigenvalue of $DT(x)$, then λ^{-1} is also an eigenvalue, except in the case $\lambda = \pm 1$. Special consideration is required in the case $\lambda = \pm 1$. Since linear involutions have determinants ± 1, $\mathrm{Det}(DT(x)$is 1 or -1. Therefore the multiplicity of eigenvalue -1 must be even or odd according as $\mathrm{Det}(DT(x))$ is 1 or -1. Then the multiplicity of eigenvalue +1 is determined by elimination, depending on $\mathrm{Det}(DT(x))$ and the parity of the dimension of the phase space. Also, by (1.2.3.4), the linear stability of a symmetric fixed point in one direction of time is the same as that in the other direction.

All the periodic orbits in reversible maps are not symmetric(see §1.2.4). Periodic orbits which are not symmetric are called unsymmetric periodic orbits. If x is a unsymmetric fixed point of a reversible map with symmetry S, then Sx is a fixed point of T, where $Sx \neq x$. The characteristic polynomial $p(\lambda)$of the unsymmetric fixed point is:

$$\begin{aligned} p(\lambda) &= \mathrm{Det}(DT(x) - \lambda I) \\ &= \lambda^2 \, \mathrm{Det}(DT(Sx) - \lambda^{-1} I)/\mathrm{Det}(DT_{Sx}). \end{aligned} \tag{1.2.3.5}$$

Therefore, if DT(x)has an eigenvalue λ, then DT(Sx) has an eigenvalue λ^{-1}. Note that for an unsymmetric fixed point, the stability in one direction is not the same as that in the other direction, in general, because generally the derivative map DT(x) is not a linear involution. But, if T is also area-preserving, then (1.2.3.5) becomes:

$$\begin{aligned} p(\lambda) &= \mathrm{Det}(DT(x) - \lambda I) \\ &= \mathrm{Det}(DT(Sx) - \lambda I) \quad . \end{aligned} \tag{1.2.3.6}$$

Hence, in this case, x and Sx have the same eigenvalue.

Secondly, I describe the connections between symmetric periodic orbits and symmetry lines. If x is a point of a symmetric orbit of a reversible map T with symmetry S, then there exists some n such that

$$S \cdot x = T^n \cdot x \tag{1.2.3.7}$$

If n is even, then

$$S \cdot T^{n/2} \cdot x = T^{n/2}\, x \quad , \tag{1.2.3.8}$$

and thus the orbit has a point $T^{n/2}x$ on Fix(S), the symmetry line of S (see § 1.1.3). If n is odd, then

$$TS \cdot T^{\frac{n+1}{2}} x = T^{\frac{n+1}{2}} x \quad , \tag{1.2.3.9}$$

and thus the orbit has a point $T^{\frac{n+1}{2}}\, x$ on Fix(TS), the symmetry line of TS. Conversely, a periodic orbit with a point x on some symmetry, e.g. Fix(S), is symmetric: since $S \cdot x = x$, $ST^k\, x = T^{-k}\, x$ for any k, and thus the periodic

orbit is invariant under S. An intersection point of two symmetry lines, Fix($T^m S$) and Fix($T^n S$), is a fixed point of T^{m-n} and thus its orbit is a symmetric periodic orbit. Conversely, a point of a periodic orbit of period q on Fix ($T^m S$) is an intersection point with Fix($T^{m+kq} S$) for any $k \in Z$. Therefore, the intersection point of the symmetry lines, Fix($T^{m+kq} S$) for all k, is a periodic point of period q.

If a periodic point x of even period 2n lies on Fix(S), then $T^n x$ also lies on Fix(S) by (1.2.3.8). Similarly, if a periodic point x of odd period (2n+1) or (2n-1), then $T^n x$ lies on Fix (ST) or fix (TS). Conversely, if x lies on Fix(S) and $T^n x$ lies on Fix(TS), or Fix(ST) or Fix(TS), then x is a periodic point, with period 2n, 2n+1, 2n-1, respectively, where 2n, 2n+1 and 2-1, in some cases, may be multiples of the period. Therefore, given a complementary pair of symmetries, a periodic orbit of even period has two points on one symmetry line and none on the other, and a periodic orbit of odd period has one on each symmetry line. These relations between symmetric periodic orbits and symmetry lines can be used usefully in locating symmetric periodic orbits: a symmetric periodic point can be evaluated by going only halfway round the orbit.

Finally, I discuss the dominant half-line for Birkhoff orbits (see §1.2.2) in reversible area-preserving maps. For example, I consider the standard map (1.1.3.14). For the standard map T with a symmetry S_1, T can be represented on a torus, because T is doubly periodic in x and y (see (1.1.3.15)).

There are two symmetry half-lines for S_1 and TS_1, respectively:

$$\text{Fix}(S_1): x = 0, \pi, \quad \text{Fix}(TS_1): x = y/2, y/2+\pi \quad .$$

Therefore, there are four half-lines. A remarkable, but not mathematically understood, observation is that periodic orbits of type(p,q) with positive residues have one point on the half-line x=0 (Shenker and Kadanoff, 1982). So, this half-line is called the dominant half-line, and the other three half-lines are called subdominant half-lines. Futhermore, on the line $x=\pi$, there is a point with positive or negative residue according as q is even or odd. On the line $x= y/2$, one finds a point with positive or negative residue according as p is even or odd, and on the line $x=y/2+\pi$ there is a point with positive or negative residue according as both p and q are odd or not. This is illustrated in figure 1.2.3.1 and tabulated in table 1.2.3.1. If a point x_0 of a Birkhoff orbit of type(p,q) lies on the initial line, then the half-way point round the orbit lies on the final line (see table 1.2.3.1). Here, the half-way point is $T^n x_0$ when q is 2n or 2n-1 . In this way, Birkhoff orbits and symmetry half-lines are related. These relations are very helpful in locating the Birkhoff orbits of type(p,q).

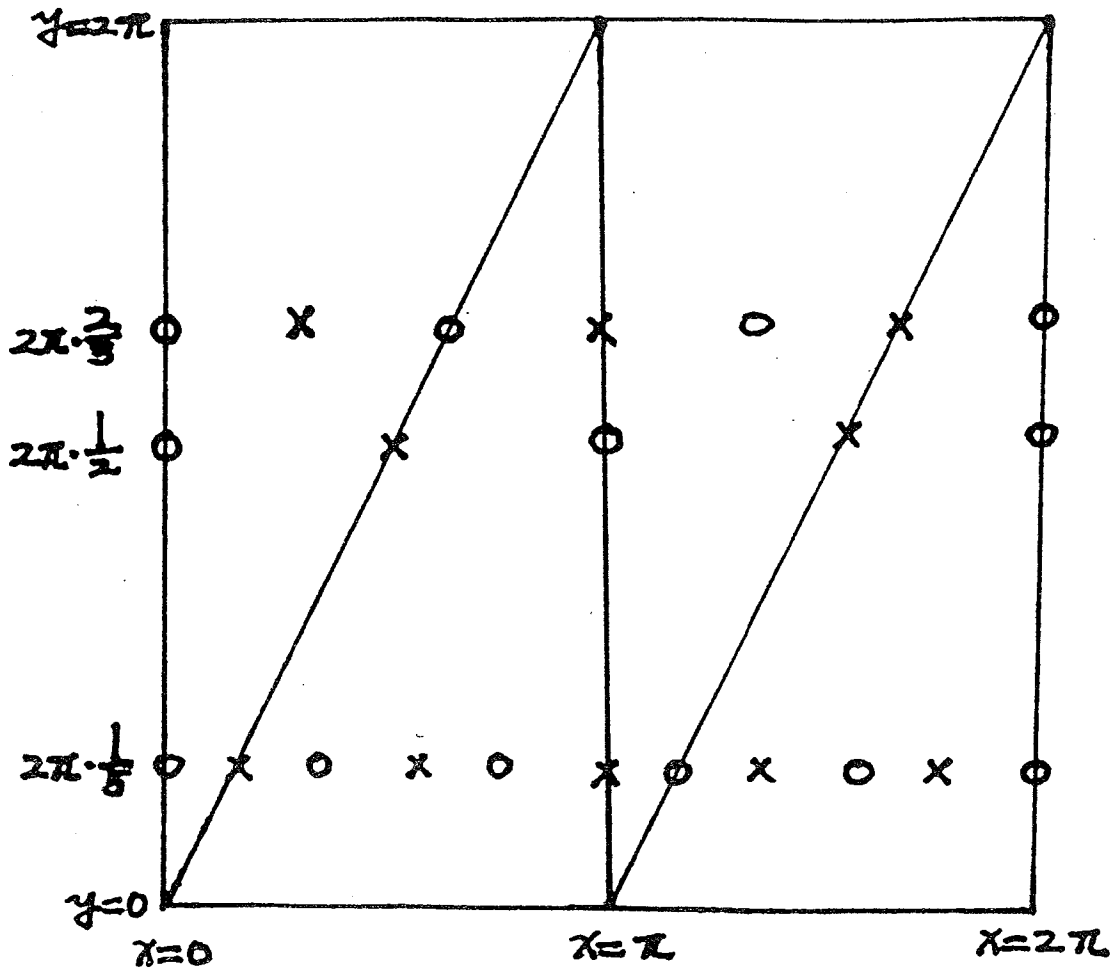

Figure 1.2.3.1 : The relations between Birkhoff orbits and symmetry lines. O denotes a minimaximizing Birkhoff orbit of type-(p,q) and X a minimizing Birkhoff orbit of type-(p,q).

p/q	R^+		R^-	
	initial line	final line	initial line	final line
odd/even	x=0	x=π	x=y/2	x=y/2+π
odd/odd	x=0	x=y/2+π	x=π	x=y/2
even/odd	x=0	x=y/2	x=π	x=y/2+π

Table 1.2.3.1: Symmetry-lines for Birkhoff orbits of type (p,q). R^+ and R^- denotes positive and negative residue, respectively.

§ 1.2.4 Bifurcations of periodic orbits

In this subsection, I discuss generic bifurcations in reversible area-preserving maps with one parameter and anomalous bifurcations in the standard map. Bifurcations mean the branching of periodic orbits as a parameter is varied.

Meyer(1970) and Rimmer(1974) have obtained the generic results for bifurcations in area-preserving maps and reversible area-preserving maps, respectively. It may be necessary to state the meaning of the genericity in dynamical systems used by mathematicans because the meaning of the genericity used by mathemathicans is weaker than that used by physicists(Abraham and Marsden 1978, Wightman 1981). What the adjective 'typical' should be defined to mean is required to study what actually happens in 'typical' Hamiltonians(or maps). Physicists usually mean by the adjective 'typical' that the exceptional set is a small uninteresting set. One notion of 'small' is measure zero with respect to some measure . However , there is no natural measure to put on the family of Hamiltonian systems (Wightman, 1981). On the other hand , there is a natural topology in the space of Hamiltonian systems, so called the Whitney topology(Abraham and Marsden 1978, Wightman 1981): two Hamiltonian systems on the phase space M are close in the C^r Whitney topology if all the derivatives of two Hamiltonians up to order r are uniformly close over all M. A small set in a topological

space is a nowhere dense set: the complement of the closure of the small set is a dense open set. Therefore, if the set of the exceptional points in the space of Hamiltonian systems is a nowhere dense set, then the set of the non-exceptional points is an open dense set. Thus, every point in the space of Hamiltonian systems has a non-exceptional point in its every neighborhood. But, in fact, a much weaker notion is useful in mathematics because for example the theorems about generic bifurcations make a statement about all bifurcations of all periodic orbits in Hamiltonian systems. In a weaker sense, the exceptional set is a meager set: a countable intersection of open dense sets, which is called a residual set. To sum up , Mathemathicans use the adjective 'generic' in a topological sense , not in a measure-theoretical sense. Therefore, a proof that a property of a system is generic does not establish necessarily that probably , a randomly chosen system has the property in a measure-theoretical sense. However , the proof establishes that systems whose Hamiltonians are sufficiently close to the system have the property.

Firstly, following Meyer(1970), I discuss generic bifurcations in area-preserving maps. Let I be an interval and $T: R^2 \times I \to R^2$ a 1-parameter family of area-preserving maps. Then, for each $\epsilon \in I$, $T_\epsilon = T|_{R^2 \times (\epsilon)}$ is area-preserving. Let (x_0, ϵ_0) be a fixed point of T :

$$T(x_0, \epsilon_0) = T_{\epsilon_0}(x_0) = x_0 \ , \ x_0 \in R^2 \ .$$

If the multipliers of the fixed point are not +1, then there

exist neighborhoods U and V, $x_0 \in U \subset R^2$ and $\epsilon_0 \in V \subset I$, and a function $f: V \to U$, such that $f(\epsilon_0) = x_0$ and $\{(f(\epsilon),\epsilon);\ \epsilon \in V\} \subset U \times V$ is the fixed point set of T in U x V. This results from the implict function theorem (Apostol, 1973). Thus, a map T_ϵ which has a parameter value ϵ sufficiently close to ϵ_0 has a unique fixed x in U. So, if a fixed point does not have multipliers +1, then it persists under sufficiently small perturbations. Therefore, the only time that a periodic orbit could be created or destroyed or collide with another periodic orbit of the same period or a submultiple is when it has a multiplier +1. Also, note that if a fixed point of T_ϵ has multipliers equal to $e^{\pm 2\pi i m/n}$, then it is also a fixed point of T_ϵ^n and has multipliers +1 under DT_ϵ^n, where m and n are coprime integers $n \geq 1$, and $0 \leq m/n \leq 1/2$. Therefore, when the multipliers of a fixed point are $e^{\pm 2\pi i m/n}$, m/n-bifurcations could occur. But I discuss only generic m/n bifurcations in generic area-preserving maps. So, all area-preserving maps are not considered, but a subset of all area-preserving maps which is a set of generic area-preserving maps is considered. An area-preserving map is called a generic area-preserving map if each periodic point in the map is either elliptic with multipliers $e^{\pm 2\pi i \alpha}$ (α: irrational number), hyperbolic, extremal, transition or n-bifurcation point with multipliers $e^{\pm 2\pi i m/n}$. The definitions of extremal, transition and n-bifurcation point will be given below.

Let us consider generic 1/2-bifurcation of a fixed point. a fixed point with multipliers -1 of T_ϵ is called a transition

point if there exist coordines (x,y) such that

$$T_\epsilon : \begin{bmatrix} x \\ y \end{bmatrix} \longrightarrow \begin{bmatrix} x' = -x+y+ex + \cdots \\ y' = -y+ax^2+bxy+c\epsilon x+dx^3+\cdots \end{bmatrix} ,$$

where $c \neq 0$, $a^2 + 2f \neq 0$; $f = d + ae + ab/2$.

Note that without loss of generality, it is possible to keep a fixed point with multipliers -1 at (0,0) because the fixed point with multiplier -1 persist under sufficiently small perturbations. So, for a sufficiently small ϵ , (0,0) is a fixed point of T_ϵ. The derivative map of T_ϵ at (0,0) is :

$$DT_\epsilon(0,0) = \begin{bmatrix} -1 & 1 \\ c\epsilon & -1 \end{bmatrix} .$$

Note that the first order effect on the diagonal terms of $DT_\epsilon(0,0)$ does not appear in evaluating the trace of $DT_\epsilon(0,0)$. So, it would appear to be necessary to calculate them to higher order. But, to avoid this one can use the area-preserving condition, as follows (Mackay,1982). This problem occurs often in analyzing generic m/n-bifurcations. Let M be a linear area-preserving map:

$$M = \begin{bmatrix} A & B \\ C & D \end{bmatrix} , \quad AD - BC = 1 .$$

Then,

$$\begin{aligned} (TrM)^2 &= (A + D)^2 \\ &= 4 + 4BC + (A - D)^2 . \end{aligned}$$

When TrM is close to +2 or -2 ,

$$TrM = \pm 2(a + BC/2 + (A-D)^2/8 + \cdots) \quad . \qquad (1.2.4.1)$$

So we can use the off-diagonal terms in evaluating the trace. Then, the trace of $DT_\epsilon(0,0)$ is :

$$Tr = -2 - c\epsilon + \mathcal{O}(\epsilon^2) \ ,$$

where I drop $DT_\epsilon(0,0)$ in $TrDT_\epsilon(0,0)$ and hereafter I will drop it for my convenience. Let $c\cdot(a^2+2f) < 0$ and then consider the case when $\epsilon > 0$ (if $c\cdot(a^2+2f) > 0$, then consider the case when $\epsilon < 0$). Make the substitutions:

$$x = \mu X \ , \ y = \mu^2 Y \ , \ \mu^2 = \epsilon \ .$$

Then,

$$T_\mu : \begin{bmatrix} X' = -X + \mu(Y + eX^2) + \mathcal{O}(\mu^2) \\ Y' = -Y + aX^2 + \mu(cX + bXY + dX^3) + \mathcal{O}(\mu^2) \end{bmatrix}$$

The derivative map of T_μ at $(0,0)$ is :

$$DT_\mu = \begin{bmatrix} -1 & \mu \\ \mu c & -1 \end{bmatrix} \quad .$$

Then, by using the trick (1.2.4.1), the trace of DT_μ is:

$$Tr = -2 - c\mu^2 = -2 - c\epsilon \ .$$

Therefore, the fixed point is an inversion hyperbolic or an elliptic point according as $c\cdot\epsilon$ is positive or negative.

Let us $(\hat{X}, \hat{Y})$ be period-2 points of T_μ. Then, they are fixed points of T_μ^2 :

$$T_\mu^2 : \begin{bmatrix} X'' = X - 2\mu(Y - aX^2/2) + \mathcal{O}(\mu^2) \\ Y'' = Y - 2\mu(cX + aXY + fX^3) + \mathcal{O}(\mu^2) \end{bmatrix} .$$

So, the period-2 points of T_μ are:

$$\hat{X} = \pm(-2c/(a^2+2f))^{1/2} , \quad \hat{Y} = -ac/(a^2+2f) .$$

In the original coordinate system (x,y), they are :

$$\hat{x} = \pm\epsilon^{1/2}(-2c/(a^2+2f))^{1/2} , \quad \hat{y} = -\epsilon ac/(a^2+2f)$$

Using the trick (1.2.4.1), one finds

$$\mathrm{Tr}DT_\mu^2 = 2 - 8\mu c + \mathcal{O}(\mu^2) = 2 - 8\epsilon^2 c .$$

Then, the period-2 point is elliptic or ordinary hyperbolic according as c is positive or negative. Therefore, in typical area-preserving maps, two types of generic 1/2-bifurcation occur according as c is positive or negative. These two cases are sketched, as follows.

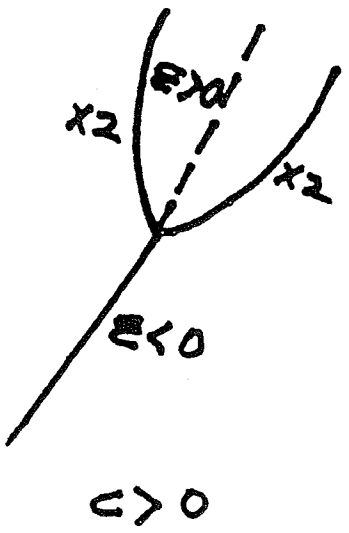

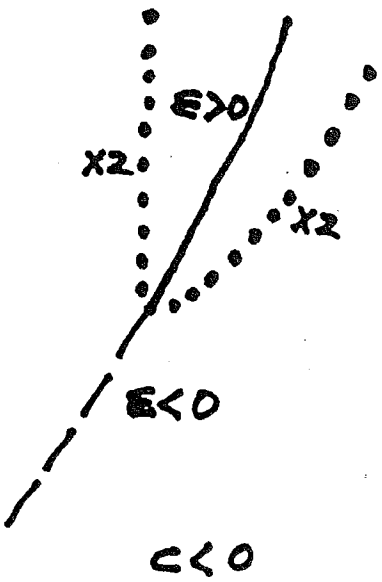

In this and future sketches, solid line indicates elliptic, dashed line inversion hyperbolic, and dotted line ordinary hyperbolic, and x n denotes that the period of a bifurcated orbit from a mother orbit is the period of the mother orbit times n.

Let us consider higher order bifurcations from a fixed point of T_ϵ whose multipliers are $e^{\pm 2\pi i m/n}$ $(n \geq 3)$. Then, there exist canonical coordinates (I,θ) (Meyer, 1970), such that

$$\theta' = \theta + 2\pi\, m/m + \epsilon\, \alpha(\epsilon)/n + \sum_{i=1}^{\frac{n-2}{2}} \beta_i(\epsilon)/n \cdot I^i + \gamma(\epsilon)/n \cdot \cos n\theta \cdot I^{\frac{n-2}{2}} + f(I,\theta,\epsilon),$$

$$I' = I + 2\cdot\gamma(\epsilon)/n \cdot \sin n\theta \cdot I^{n/2} + g(I,\theta,\epsilon),$$

$$\frac{\partial^j f}{\partial \rho^j}(\theta,0,0) = 0 \ , \ j = 0,\ 1,\ 2,\ \ldots\ n-1,$$

$$\frac{\partial^j g}{\partial \rho^j}(\theta,0,0) = 0, \quad j = 0,\ 1,\ 2,\ \ldots,\ n+1,$$

$$\rho = I^{1/2} \ , \ x = (2I)^{1/2} \cos\theta, \ y = (2I)^{1/2} \sin\theta \ . \quad (1.2.4.2)$$

This is called a normal form of T_ϵ . A fixed point is called a n-bifurcation point if α and γ are not zero when $n=3$, α,γ and $\beta \pm \gamma$ are not zero when $n=4$, and α, β and γ are not zero when $n \geq 5$, where $\alpha = \alpha(0)$, $\beta = \beta_1(0)$ and $\gamma = \gamma(0)$.

Let us consider the case when $n=3$. Make the substitution in (1.2.4.2): $I = \epsilon^2 r$. Then, T_ϵ becomes :

$$r' = r + 2|\epsilon| \cdot \frac{\gamma}{3} \cdot \sin 3\theta\ r^{\frac{3}{2}} + \mathcal{O}(\epsilon^2),$$

$$\theta' = \theta + 2\pi \cdot 1/3 + \epsilon \cdot \frac{\alpha}{3} + \frac{\gamma}{3} \cdot |\epsilon| \cdot \cos\ 3\theta \cdot r^{1/2} + \mathcal{O}(\epsilon^2) \ .$$

Let us $(\hat{r},\hat{\theta})$ be period-3 points of T_ϵ. Then they are fixed points of T_ϵ^3 :

$$r^{(3)} = r + 2\,|\epsilon|\cdot\gamma\cdot\sin 3\theta\cdot r^{3/2} + \mathcal{O}(\epsilon^2),$$
$$\theta^{(3)} = \theta + \epsilon\cdot\alpha + |\epsilon|\cdot\gamma\cdot\cos 3\theta\cdot r^{1/2} + \mathcal{O}(\epsilon^2) \quad .$$

Let $\alpha\cdot\gamma>0$ (otherwise, $\alpha\gamma<0$). Then, the period-3 points are:

$$\sin 3\hat{\theta} = 0 \ , \ \cos 3\hat{\theta}\cdot\hat{r}^{1/2} = -\frac{\epsilon}{|\epsilon|}\cdot\frac{\alpha}{\gamma} \ ,$$

if $\epsilon > 0$, then $3\hat{\theta} = (2k+1)\pi$, otherwise $3\hat{\theta} = 2k\pi$, $k=0,1,2$, and $\hat{r}^{1/2} = \alpha/\gamma$. In the original system (I,θ), $\hat{I}^{1/2} = |\epsilon|\cdot\hat{r}^{1/2} = |\epsilon\alpha/\gamma|$. Using the trick (1.2.4.1), the trace of DT_ϵ^3 is :

$$\mathrm{Tr}DT_\epsilon^3 = 2 + 3\epsilon^2\alpha^2 \quad .$$

Therefore, the period-3 points are ordinary hyperbolic. So, we get a 1/3-bifurcation diagram like:

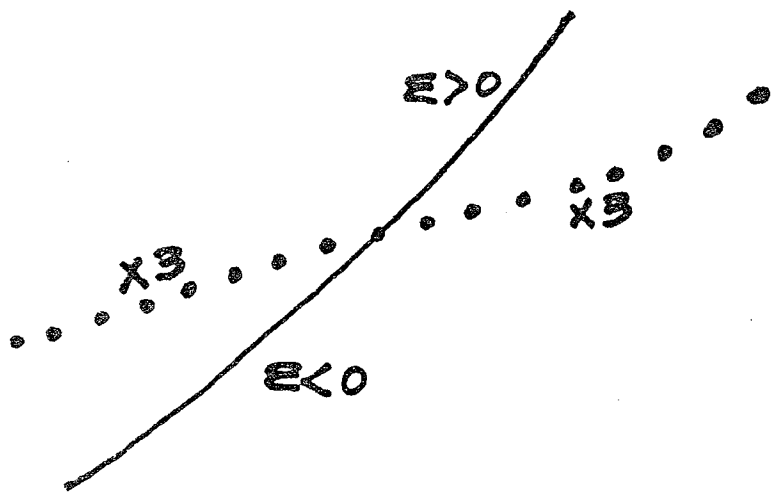

Note that often one sees that the period-3 points are born by a tangent bifurcation which will be explained below (e.g. see §2.2), but this is outside the range of local analysis.

So, a typical 1/3-bifurcation diagram is:

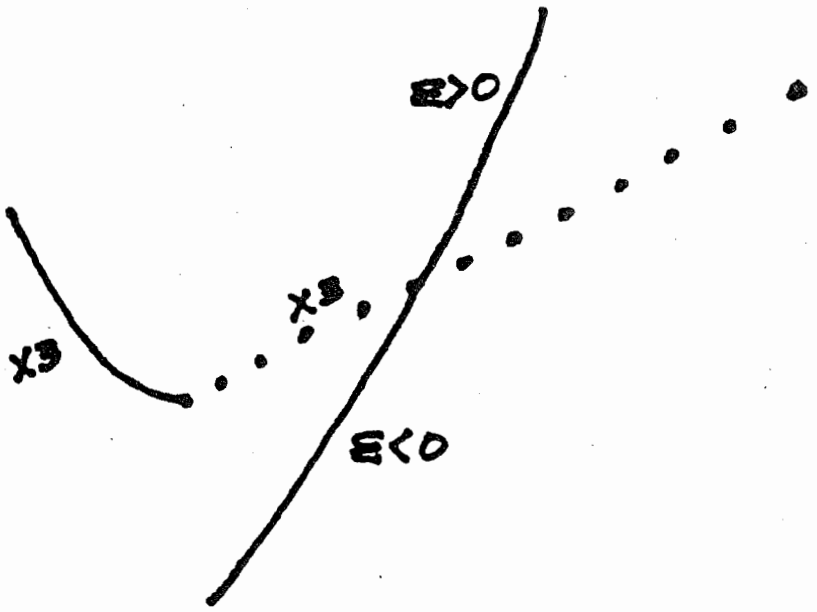

Let us consider the case when n=4. Make the substitution in (1.2.4.2) ; $I=\epsilon r$. Then T_ϵ becomes :

$$r' = r + 2\cdot\frac{\gamma}{4}\cdot\epsilon\cdot\sin 4\theta\cdot r^2 + \mathcal{O}(\epsilon^2),$$

$$\theta' = \theta + 2\pi\cdot\frac{1}{4} + \frac{\epsilon}{4}(\alpha+\beta r) + \frac{\epsilon}{4}\gamma\cos 4\theta\cdot r + \mathcal{O}(\epsilon^2) .$$

Let $(\hat{\theta},\hat{r})$ be period-4 points of T_ϵ. Then they are fixed points of T_ϵ^4 :

$$r^{(4)} = r + 2\epsilon\cdot\gamma\cdot\sin 4\theta\ r^2 + \mathcal{O}(\epsilon^2) ,$$

$$\theta^{(4)} = \theta + \epsilon(\alpha+\beta r) + \epsilon\cdot\gamma\cdot\cos 4\theta\cdot r + \mathcal{O}(\epsilon^2) .$$

A system of equations to solve to obtain fixed points of T_ϵ^4 is :

$$\alpha + (\beta + \gamma\cos 4\hat{\theta})\cdot\hat{r} = 0 , \quad \sin 4\hat{\theta} = 0 .$$

In the original coordinate system (I,θ), they are:

$$\epsilon\alpha + (\beta+\gamma\cos 4\hat{\theta})\cdot\hat{I} = 0, \qquad \sin 4\hat{\theta} = 0$$

when $|\beta|>|\gamma|$, if $\epsilon\beta > 0$, then there is no fixed point since $I< 0$, which is a contradiction to the fact $I>0$, otherwise

$$\hat{I} = \left|\frac{\alpha\cdot\epsilon}{\beta\pm\gamma}\right| ,$$

$4\hat{\theta} = 2k\pi$ or $(2k+1)\pi$ according as the sign in $\hat{I}$ is + or -,

$k=0,1,2,3.$

When $|\beta|<|\gamma|$, if $\epsilon\gamma > 0$, then

$$\hat{I} = \left| \frac{\alpha\epsilon}{\beta-\gamma} \right| \quad \text{and } 4\hat{\theta} = (2k+1)\pi, \text{ otherwise}$$

$$\hat{I} = \left| \frac{\alpha\epsilon}{\beta+\gamma} \right| \quad \text{and } 4\hat{\theta} = 2k\pi .$$

The stability of period-4 points are given by

$$\mathrm{Tr}DT_{\epsilon}^{4} = 2-8\epsilon\alpha\gamma\cos 4\hat{\theta} .$$

Let $\alpha>0$ (otherwise, $\alpha<0$). Then, When $|\beta|>|\gamma|$, if $\epsilon\gamma>0$, then the period-4 points are elliptic or ordinary hyperbolic according as $4\hat{\theta} = 2k\pi$ or $(2k+1)\pi$, otherwise vice versa. When $|\beta|<|\gamma|$, if $\epsilon\gamma > 0$, then the period-4 points are ordiary hyperbolic, otherwise vice versa. Therefore, the former case ($|\beta|>|\gamma|$) is like $\frac{1}{n}$ -bifurcation case ($n\geq 5$), while the latter case is like 1/3 - bifurcation case. The two cases are sketched, as follows .

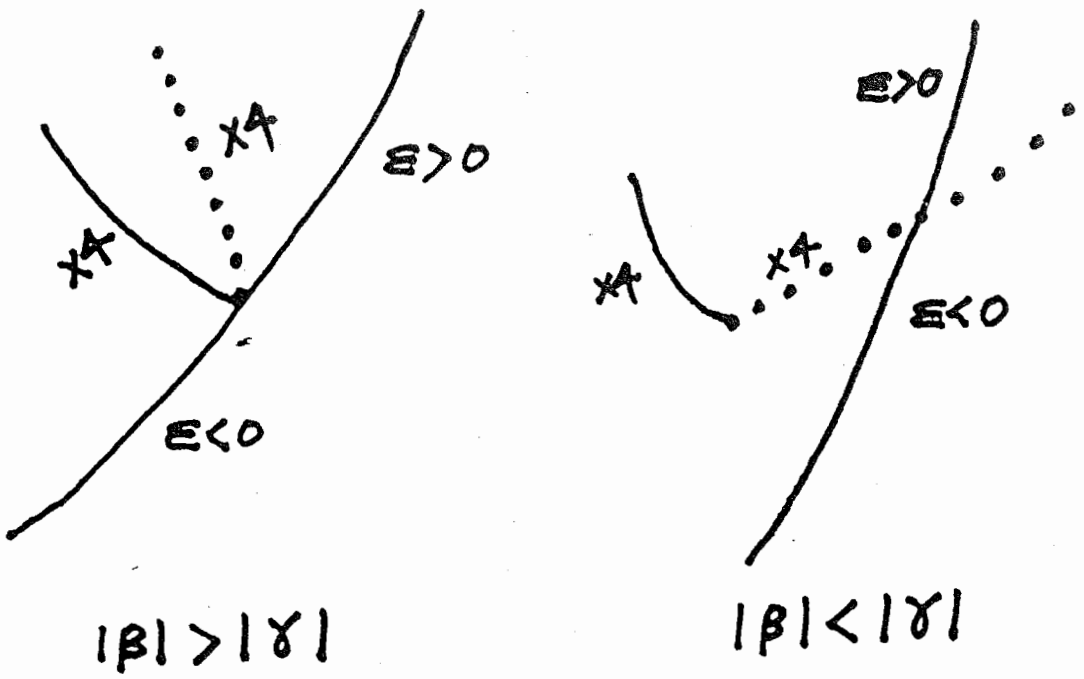

$|\beta| > |\gamma|$ $|\beta| < |\gamma|$

Note that like the 1/3-bifurcation, when $|\beta|<|\gamma|$, period -4 points are often born by tangent bifurcation.

When $n \geq 5$, T_ϵ becomes:

$$r' = r + \epsilon^{-1} \cdot \frac{2\gamma}{n} \cdot \sin(n\theta)(\epsilon r)^{n/2} + \sigma(\epsilon^{n/2}) ,$$

$$\theta' = \theta + 2\pi \cdot m/n + \epsilon \cdot \frac{\alpha}{n} + \epsilon \cdot \frac{\beta}{n} \cdot r + \sigma(\epsilon^{\frac{3}{2}}) ,$$

where $I = \epsilon r$.

The period-n points are fixed points of T_ϵ^n:

$$r^{(n)} = r + \epsilon^{-1} \cdot 2\gamma \cdot \sin(n\theta)(\epsilon r)^{n/2} + \sigma(\epsilon^{n/2}) ,$$

$$\theta^{(n)} = \theta + \epsilon(\alpha + \beta r) + \sigma(\epsilon^{\frac{3}{2}}) .$$

The n-periodic points $(\hat{\theta}, \hat{r})$ of T_ϵ are given by a system of equations:

$$\sin(n\hat{\theta}) = 0 , \quad \alpha + \beta\hat{r} = 0 .$$

In the original coordinate system, this system of equations ar

$$\sin(n\hat{\theta}) = 0 , \quad \hat{I} = -\epsilon \cdot \alpha/\beta .$$

Let $\alpha>0$ (otherwise, let $\alpha<0$). Then, if $\beta\epsilon>0$, then there are no n-periodic points because $\hat{I} < 0$, otherwise

$$\hat{I} = |\epsilon\frac{\alpha}{\beta}| \quad , \; n\hat{\theta} = 2k\pi \text{ or } (2k+1)\pi$$

$$k = 0,1,2,\ldots,n-1 \quad .$$

Using the trick (1.2.4.1), one finds

$$TrDT_{\epsilon}^{n} = 2 + 2n\cdot|\epsilon\cdot\alpha/\beta|^{n/2}\cdot\gamma\beta\cdot\cos\, n\hat{\theta} \quad .$$

So, if $\gamma\beta>0$, then periodic n-points are ordinary hyperbolic or elliptic according as $n\hat{\theta} = 2k\pi$ or $(2k+1)\pi$, otherwise vice versa. The m/n-bifurcation($n\geq 5$)diagram is sketched below.

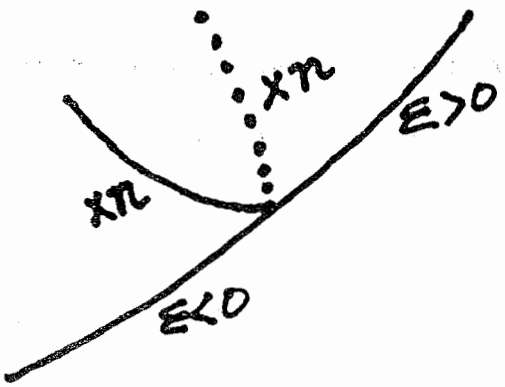

When n=1, a fixed point is called an extremal point if it satisfies some conditions (for details, see Meyer(1970)). Only I sketch two generic 0/1-bifurcations, as follows.

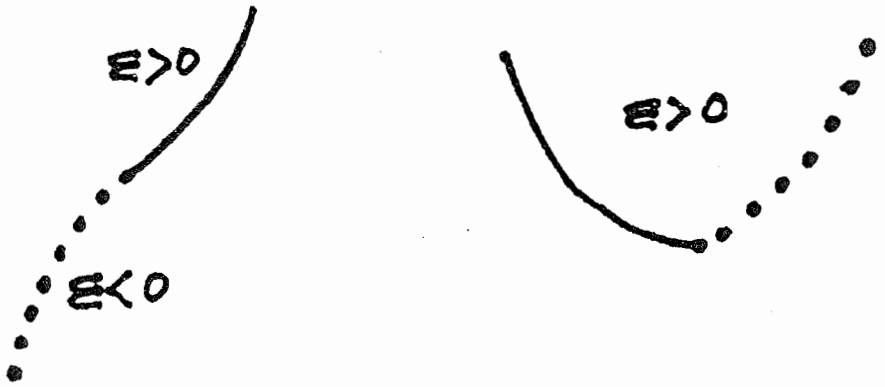

Note that in the second case in the sketches, two fixed points which are elliptic are ordinary hyperbolic respectively pop up when $\epsilon>0$. This is called a tangent bifurcation.

Secondly, following Rimmer(1974),I discuss generic bifurcations of symmetric fixed points in reversible area-preserving maps. The main differences between generic bifurcations in area-preserving maps and those in reversible area-preserving maps come in the case of multipliers +1,where there are two typical cases. One case is the same as that in area-preserving maps. The other case is sketched below.

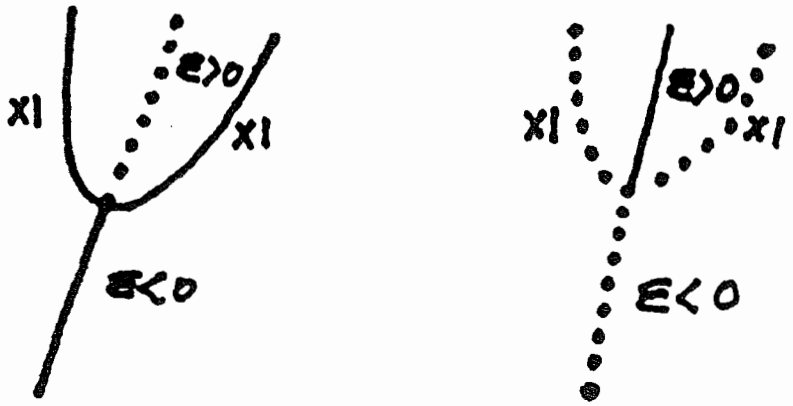

As shown in the sketches, in this case, two further families of unsymmetric points are produced from the mother orbit. Except this case, all periodic orbits produced by generic bifurcations of a symmetric periodic orbits are also symmetric.

Finally, follwing Mackay(1982), I discuss nongeneric anomalous bifurcations in the standard map (1.1.3.14). Various authors(Benettin et al, 1980,Schmidt and Bialek,1982,Greene, Karney, and Bak and Jensen referred to by Mackay,1982) have reported anomalous bifurcations of periodic orbits in the standard map. Note that the map $T:(X,Y)\to(X',Y')$ studied by

Benettin et al can be transformed into the standard map by some coordinate change:

$$X'=x \ , \ X=x' \ , \ Y' = -y, \ Y= -y' \ .$$

Their observations in the standard map can be summarized as follows. The fixed point at (0,0) and period-2 orbit at(o,π), (π,π) have generic m/n-bifurcations at multipliers $e^{\pm 2\pi i m/n}$, when n is even, but anomalous double m/n-bifurcation when n is odd: when n is odd, two families of periodic orbits whose periods are n times as long as the period of the mother orbit are born. The multipliers of the daughters of period an even multiple of that of the mother orbit, +1 at birth, travel round the unit circle, pass through each other at -1,continue to go round the unit circle to +1,and split along the positive real line, as a parameter is varied. During this change of multipliers, generic or anomalous double m/n-bifurcations occur: when the multipliers are $e^{\pm 2\pi i m/n}$, generic m/n-bifurcations occur when m is even, but anomalous double m/n-bifurcations when m is odd. When the multipliers go through +1, a generic bifurcation occur: two further families of periodic orbits of the same period as that of the mother are born.

These anomalous bifurcations in the standard map may be explained as follows. The standard map T is doubly periodic in (x,y), and thus the map can be considered to be acting on a torus. Furthermore, the map has an inversion symmetry:

$$T = U \cdot T \cdot U \ , \qquad U: \ x' = -x \ , \ y' = -y \ .$$

Then, identifying points on a torus which are related by U, one can consider the map to be acting on a sphere with four corners(see figure 1.2.4.1). The four corners are fixed points under U. Recall that the standard map has two reversible symmetry S_1 and S_2 (see (1.1.3.15)), $S_2 = US_1$ and $TS_2 = U(TS_1)$. So, on a sphere with four corners, two symmetries, S_1 and S_2 are reduced to one symmetry.

If $\{T \cdot x \quad x \in T$ (a torus), $n \in Z\}$ is an orbit, then $\{UT\ x, n \in Z\}$ is also an orbit. An U-symmetric orbit is an invariant orbit under U. Let x be an U-symmetric point. Then $U \cdot x = T^m x$, for some m. So, $T^{2m} \cdot x = x$, and thus an U-symmetric orbit must be periodic. Let p be the period. Then, without loss of generality, $0 \leq m < p$. If m is zero, then $U \cdot x = x$, x on a torus. So, in this case, the orbit is composed of some fixed points of U. This orbit is called a strongly symmetric orbit (Mackay, 1982). If m is not zero, then 2m must be a multiple of p. Since $0 < m < p$, $m = p/2$, p even. In this case, the orbit is called a weakly symmetric orbit (Mackay, 1982). In the standard map acting on a torus, the period-1 orbits and period-2 orbit at$(0, \pi), (\pi, \pi)$ are strongly symmetric orbit. When the multipliers of these strongly symmetric orbits are $e^{2\pi i m/n}$, if n is even, then generic m/n-bifurcations may occur, otherwise anomalous double m/n-bifurcations. This is because a periodic orbit of even period could be a weakly symmetric orbit, on the other hand a periodic orbit of odd period can not be a weakly symmetric orbit and a pair of unsymmetric orbits exists. Assume that all the orbits of even

period born from the strongly symmetric orbits are weakly symmetric. If x is a weakly symmetric point of period even p, then x is also a fixed point of $U \cdot T^{p/2}$. Note that T^p can be factorized into a product:

$$T^p = Q \cdot Q \quad , \quad q = U \cdot T^{p/2} \quad .$$

If the residue R of x as a fixed point of Q is $\sin(\pi\omega)$, then the residue R' as a fixed point of T^p is :

$$R' = 4R(1-R) = \sin^2(2\pi\omega) \quad .$$

Assume that R increases monotonically as a parameter is increased and generic bifurcations occurs when $\omega = m/n$. Then R', 0 at birth, increases to +1 and decreases to 0. Note that if there is a periodic orbit of period even p in Q, then a pair of periodic orbits of period p/2 exist in T^p. Thus, when the multipliers of x in T^p are $e^{\pm 2\pi i m/n}$, if m is even, then generic m/n-bifurcations occur, otherwise double m/n-bifurcation. So, the inversion symmetry U is responsible for anomalous bifurcation .

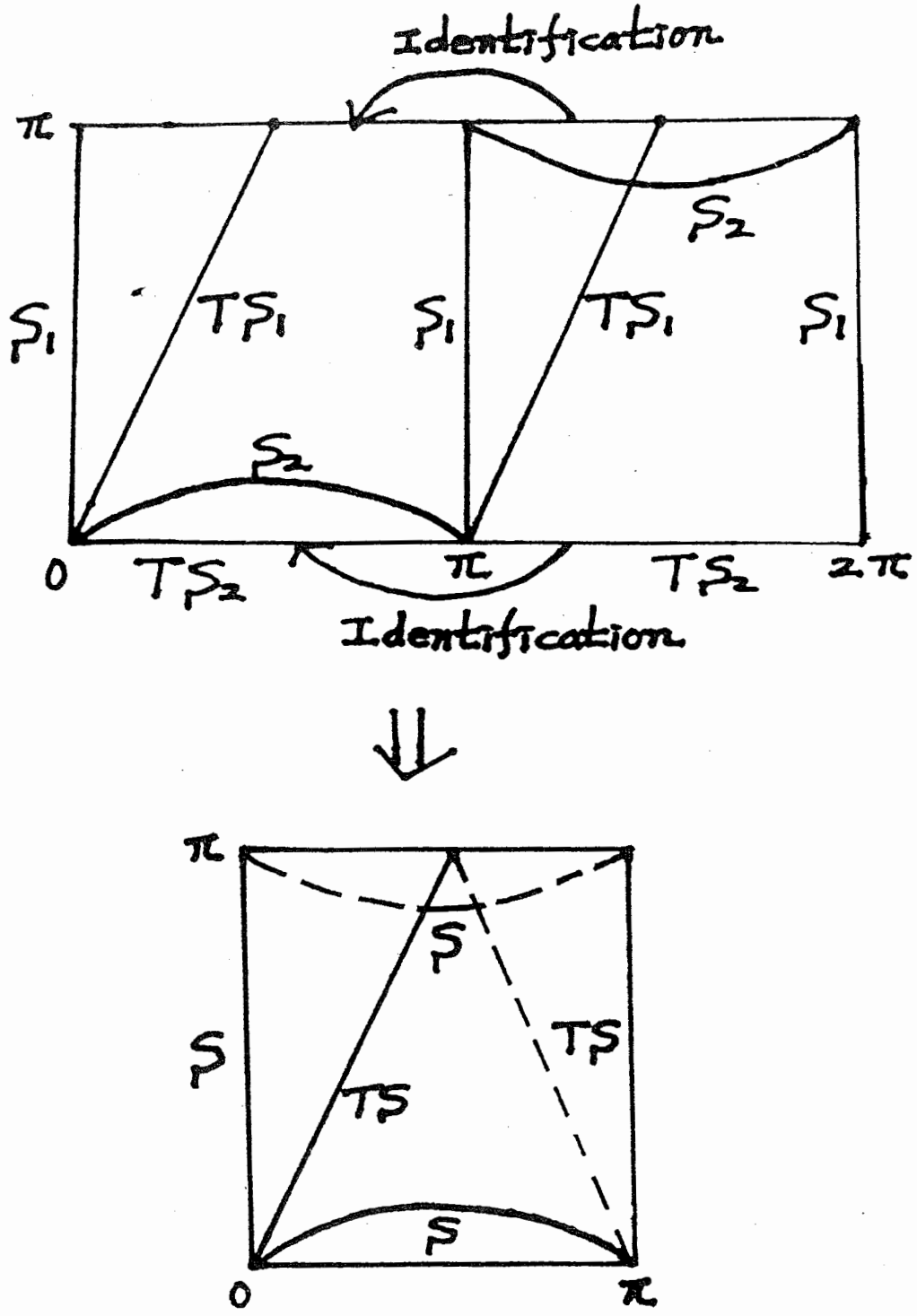

Figure 1.2.4.1 : A sphere with four corners made by identification of points on a torus related by U. Dashed lines are on the back of the four-cornered sphere.

§ 1. 3 Quasi-Periodic orbits

In this section, I discuss quasi-periodic orbits in periodic area-preserving twist maps with zero net flux, namely, those which lie on invariant circles or cantori.

In § 1.3.1 , in periodic maps rotation numbers of orbits are defined. Then, I discuss the stationary action principle for quasi-periodic orbits whose rotation numbers are irrational. Like the case of periodic orbits (see §1.2.2), minimizing quasi-periodic orbits exist in the range of twist. The closure of a minimizing quasi-periodic orbit may be a circle or a cantorus. In the case of a cantorus, the projection of the cantorus on the angle coordinate is the complement of a dense set of gaps and a minimaximizing quasi-periodic orbit homoclinic to the cantorus lies in the gaps. When it is an invariant circle, all the orbits below the invariant circle are confined, and thus there is no flux through it. On the other hand, when it is a cantorus, there is flux through the gaps. The flux depends upon closed curves which close all the gaps. The more important closed curves is the closed curves through which the flux is minimum. These closed curves are those which pass through the cantorus and the minimaximizing orbit, and the flux is given by the difference in the actions between a minimizing orbit and the minimax orbit. Finally, I discuss the Moser's twist theorem which guarantees persistence of invariant circles with sufficiently irrational rotation numbers in the integrable twist map under sufficiently small and smooth perturbations .

In § 1.3.2 , I discuss when extended chaos occurs by various criteria.

The first is Greene's residue criterion which connects the existence of an invariant circle with the stabilities of nearby Birkhoff periodic orbits. The second is Chirikov's resonance overlap criterion which connects the existence of an invariant circle with the widths of nearby resonances. The criteria of Greene and Chirikov are not mathemathically proved, but their criteria give us practical ways to see whether or not an invariant circle exists. In particular, Greene's residue criterion is now the best practical criterion. The third is a theorem of Mather which gives the necessary and sufficient condition for existence of an invariant circle in terms of the difference in the actions of nearby Birkhoff orbits. Finally I discuss the cone-crossing criterion for nonexistence of all the rotational invariant circles.

§ 1. 3. 1 Invariant circles and Cantori

In this subsection, I consider C^1 periodic area-preserving twist map T with zero net flux whose generating function is $L(x,x')$:

$$(x',\ p') = T(x,p) \to (x' + 1,\ p') = T(x+1,\ p),$$
$$\partial^2 L/\partial x \partial x' < 0\ ,\ L(x+1,\ x'+1) = L\ (x,x'). \qquad (1.3.1.1)$$

Equivalently, the map T can be represented on a cylinder, where $2\pi x$ is an angle variable.

One can define rotation number ν for some orbit of a periodic map T. Let (x_0, p_0) be a point in the plane. Then, its orbit $\{(x_n,p_n)=T^n(x_0,p_0),\ n\epsilon Z\}$ is said to have rotation number ν :

$$\nu = \lim_{l-l'\to\infty} (x_l - x_{l'}) / (l-l') ,$$

if the limit exists and does not depend upon the way by which $(l-l')$ goes to infinity. Aubry(1983) and Mather(1982) has shown that every minimizing orbits have rotation number, and conversely, for every ν in the range of twist, there exist a minimizing orbit. When a minimaximizing orbit that is the companion of a minimizing orbit exists, it has the same rotation number. In the previous section, I discussed minimizing and minimaximizing periodic orbits whose rotation numbers are rational. In this section, I discuss minimizing and minimaximizing quasi-periodic orbits whose rotation numbers are irrational. A quasi-periodic orbit is dense on a circle or a Cantor set. When the closure of a quasi-periodic orbit is a circle, we call it an invariant circle and its companion, i.e. a minimaximizing orbit, does not exist. On the other hand, when the closure is a Cantor set, we call it a cantorus and there exists a minimaximizing orbit homoclinic to the cantorus .

There are two types of invariant circles. If an invariant circle encircles the cylinder, then the invariant circle is called a rotational invariant circle, otherwise a vibrational invariant circle. Particularly, rotational invariant circles are more important because they are necessary for confinement,

by a corollary of Birkhoff's theorem(Mackay and Percival,1985):

Theorem(Birkhoff): For the above class of maps, the boundary of any open invariant set homeomorphic to the cylinder and containing all points below some level(p=some constant) and none above some other level, is the graph $\{(x, f(x)):x \in S^1\}$ of some continuous function $f: S^1 \to R$. Particularly, it is a rotational invariant circle.

There are three important corollaries of this theorem (Mackay and Percival, 1985).

The first is Confinement Corollary:
if the orbits of all points below some level p_- remain below some other level p_+, then there exist a rotational circle between p_- and p_+.

The second is Circle Corollary:
every rotational invariant circle is the graph of some continuous function $f: S^1 \to R$.
Then, every rotational circle intersects each vertical line (x=some constant) only once.

The third is Lipschitz Corollary:
the function f(x) in Birkhoff's theorem is Lipschitz.
A function $f: R \to R$ is said to be Lipschitz if the slopes:

$$S(x_1, x_2) = \frac{f(x_2)-f(x_1)}{x_2-x_1} \quad , \; x_1 \neq x_2$$

are uniformly bounded, i.e.

$$\exists D^{\pm} \quad \text{s.t.} \quad D^- \leq S(x_1, x_2) \leq D^+ \quad .$$

Such a range of slopes is called a Lipschitz cone. The domain

of f in Birkhoff's theorem is S^1 to its covering space R, i.e. do not take mod 1 in x. So, though f(x) is not necessary differentiable, it is at least Lipschitz. These theorem and corollaries will be used in the next subsection for the discussion of the nonexistence of all the rotational invariant circles.

Like the case of periodic orbits(see §.1. 2. 2), there are a couple of stationary action principles for quasi-periodic orbits(Percival, 1979, Mather, 1982, Aubry, 1983): one was introduced by Percival and developed by Mather, and the other was introduced by Aubry.

Firstly, I discuss the first one(Percival, 1979, Mather, 1982). Let Y_ν be the set of all increasing functions $\varphi:R\to R$ such that $\varphi(\theta+1)=\varphi(\theta)+1$ and ν is the rotation number of a quasi-periodic orbit under consideration. For $\varphi \in Y_\nu$, Mather defined an action for φ :

$$A_\nu(\varphi) = \int_0^1 d\theta \cdot L(\varphi(\theta), \varphi(\theta+\nu)) \quad ,$$

where L is the generating function for a map under consideration and proved existence of a minimizing $\varphi(\theta)$. Then, it follows that the minimizing $\varphi(\theta)$ satisfies the following Euler-Lagrange equation.

Mather defined :

$$V(\varphi, \theta) = \frac{\partial}{\partial x'} [L(x,x') + L(x',x'')]$$

evaluated at

$$x = \varphi(\theta - \nu),\ x' = \varphi(\theta),\ x'' = \varphi(\theta + \nu) \quad .$$

Then, the minimizing $\varphi(\theta)$ satisfies the Euler-Lagrange euqation:

$$V(\varphi, \theta) = 0 \quad \text{for all } \theta \in R \quad .$$

This gives rise to an invariant set parametrized by θ:

$$x = \varphi(\theta), \quad p = -L_1(\varphi(\theta), \varphi(\theta+\nu)),$$

where subscript 1 denotes the derivative with respect to the first argument, and x and p are dynamical variables in the map T. It may be an invariant circle or a Cantor set according as $\varphi(\theta)$ is continuous or discontinuous. When $\varphi(\theta)$is discontinuous, it has two determinations $\varphi^{\pm}(\theta)$: φ^{+} and φ^{-} are the right continuous and the left continuos determination of the same discontinous $\varphi(\theta)$. In other words,

$$\lim_{\substack{\epsilon\to 0 \\ \epsilon>0}} \varphi^{-}(\theta+\epsilon) = \varphi^{+}(\theta) \ ,$$

and

$$\lim_{\substack{\epsilon\to 0 \\ \epsilon<0}} \varphi^{+}(\theta+\epsilon) = \varphi^{-}(\theta) \quad .$$

If $\varphi^{\pm}$ is discontinuous at θ_0, then $\varphi^{\pm}$ is also discontinuous for $\theta=\theta_0 + h\cdot\nu + k$, where h and k are integers. So, the set of discontinuity points is dense on the real line. In fact, $\varphi^{\pm}$ can be written as a sum of step functions:

$$\varphi^{\pm}(\theta) = \sum_i a_i \cdot Y^{\pm}(\theta - \theta_i) \ ,$$

where at θ_i $\varphi^{\pm}$ is discontinuous, $Y^{\pm}(x) = 0$ for $x<0$, $Y^{\pm}(x)=1$ for $x>0$, $Y^{+}(0)=1$, $Y^{-}(0)=0$, and a_i is the amplitude of the

step function located at θ_i (Aubry, 1983).

Secondly, Aubry(1983) introduced a similar stationary action principle. Let $\{x_i, i\in Z\}$ be an infinite sequence. Then, the action for this sequence is:

$$A = \sum_{i=-\infty}^{\infty} L(x_i, x_{i+1}) \quad .$$

If an infinite sequence $\{x_i, i\in Z\}$ is a minimizing orbit, then for any sequence $\{\delta_i, i\in Z\}$ s.t. there exists $N' < N$ with $\delta_i = 0$ for $i>N$ and $i<N'$, the action variation:

$$\delta A = \sum_{i=N'-1}^{N} [L(x_i+\delta_i, x_{i+1}+\delta_{i+1}) - L(x_i, x_{i+1})]$$

is positive or zero and its has a rotation number ν, and conversely. The closure of this minimizing orbit may be an invariant circle or a Cantor set.

When the invariant set is a Cantor set, there exists a minimaximizing quasi-periodic orbit homoclinic to the Cantor set, i.e. one which converges to the Cantor set as $t\to\pm\infty$ (Mather, 1982, Aubry, 1983). The projection of a Cantor set on the angle coordinate is the complement of a dense set of gaps. All the gaps fall into families: if G is a gap, then any gap $T^nG(n\in Z)$ belongs to the same family. The quasi-periodic orbit homoclinic to the Cantor set is minimaximizing in the following sense(Mackey, 1982). Given a Cantor set, choose one gap. Write $\underset{\sim}{x}^{\ell}$ and $\underset{\sim}{x}^{r}$ for the orbits of the endpoints of the chosen gap. For any sequence $\underset{\sim}{x}$ satisfying:

$$x_i^{\ell} \leq x_i \leq x_i^{r} \quad ,$$

the difference in actions between $\underset{\sim}{x}$ and $\underset{\sim}{x}^{\ell}$:

$$F(\underset{\sim}{x})=\sum_{i=-\infty}^{\infty}[L(x_i, x_{i+1})-L(x_i^{\ell}, x_i^{\ell+1})]$$

is convergent and non-negative. Consider a set:

$x_a = \{\underset{\sim}{x} : F(\underset{\sim}{x}) \leq a$, and $\underset{\sim}{x}^{\ell}$ and $\underset{\sim}{x}^{r}$ lie in the same connected component$\}$ and let a_{min}= inf{a: a is a possible value which x_a can have}. This infimum is attained. Then, any $\underset{\sim}{x}$ for which $F(\underset{\sim}{x}) = a_{min}$ is an orbit homoclinic to the orbits of the endpoints of the chosen gap. Mather defined

$$F(\nu)=\max\{a_{min}\}, \qquad (1.3.1.2)$$

taking over all gaps.

This maximum is attained. Then, Mather showed that the Cantor set lies on an invariant circle iff $F(\nu)=0$. In other words, it does not lie on an invariant circle iff there is some gap for which a_{min} is positive. One can include the case where $\varphi(\theta)$ is continuous. In this case, $F(\nu)=0$. So, there is an invariant circle of irrational rotation number ν iff $F(\nu)=0$.

Choose a family and one particular gap(ℓ_0, r_0) of the family. Then a_{min} can be interpreted as the flux through that family of gaps in the Cantor set when only one quasi-periodic orbit exist between $\underset{\sim}{x}^{\ell}$ and $\underset{\sim}{x}^{r}$ (Mackay et al, 1983). Define the stable set $C^{+}(x, p)$ and the unstable set $C^{-}(x,p)$ of points (x',p') s.t. the distance between $T^n(x',p')$and $T^n(x,p)$ goes to zero as $n\to \pm\infty$, respectively. Since the widths of the forward and the backward image gaps, i.e. T^n(a chosen gap), $n\in Z$, go to zero as $n\to \pm\infty$, both endpoints of the chosen gap

have the same C^+ and C^-. Also, the minimax quasi-periodic orbit belongs to both sets, since it is homoclinic to the Cantor set. Then, one can close the forward image gaps with the images of C^+ and the backward image gaps with the image of C^- and form a partial barrier with one turnstile in the chosen gap. Thus, one can blame all the transport on the chosen gap (see figure 1.3.1.1).

Let us describe C^+ and C^- by functions $p^+(x_o)$ and $p^-(x_o)$. Then, the flux through the turnstile is:

$$\int_{\mathbb{1}_o}^{C_o} dx_o \; [\, p^-(x_o) - p^+(x_o)]$$

$$= \int_{\mathbb{1}_o}^{C_o} dx_o \; [\, \frac{\partial L}{\partial x_o}(x_{-1}, x_o) + \frac{\partial L}{\partial x_o}(x_o, x_1)] \quad .$$

If x_{t-1}, x_t and x_{t+1} are three successive points on an orbit, then

$$\frac{\partial L}{\partial x_t}(x_{t-1}, x_t) + \frac{\partial L}{\partial x_t}(x_t, x_{t+1}) = 0 \quad .$$

Then,

$$\int_{\mathbb{1}_o}^{C_o} dx_o \; [p^-(x_o) - p^+(x_o)]$$

$$= \int_{\mathbb{1}}^{C} dA \;, \qquad A = \sum_{t=-\infty}^{\infty} L(x_{t-1}, x_t) \quad .$$

So, the difference in actions between minimizing and mini-maximizing quasi-periodic orbit is just the flux through the gaps of the chosen family in the Cantorus. If there is more than one family of gaps, then the total flux through the Cantorus is given by the sum of each flux through each family.

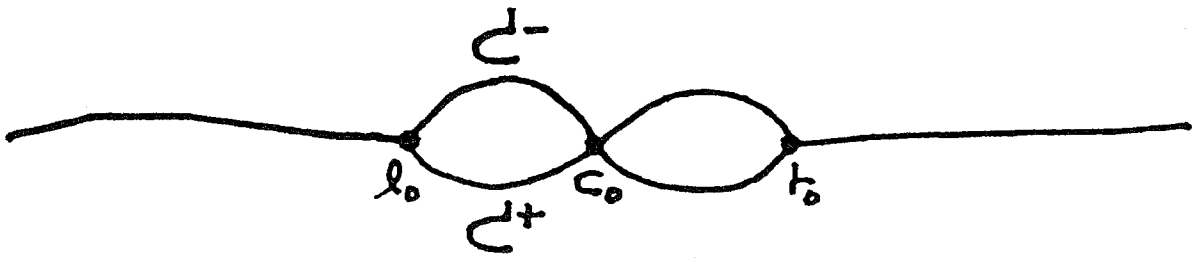

Figure 1.3.1.1 : Formation of a partial barrier with a turnstile. (l_0, r_0) denotes the endpoints of the chosen gap and c_0 a minimax point.

Hence, the quantity(1.3.1.2) defined by Mather corresponds to the maximum flux among the fluxes through the gaps of families when only one minimax quasi-periodic orbit exists between $\underset{\sim}{x}$ and $\underset{\sim}{x}^r$.

Finally, I discuss persistence of sufficiently irrational invariant circles in integrable twist maps under sufficiently small and smooth perturbations.

First, I introduce some terminology. ν is called a diophantine number (Niven, 1963) if

$$\exists\ c>0,\ \tau \quad \text{s.t.} \quad \left| \nu - \frac{p}{q} \right| > c/q^{\tau} \qquad \forall p,q \in Z,\ q>0 \ .$$

A number ν is said to have Liouville exponent τ if

$$\exists\ c>0 \qquad \text{s.t.} \quad \left| \nu - \frac{p}{q} \right| > c/q^{\tau} \qquad \forall p,q \in Z\ ,\ q>0 \ .$$

Let LE_τ be the set of numbers with Liouville exponent τ. Then,

$$LE_\tau < LE_{\tau'} \quad , \text{ for } \quad \tau < \tau' \ .$$

Niven(1963) showed that

$$LE_\tau = \varphi \quad \text{for} \quad \tau < 2 \ .$$

For $\tau > 2$, it is easy to show that the measure of LE_τ goes to one as $c \to 0$. Give c and τ, one deletes the closed intervals of length $2 \cdot c/q^2$ centered at each rational p/q. The union of all points in these deleted intervals is the complement of LE_τ . The total measure of deleted intervals is less than $\sum_{q=1}^{\infty} (2c/q^2) \cdot q$. Then, for $\tau > 2$, the total measure of deleted intervals goes to zero as $c \to 0$. Here we

assume that $0 \leq \nu < 1$ and it is sufficient.

There is a theorem,so called Moser's twist theorem, which gives some answers about questions of persistence of invariant circles :

Theorem (Moser, 1973): All the invariant circles of Liouville exponent τ in any integrable C^r twist map persist under sufficiently small C^r perturbations $(r > 2\tau-1)$.
Here, an integrable twist map is:

$$T : \begin{bmatrix} I \\ \theta \end{bmatrix} \rightarrow \begin{bmatrix} I' = I \\ \theta' = \theta + \nu(I) \end{bmatrix}, \qquad \nu' \neq 0 . \qquad (1.3.1.3)$$

It may be necessary to see the meaning of persistence in more detail. Consider the uniform rotation of rotation number ν on a circle: $T_o : r' = r , t' = t + r , r = \nu , t \in S^1$.
Then, an invariant circle of ratation number ν in the perturbed map T_ϵ: $(I,\theta) \rightarrow (I',\theta')$ has the form:

$$\begin{aligned} I(t) &= r + u(t) \\ \theta(t) &= t + v(t) \end{aligned}, \qquad r = \nu .$$

Moser showed that u(t)and v(t) are at least C^1. Then, the motion on the invariant circle of rotation number ν is at least C^1-conjugate to uniform rotation on a circle:

$\exists$ a C^1 coordinate change $U:(r,t) \rightarrow (I, \theta)$,

$r = \nu$ s.t. $T_o = U^{-1} \cdot T_\epsilon \cdot U$.

An invariant circle is said to be smooth if the motion on it

is differentiably conjugate to uniform rotation on a circle. The number of derivatives of u and v depends on the Liouville exponent τ of a Diophantine rotation number and the smoothness of the perturbed C^r-map. For example, Herman (referred to by Mackay, 1982) gets invariant circles with $\tau = 2$ for C^r, $r>3$, which are C^{r-1}-conjugate to uniform rotation. In the analytic case, Gallavotti(referred to by Mackay, 1982) showed that invariant circles are C^{ω}-conjugate to uniform rotation. On the other hand , in the case of cantori , the functions u and v are discontinuous.

§ 1. 3. 2 Transition to extended chaos

Just after the last rotational invariant circle is broken into a cantorus, no confinement exists, and thus extended chaos occurs. I discuss when extended chaos occurs by various criteria. The first and the second criterion to be discussed are Greene's residue criterion and Chirikov's overlap criterion. They connected the existence of invariant circles with some property of nearby periodic orbits.

Practically, it is necessary to approximate an irrational rotation number ν by an infinite sequence of rational approximants (p_n/q_n), and thus one can approximate the irrational invariant circle by a nearby periodic orbit of rotation number p_n/q_n . As n increases , one can approximate it better.

Any irrational number has a unique infinite continued fraction representation (Niven, 1963):

$$\nu = m_0 + \cfrac{1}{m_1 + \cfrac{1}{m_2 + \cdots}}$$

$$= [\, m_0 , m_1 , m_2 , \cdots] \ ,$$

$$m_0 \in Z \ , \ m_i \in Z^+ , \qquad \text{for} \quad i \in Z^+$$

The rational approximant r_n of ν is:

$$r_n = p_n/q_n = [\, m_0 , m_1 , \cdots , m_n \,] \ ,$$

$$p_n = m_n p_{n-1} + p_{n-2} \ , \ p_{-2} = 0 \ , \ p_{-1} = 1 \ ,$$

$$q_n = m_n q_{n-1} + q_{n-2} \ , \ q_{-2} = 1 \ , \ q_{-1} = 0 \ .$$

These rational approximants are alternatively greater and less than ν and converge to ν :

$$r_0 < r_2 < r_4 < \cdots < r_5 < r_3 < r_1 \ ,$$

$$\lim_{n\to\infty} r_{2n} = \nu = \lim_{n\to\infty} r_{2n+1} \ .$$

This continued fraction expansion is the best approximation in the sense that p_n/q_n is the number which minimize $|q\nu - p|$ over all rationals p/q with the same or smaller denominator. In a weak sense, p_n/q_n is the closest number to ν among all the rationals with the same or smaller denominators.

It is observed that given a periodic orbit, nearby invariant circles and nearby longer periodic orbits are strongly perturbed due to the separatrix splitting of the perturbing periodic orbit. The separatrix splitting will be discussed in the next section. In perturbation theory, this effect appears to be a problem of small denominators, where the denominator is a measure of distance between the perturbing

periodic orbit and a nearby orbit. Let the rotation number of the perturbing periodic orbit be p/q whose continued fraction expansion is $[\, m_0 , m_1 , \cdots, m_n \,]$. Then, $[m_0 , m_1 , \cdots, m_n , m_{n+1}]$ approaches to p/q as $m_{n+1} \to \infty$. Thus, the magnitude of m_i indicates the degree of isolation from the perturbing periodic orbit. In this sense, the most irrational number has $m_i = 1$ for all i : $\nu = [(1, \,)^{\infty}] = (1+\sqrt{5})/2$. This number is called the Golden Mean which has the largest possible value for C (when the Liouville exponent $\tau = 2$) of $1/\sqrt{5}$ (Niven, 1963, see the previous section). So, one expects that the Golden-Mean invariant circle may be the last invariant circle to be destroyed as a parameter is varied.

Greene(1979) studied the Golden-Mean invariant circle in the standard map(1.1.3.14). He connected the existence of a invariant circle with the linear stability of nearby Birkhoff orbits.

Numerically, he observed the three cases:

1) subcritical case: $R_n^{\pm} \to 0$, and it appears as if the Birkhoff island chain of type-(p_n, q_n) converges to a smooth invariant circle of rotation number ν,
2) Critical case : $R_n^{\pm}$ are eventually bounded away from 0 and $\pm\infty$, and it appears as if the Birkhoff island chain of type- (p_n , q_n) converges to a non-smooth invariant circle of rotation number ν ,
3) supercritical case: $R_n^{\pm} \to \pm\infty$, and it appears as if there is no invariant circle of rotation number ν ,

where $R_n^{\pm}$ is the residue defined in (1.2.1.8) of minimaximizing

and minimizing Birkhoff orbits of type-(p_n, q_n) and p_n/q_n is the nth rational approximant of irrational rotation number ν in the continued fraction expansion.

He obtained the critical parameter value:

$$k_c = 0.9716\cdots \quad .$$

Also, at this critical value,

$$R_n^+ = 0.250\cdots \ , \ R_n^- = -\ 0.255\cdots \quad .$$

So, the Golden-Mean invariant circle appears to be on the edge of disappearance when the residues of nearby minimaximizing Birkhoff orbits are roughly 1/4. In other words, when nearby minimaximizing Birkhoff orbits bifurcate out orbits of period six times longer than that of a mother orbit, the Golden-Mean invariant circle appears to be about to be broken. Just after the cirtical value, nearby minimaximizing Birkhoff orbits of higher periods becomes abruptly unstable, and thus the invariant circle appears to be destroyed. Based upon his numerical results, Greene's residue criterion is that one could replace ' and it appears as if ' in the above three cases by 'which implies that'. That is, Greene's residue criterion assumes that invariant circles exist if nearby minimaximizing Birkhoff orbits are stable and they do not exist if nearby minimaximizing Birkhoff orbits are unstable.

Chirikov (1979) connected the existence of invariant circles with the widths of island chains. His resonance overlap criterion is that if two island chains overlap, then it is unlikely that there is any invariant circle between them.

He applied his criterion to the standard map. Following him, I reproduce his results, and then one can compare his result with Greene's result in the standard map.

Let us consider a Hamiltonian;

$$H = I^2/2 + \epsilon \cdot \cos 2\pi\theta \cdot \sum_{l=-\infty}^{\infty} \delta(t-l)$$

$$= I^2/2 + \epsilon \cdot \sum_{l=-\infty}^{\infty} \cos\, 2\pi(\theta - lt) \ , \qquad (1.3.2.1)$$

$$\text{where} \quad \sum_{l=-\infty}^{\infty} \delta(t-l) = 1 + 2 \sum_{l=1}^{\infty} \cos\, 2\pi l t \quad .$$

Here the perturbation represents a 'kick' per unit time. By constructing a surface of section at t=0 (mod 1) in the (I, θ, t)-space, the standard map can be obtained:

$$T : \begin{bmatrix} I_n \\ \theta_n \end{bmatrix} \longrightarrow \begin{bmatrix} I_{n+1} = I_n + \frac{k}{2\pi} \sin 2\pi\theta_n \\ \theta_{n+1} = \theta_n + I_{n+1} \end{bmatrix} \ ,$$

$$k = (2\pi)^2 \epsilon \quad .$$

In the Hamiltonian (1.3.2.1), only integer resonances appear : $\dot{\theta} = l$(integer). So, let us consider the overlap between integer resonances. Under a sufficiently small perturbation, one can obtain the set of first approximation resonances: $I_l = l$. Note that all these integer resonances are identical except a integer-shift in I. So, it is sufficient to consider only one integer resonance, e.g. $l = 0$. The resonant Hamiltonian governing the phase flow near the l-resonance is:

$$H_l = I^2/2 + \epsilon \cos 2\pi(\theta - lt) \quad . \qquad (1.3.2.2)$$

Transformation to new canonical variables(p,ψ) by means of a generating function:

$$F = -(I-I_{\ell})\cdot(\psi+\ell t)$$

yields

$$H_{\ell} = p^2/2 + \epsilon \cos 2\pi\psi \quad ,$$

$$p = -\partial F/\partial\psi \quad , \quad \theta = -\partial F/\partial I \quad .$$

Note that H_{ℓ} reduces to the pendulum Hamiltonian. So the half-width of the ℓ-resonance is the distance from the resonance center to the separatrix. So, the half-width of a integer resonance is :

$$\delta I_{\ell} = 2\sqrt{\epsilon} \quad .$$

On the other hand, the resonance-spacing between nearby integer resonances is:

$$\Delta I_{\ell} = 1 \quad .$$

Define the stochasticity parameter:

$$S = \frac{\text{sum of half-widths of two resonances}}{\text{resonance spacing between two resonances}} \quad .$$

In this case, $S = 4\sqrt{\epsilon}$. When the stochasticity parameter is 1, one can expect that there is no rotational invariant circles due to the resonance overlap. So, the critical parameter value is:

$$\epsilon_c = 1/16 \quad \text{or} \quad k_c = (2\pi)^2\epsilon_c = \pi^2/4 \quad .$$

In the same approximation, the resonant Hamiltonian can be used to calculate the residue of the resonance center. The linearized equation about the resonance center is:

$$\dot{\zeta} = \eta \ , \ \dot{\eta} = (2\pi)^2 \cdot \epsilon \cdot \zeta \ ,$$

$$\zeta = \theta - \hat{\theta} \ , \ \eta = I - \hat{I} \ ,$$

where $(\hat{\theta} \ , \ \hat{I})$ is the resonance center.

The solution for the time displacement operator M(t)satisfying

$$\begin{bmatrix} \zeta(t) \\ \eta(t) \end{bmatrix} = M(t) \begin{bmatrix} \zeta(0) \\ \eta(0) \end{bmatrix}$$

is:

$$M(t) = \begin{bmatrix} \cos \hat{\omega} t & \frac{1}{\hat{\omega}} \sin \hat{\omega} t \\ -\hat{\omega} \sin \hat{\omega} t & \cos \hat{\omega} t \end{bmatrix} ,$$

where $\hat{\omega}^2 = (2\pi)^2 \epsilon = k$.

In the time-1 Poincare map, the residue of the resonance center is :

$$R = (2 - \mathrm{Tr}M(1))/4$$

$$= \sin^2 \hat{\omega}/2$$

$$\approx k/4$$

So, at the critical value obtained by Chrikov , the residue is :

$$R \approx \pi^2/16 \ .$$

This value is larger than that obtained by Greene. The reason can be seen by expressing the stochasticity parameter in terms of the residue of the resonance center:

$$S = \frac{2}{\pi}\sqrt{K} \propto \frac{4}{\pi}\sqrt{R} \quad .$$

At the critical case, the residue of the resonance center obtained by Greene is roughly 1/4. So, $S \propto 2/3$.
In other words, Greene's residue criterion says that when the stochasticity parameter is 2/3, there are no rotational invariant circles between the two resonances. This is called the 'two-thirds' rule. On the other hand, in the Chirikov's criterion, S=1. So, Chirikov's resonance overlap criterion gives the order of magnitude. But one can improve the critical value, taking account of higher order resonances.

Assuming ϵ to be small, we take $H_0 = I^2/2$ as the unperturbed Hamiltonian and introduce a canonical transformation $(I,\theta) \rightarrow (\bar{I}, \bar{\theta})$ such as to 'kill' the perturbation of order ϵ. Let us look for a generating function of the usual form:

$$F(\bar{I},\theta) = \bar{I}\cdot\theta + \epsilon\cdot\Phi\,(\bar{I},\theta,t) \quad , \qquad (1.3.2.3)$$

$$I = \bar{I} + \epsilon\,\Phi \quad , \quad \bar{\theta} = \theta + \epsilon\cdot\Phi_{\bar{I}} \quad ,$$

$$\bar{H} = H + \epsilon\,\Phi_t \quad ,$$

where the subscript denotes the partial derivative with respect to the subscript.
Substituting (1.3.2.3) into (1.3.2.2), we obtain the condition for 'killing' the perturbation of order ϵ :

$$\bar{I}\cdot\Phi + \Phi_t + \sum_{\ell=-\infty}^{\infty} \cos 2\pi(\theta-\ell t) = 0 \quad . \qquad (1.3.2.4)$$

Then, the solution Φ for (1.3.2.4) is:

$$\Phi\,(\theta,\bar{I},t) = \sum_{\ell} \frac{\sin 2\pi(\theta-\ell t)}{2\pi(\ell-\bar{I})} \quad ,$$

and the new Hamiltonian $\bar{H}$ is :

$$\bar{H} = \bar{I}^2/2 + \epsilon^2/2 \sum_{\ell,m} \frac{\cos 2\pi(\theta-\ell t)\cdot\cos 2\pi(\theta-mt)}{(\ell-\bar{I})\cdot(m-\bar{I})}$$

In the new coordinates$(\bar{\theta}, \bar{I})$, $\bar{H}$ is :

$$\bar{H} = \bar{I}^2/2 + \epsilon^2/2 \sum_{\ell,m} \frac{\cos 2\pi(\bar{\theta}-\ell t)\cos 2\pi(\bar{\theta}-mt)}{(\ell-\bar{I})\cdot(m-\bar{I})}$$

$$+\epsilon^3/2 \sum_{\ell,m,n} \frac{\sin 2\pi[2\bar{\theta}-(\ell+m)t]\cdot\sin 2\pi(\bar{\theta}-nt)}{(\ell-\bar{I})(m-\bar{I})\cdot 2\pi(n-\bar{I})^2}$$

$$+ \mathcal{O}(\epsilon^4) \; . \qquad (1.3.2.5)$$

Here, it makes sense to retain the terms of order ϵ^3, since the next canonical transformation to 'kill' the terms of order ϵ^2 also kill the terms of order ϵ^3 and thus the order of the perturbation will be ϵ^4. Note that the perturbation of order ϵ^2 has terms resulting in half-integer resonances: $\bar{I}_r = r + \frac{1}{2}$ for any integer r. Characteristice of a half-integer resonances are determined by the sum:

$$U = \sum_{\ell+m=2r+1} \frac{1}{(\ell-r-\frac{1}{2})(m-r-\frac{1}{2})} = -\pi^2 \; .$$

Note that the sum U is independent of r. So, all half-integer resonances are identical except a integer-shift in I and thus it is sufficient to consider only a half-integer resonance, e.g. r=0. For r=0, the resonant Hamiltonian governing the phase flow near ½-resonance is :

$$\bar{H}_{\frac{1}{2}} = \bar{I}^2/2 - \frac{\pi^2}{4}\epsilon^2 \cos 2\pi(2\bar{\theta}-t) \; .$$

Applying the technique used in the case of integer resonance,

one can obtain the half-width of a half-integer resonance:

$$\delta I_{\ell+\frac{1}{2}} = \pi \cdot \epsilon \quad .$$

Now, one can improve the critical parameter value, taking account of the overlap between a integer resonance and a nearby half-integer resonance. In this case, the stochasticity parameter is:

$$S = 2 \cdot (2\sqrt{\epsilon} + \pi\epsilon) \quad .$$

So, the critical parameter value is:

$$\epsilon_c = 0.03686 \ , \ k_c = 1.46 \quad .$$

Note that the perturbation of order ϵ^3 in (1.3.2.5) has terms resulting in 3rd order resonance. Chirikov also calculated the width of 3rd order resonances, and taking account of the overlap of a half-integer resonance and a nearby 3rd order resonance, he obtained more improved value:

$$\epsilon_c = 0.03423, \ k_c = 1.35 \quad .$$

A necessary and sufficient condition for existence of an invariant circles with irrational rotation number has been proved by Mather(referred to by Mackay, 1982) . I restrict my consideration to the case that given a rational p/q, there exist only one pair of Birkhoff periodic orbits of type-(p,q). For example, the standard map belongs to this case. For an irrational ν, some quantity $F(\nu)$ is defined in (1.3.1.2). For rationals, define $F(p/q)$ to be the difference in actions

between the two minimizing and minimaximizing Birkhoff orbits of type-(p,q):

$$F(p/q) = A_{minimax} - A_{min} \quad .$$

In this case, F(p/q) can be interpreted as the flux(see §1.2.). Mather showed that $F(\nu)$ is continuous in ν at irrationals. Thus, it follows that given a sequence of rationals $p_n/q_n \to \nu$ (irrational), there exists an invariant circle of rotation number ν iff $F(p_n/q_n) \to 0$. Hence, in both the subcritical and the critical cases, $F(p_n/q_n) \to 0$ and in the supercritical case, $F(p_n/q_n)$ converges to some positive value. Mather also showed that $F(\nu)$ depends continuously on perturbations of the map at irrationals. So, just above the critical value, $F(\nu)$ is very small. So, pratically, it is difficult to calculate the critical parameter value by means of Mather's criterion.

Finally, I discuss the Cone-Crossing criterion developed by Mackay and Percival(1985). Let T be a C^1 area-preserving twist map with zero net flux and DT the tangent map of T:

$$(T, DT)\cdot(X,v) = (T(X), DT_X\cdot(v))$$

$$X = (x, p) \ , \ v = (\delta x \ , \ \delta p) \quad .$$

Then, the Lipschitz corollary described in § 1.3.1 gives a criterion for nonexistence of rotational invariant circles in T. A rotational invariant circle separates the cylinder into two invariant components. So, if one finds a tangent orbit of a base orbit $T^n(X)$ for which v sometimes lies above the Lipschitz cone and sometimes below it(see figure 1.3.2.1), then the base orbit does not lie on a rotational circle.

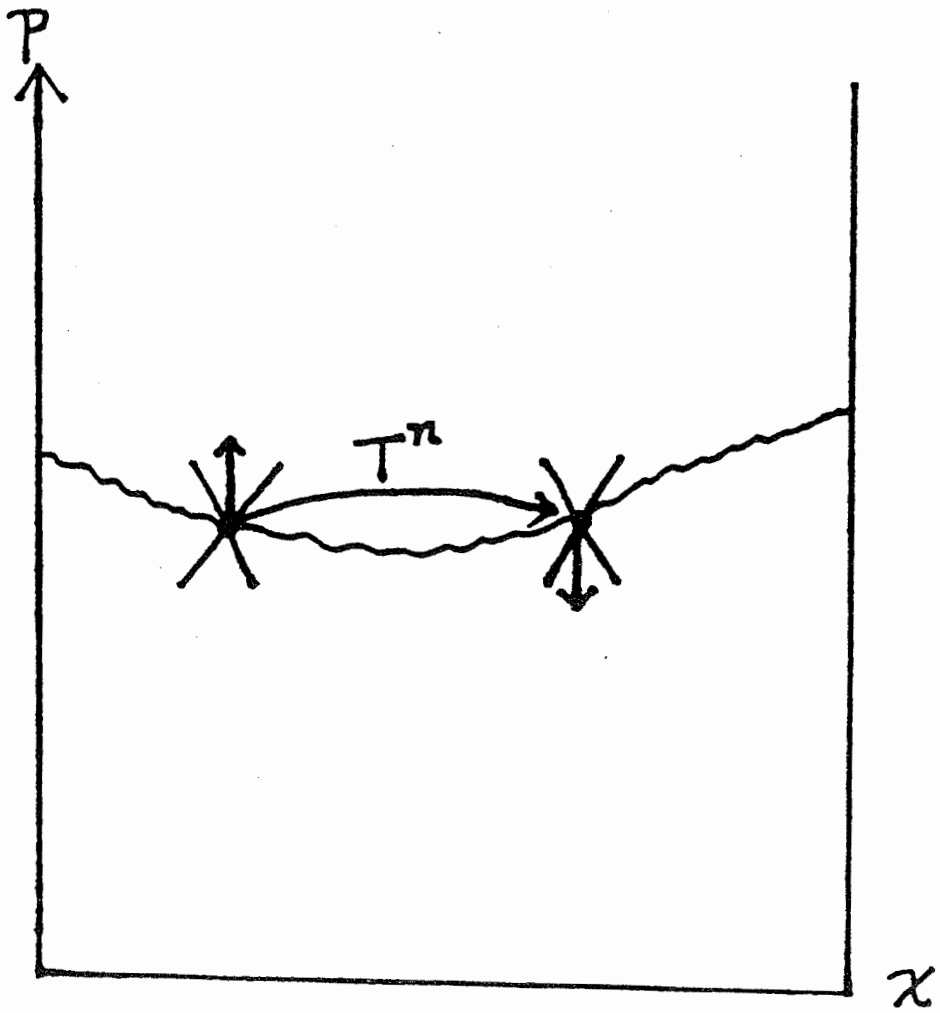

Figure 1.3.2.1 : Impossible situation because a tangent vector above the invariant circle crosses it.

This is called the cone-crossing criterion.

Let $((x_n^1 , p_n^1),\ n \in Z\ )$ and $((x_n^2 , p_n^2),\ n \in Z\ )$ be any two different orbits on a rotational invariant circle. Then, since the orientation is preserved on the invariant circle, one has :

$$x_n^1 < x_n^2 \quad \text{or} \quad x_n^1 > x_n^2 \quad \text{for all } n$$

In other words,

$$0 < \frac{x_1' - x_2'}{x_1 - x_2} < \infty \quad ,$$

where (x_1 , p_1) and (x_2 , p_2) are any two different points on the invariant circle and $(x', p') = T(x,p)$. To use this orientation-preserving condition, it is more convenient to change to (x,z)coordinates:

$$z(x,p) = \pi_1 \cdot T(x,p) \ , \text{ where } \pi_1 : S^1 \times R \to S^1$$

is the projection onto the first coordinate.
Then, in the new coordinates, the orientation preserving condition is:

$$0 < \frac{z_1 - z_2}{x_1 - x_2} < \infty \ , \ x_1 \neq x_2 \ ,$$

for points (x_1 , z_1) and (x_2 , z_2) on a rotational invariant circle. Note that this confines the slopes of rotational circles to a right angle and also this is independent of the map. So, in the (x, z) - coordinates, the orientation-preserving condition becomes the cone-condition : the upper cone constant is ∞ and the lower one zero. Since the cone-condition is obtained, the cone-crossing Criterion can be

stated explictly as follows. If (δx_t) are the δx-components of a tangent orbit to an base orbit (X_t),

with $\delta x_0 \leq 0$,

$\delta x_1 > 0$,

$\delta x_n \leq 0$ for some $n > 1$,

then the base orbit (X_t) does not lie on a rotational invariant circle.

For example, let us apply this criterion to a map T:

$$T : \begin{bmatrix} p' = p + f(x) \\ x' = x + p' \end{bmatrix} \text{ in } (x,p) \text{ coordinates ,}$$

$$T : \begin{bmatrix} z' = g(z) - x \\ x' = z \end{bmatrix} \text{ in } (x,z) \text{coordinates .} \qquad (1.3.2.4)$$

When $f(x) = -\frac{k}{2\pi} \sin 2\pi x$, then the map is the standard map. The δx-components of a tangent orbit to a base orbit ((x_t, z_t), $t \in Z$) satisfies :

$$\delta x_{t+1} = g'(x_t)\, \delta x_t - \delta x_{t-1} \quad .$$

So, choosing $\delta x_0 = 0$, $\delta x_1 > 0$, one gets

$$\delta x_2 = g'(x_1) \cdot \delta x_1 \quad .$$

So, if $g'(x_1) \leq 0$, then $\delta x_2 \leq 0$,

and thus there are no rotational circles crossing the vertical line $x = x_1$. Recall that every rotational invriant circle must cross each vertical line. Therefore, there are no invariant circles if

$$m = \min_{x} g'(x) \leq 0 \quad .$$

In the standard map ,

$$m = 2 - |k| \quad ,$$

and thus there are no invariant circles ,

$$\text{if} \quad |k| \geq 2 \quad .$$

One can obtain more improved results, applying the criterion with n>2. But one can save having to take n too large by improving the cone condition. Note that the direction of a tangent vector v at X gives a slope and the derivative DT on the tangent vector induces an operator on slopes D at X → D' at X' :

$$X = (x,z),\ v = (\delta z\ ,\ \delta x),\ D = \delta z/\delta x\ ,$$

$$(T,\ DT)(X,\ v) = (X',\ v'),\ X' = (x',z'),$$

$$v' = (\delta z',\ \delta x')\ ,\ D' = \delta z'/\ \delta x' \ .$$

So, in the map (1.3.2.4),

$$D' = g'(z) - 1/D \quad .$$

Let some Lipschitz cone constants be D°_{+} and D°_{-} :

$$D^{\circ}_{-} \leq \frac{z_1 - z_2}{x_1 - x_2} \leq D^{\circ}_{+} \quad , \ x_1 \neq x_2 \quad .$$

Then D°_{+} can be obtained as follows .

If $\frac{z_1 - z_2}{x_1 - x_2} \leq D_{+}$, then

$$\frac{z_1' - z_2'}{x_1' - x_2'} \leq D_+' \text{ , where}$$

$$D_+' = \max_z \left(g'(z) - 1/D_+\right) = M - 1/D_+ \text{ ,}$$

$$M = \max_z g'(z) \text{ .}$$

Note that $D_+' < D_+$. So, if one iterates this infinite times, then D_+ goes to the limit value:

$$D_+ = M - 1/D_+ \text{ .}$$

Then, the upper cone constant D_+° is the largest root of the above equation:

$$D_+^\circ = M/2 + \sqrt{M^2/4 - 1} \text{ .}$$

Similarly, the lower cone constant D_-° is the smallest root of a equation:

$$D_- = \min_z \left(g'(z) - 1/D_-\right) \text{ .}$$

So, $D_-^\circ = M/2 - \sqrt{M^2/4 - 1}$.

Now, let us apply the cone-crossing criterion with the improved cone-condition. Choosing $\delta x = 1$, $\delta z = D_+^\circ$, one gets:

$$D' = g'(z) - 1/D_+^\circ \text{ .}$$

If $\min_z D'$ is less than D_-° , then there are no rotational invariant circles crossing the vertical line $x=z_0$, at which D' is minimum. That is, if $m < M - \sqrt{M^2 - 4}$, then there are no rotational invariant circles crossing the line $x = z_0$ and thus none

at all. So, there are no rotational invariant circles if $|k| > 4/3$.

One can obtain more improved results, applying the cone-crossing criterion with higher n. Mackay and Percival(1985) showed, applying the criterion with higher n, that the standard map has no rotational invariant circles if $|k| \geq 63/64$. This value is very close to the critical value obtained by Greene.

§ 1. 4. Stochastic layers

A integrable twist map (1.3.1.3), e.g. the standard map (1.1.3.14) for k=0, has rational invariant circles, the orbits on them are periodic and the residues of the periodic orbits are zero. But generically, the residues of all periodic orbits in an area-preserving twist map with zero net flux are nonzero and thus they are isolated from points of the same period. For example, for nonzero k in the standard map, it is observed that there exist no rational invariant circles.

For sufficiently small k in the standard map, there exist a pair of stable and unstable periodic orbits of all possible rational rotation number by Poincare - Birkhoff theorem (see § 1.2). At any unstable periodic point H, four invariant curves meet(see figure 1.4.1). Two of these are contracting curves H_+, and the other two are dilating curres H_-. The orbits on the contracting curve converge to the unstable point H under the forward iterations of the map, while the orbits on the dilating curve converge to H under the backward iterations of the map.

The only way to get a rational invariant circle with no periodic points of residue zero is by joining a dilating curve of an unstable periodic point to a contracting curve of a nearby unstable periodic point smoothly, i.e. saddle connection, and then there exists a separatrix(see figure 1.4.2). But generically, there are no saddle connections (Robinson, 1970). They can be broken by arbitrarily small perturbations

giving transeverse intersection of the dilating curve and the contracting curve (see figure 1.4.3). This phenomenon is called the separatrix splitting(Arnold,1978). The intersection points are called homoclinic points, since the orbits of homoclinic points converge to the unstable periodic orbit under both the forward and the backward iterations of the map. So,homoclinic orbits have the same rotation number as that of the unstable orbit. But they are not periodic.Like the case of a periodic and a quasi-periodic orbit, there are two types of homoclinic orbits. One is a minimizing homoclinic orbit and the other a minimaximizing orbit(Mackay et al 1984). The limit of minimizing orbits of rotation number ν, as $\nu \to m/n$ monotonically from above or below, gives a minimizing homoclinic orbit of rotation number m/n. In the same way that there is a minimax point between the two endpoints of a gap in a minimizing Cantor set(see §1. 3. 1), there is a minimax homoclinic point between any two minimizing homoclinic point. Like the case of a cantorus(see § 1.3.1),the difference in the actions between a minimizing homoclinic orbit and a minimaximizing homoclinic orbit can be interpreted as the flux through a broken separatrix (see figure 1.4.4) .

If a separtrix exist like the case of a pendulum ,then the separatrix separates the rotation region from the vibration region completely. But, due to a separatrix splitting, generically there exists a flux through the broken separatrix. In other words, points near the broken separatrix wander from the rotation region to the vibration region and vice versa.

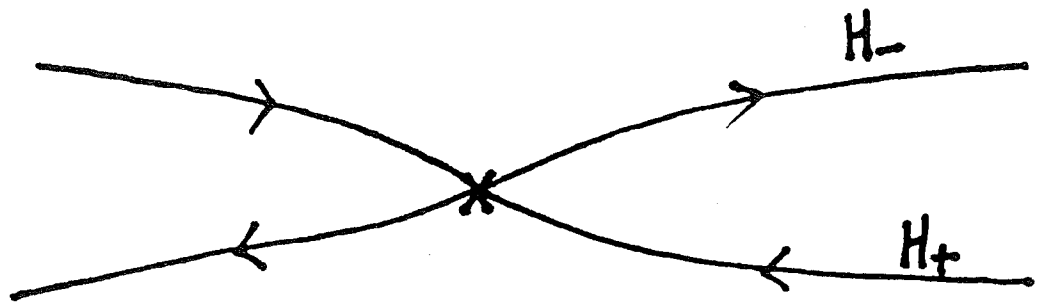

Figure 1.4.1 : Four invariant curves

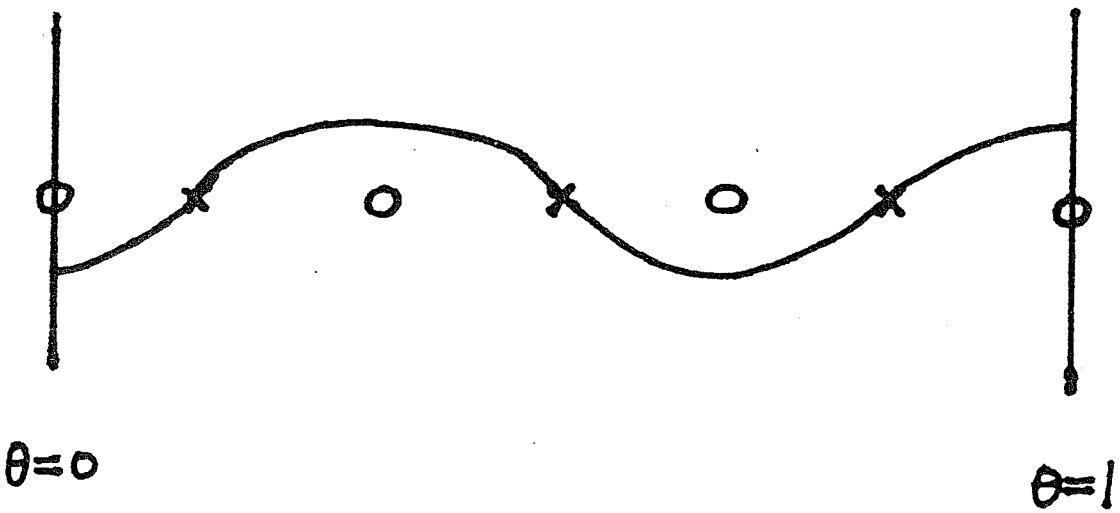

Figure 1.4.2 : A saddle connection

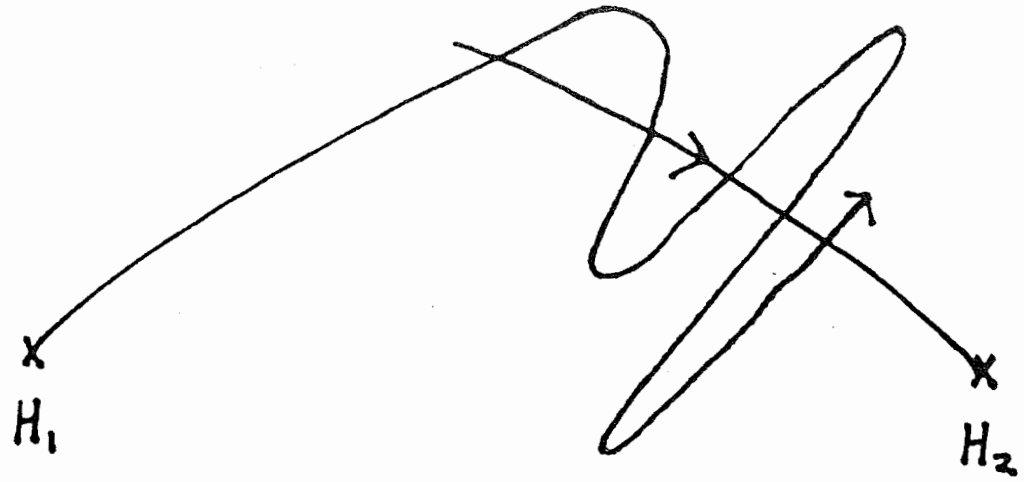

Figure 1.4.3 : A transversal intersection of a dilating curve and a contracting curve. H_1 and H_2 are two nearby hyperbolic points.

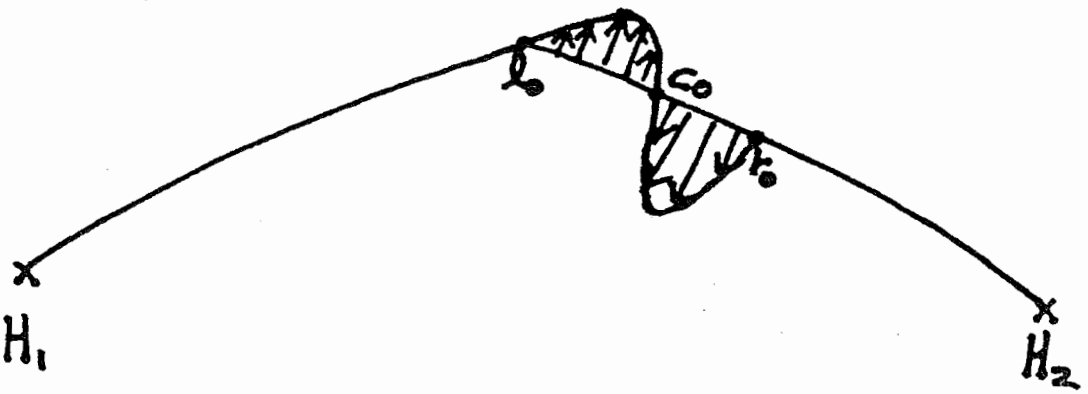

Figure 1.4.4 : Flux through a broken separatrix. (l_0, t_0) denotes minimizing points and c_0 a minimax point.

Thus , a stochastic layer is formed near the broken separatrix (Chirikov, 1979).

Following Chirikov(1979), let us estimate the size of a stochastic layer around the broken separatrix. He considered a pendulum as a model of nonlinear resonance, under a periodic parametric perturbation described by a Hamiltonian:

$$H(p,\varphi,\tau) = H_0(p,\varphi) + \epsilon\cdot V(\varphi,\tau), \qquad (1.4.1)$$

$$H_0 = p^2/2 - \omega_0^2\cos\varphi\ , \quad V = \omega_0^2\ \cos\varphi\cdot\cos\tau\ ,$$

$\tau = \Omega\cdot t + \tau_0$, where Ω and τ_0 are the perturbation frequency and the initial phase, respectively. By constructing a surface of section at $\varphi = 0$, he obtained the separatrix map describing the motion of system(1.4.1) near the separatrix when Ω/ω_0 is very large. The separatrix map is :

$$\begin{aligned} w' &= w - \zeta \sin\tau_0\ , \\ \tau_0' &= \tau_0 + \lambda\ \mathit{ln}\ (32/|w'|)\ , \\ \zeta &= 4\pi\epsilon\lambda^2\ e^{-\pi\lambda/2}\ ,\ \lambda = \Omega/\omega_0\ . \end{aligned} \qquad (1.4.2)$$

Here, w is the quantity to indicate the degree of relative deviation of H_0 from the unperturbed separatrix energy ω_0^2 :

$$w = (H_0 - \omega_0^2\ )/\omega_0^2\ .$$

The fixed points of the separatrix map(1.4.2) $(\hat{w}\ ,\hat{\theta})$ are:

$$|\hat{w}| = 32\cdot\exp(-2\pi n/\lambda)\ , \qquad \hat{\theta} = 0 \text{ or } \pi\ .$$

The residues defined in (1.2.1.8) of these fixed points are:

$$R = \zeta\cdot\lambda\cdot\cos\hat{\theta}\ /(4\cdot\hat{w})\ .$$

Thus , a stochastic layer is formed near the broken separatrix (Chirikov, 1979).

Following Chirikov(1979), let us estimate the size of a stochastic layer around the broken separatrix. He considered a pendulum as a model of nonlinear resonance, under a periodic parametric perturbation described by a Hamiltonian:

$$H(p,\varphi,\tau) = H_0(p,\varphi) + \epsilon \cdot V(\varphi,\tau), \qquad (1.4.1)$$

$$H_0 = p^2/2 - \omega_0^2 \cos\varphi \ , \quad V = \omega_0^2 \cos\varphi \cdot \cos\tau \ ,$$

$\tau = \Omega \cdot t + \tau_0$, where Ω and τ_0 are the perturbation frequency and the initial phase, respectively. By constructing a surface of section at $\varphi = 0$, he obtained the separatrix map describing the motion of system(1.4.1) near the separatrix when Ω / ω_0 is very large. The separatrix map is :

$$\begin{aligned} w' &= w - \zeta \sin\tau_0 \ , \\ \tau_0' &= \tau_0 + \lambda \ln (32/|w'|) \ , \\ \zeta &= 4\pi\epsilon\lambda^2 \ e^{-\pi\lambda/2} \ , \ \lambda = \Omega / \omega_0 \ . \end{aligned} \qquad (1.4.2)$$

Here, w is the quantity to indicate the degree of relative deviation of H_0 from the unperturbed separatrix energy ω_0^2 :

$$w = (H_0 - \omega_0^2)/\omega_0^2 \ .$$

The fixed points of the separatrix map(1.4.2) $(\hat{w}, \hat{\theta})$ are:

$$|\hat{w}| = 32 \cdot \exp(-2\pi n/\lambda) \ , \quad \hat{\theta} = 0 \text{ or } \pi \ .$$

The residues defined in (1.2.1.8) of these fixed points are:

$$R = \zeta \cdot \lambda \cdot \cos\hat{\theta} \ / (4 \cdot \hat{w}) \ .$$

Note that the residue is dependent on the fixed point $(\hat{w},\hat{\theta})$. Also, recall that in the standard map, all the fixed points have the same residues. All the fixed points in the region where $|w| < \zeta\cdot\lambda/4$ are unstable, while all the fixed points on the line $\theta = 0$ are unstable, those on the line $\theta=\pi$ stable when $\hat{w} > \zeta\cdot\lambda/4$, and vice versa when $\hat{w} < -\zeta\cdot\lambda/4$ (see figure 1.4.5) So, since in the region where $|w| <\zeta\cdot\lambda/4$ all the fixed points are unstable, one can expect that there are no invariant circles in the region by Greene's residue criterion (see §1.3.2). Therefore, one can expect that in the region, the motion may be stochastic.

For $\lambda << 1$, the change of w is small, and thus one can linearize the separatrix map in w about a fixed point$(\hat{w}, \hat{\theta})$ to get a new map:

$$
\begin{aligned}
I' &= I + K \sin\theta \ , \\
\theta' &= \theta + I', \qquad\qquad (1.4.3) \\
K &= \frac{\lambda}{\hat{w}}\,\zeta \ , \qquad I = -\frac{\lambda}{\hat{w}}\,(w - \hat{w}) \ , \qquad \theta = \tau_0 \ .
\end{aligned}
$$

Note that the above map is just the standard map and the parameter is dependent on the fixed points. Recall that in the standard map, extended chaos occurs when $|K| > 1$ (see § 1.3.2). So, in the region where $|w| < \lambda\cdot\zeta$, there are no invariant circles and near the fixed points for which $|\hat{w}|\simeq\lambda\cdot\zeta$, there exist the boundary invariant circles (see figure 1.4.5). Therefore, the half-width of the stochastic layer is :

$$
\begin{aligned}
w_s &= \lambda\cdot\zeta \\
&= 4\pi\cdot\epsilon\cdot\lambda^3 e^{-\pi\lambda/2}
\end{aligned}
$$

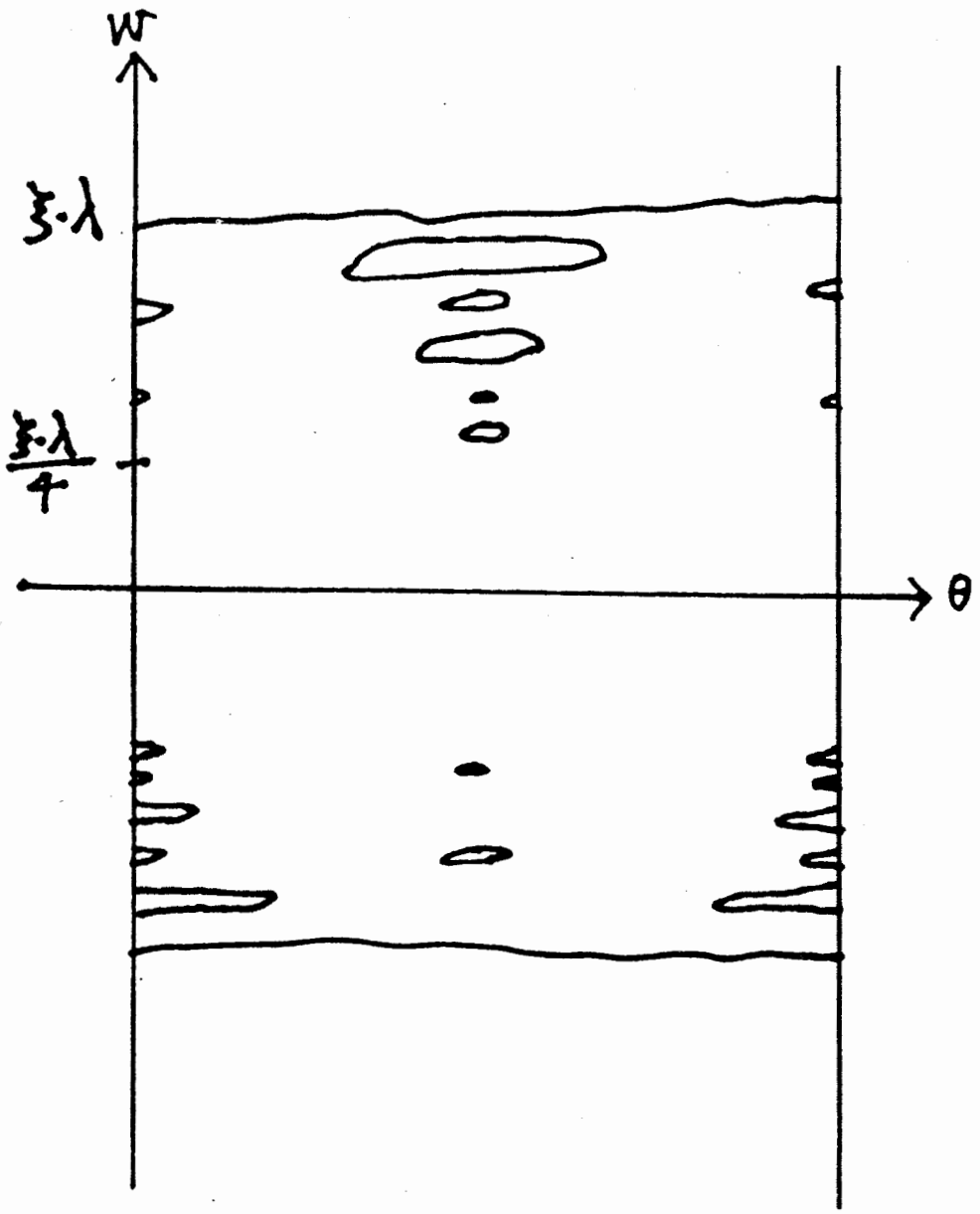

Figure 1.4.5 : The structure of a stochastic layer near a broken separatrix

It is worth noting that for arbitrarily small ϵ , w_s is non-zero.

Roughly speaking, the stochastic layer consists of the two parts. One part is the central one ($|w| < \zeta\cdot\lambda/4$) in which there are no islands and the other part($\zeta\cdot\lambda/4 < |w| < w_s$) is the peripheral one in which islands are imbedded, but there exist no rotational invariant circles. In this way, the structure of the stochastic layer is intricate: it has the divided space in which regular and stochastic components coxeist.

The diffusion is a distinctive random process. So if one considers the motion in the stochastic layer as being similar to a random one, a diffusion in w must occur.

Let us see the statistical properties of the motion in the standard map (1.4.3) when $|K| > 1$. Then, one can see the statistical properties of the motion near a fixed point of the separatrix map (1.4.2) since the standard map describes the behavior of motion near a fixed point of the separatrix map.

The force correlation in the standard map is defined by

$$C_R(\tau) = < a_t \cdot a_{t+\tau} >_R \quad , \qquad (1.4.4)$$

where $a_t = I_{t+1} - I_t = K\cdot\sin\theta_t$ and the averaging is performed over an ergodic component of the motion R. Also,the diffusion coefficient is defined by :

$$D_R = \lim_{t\to\infty} D_R(t) \quad , \qquad (1.4.5)$$

$$D_R(t) = 1/2t <(I_t - I_0)^2>_R \ .$$

Then, the diffusion coefficient can be expressed in terms

of the force correlation:

$$D_R = \frac{1}{2} C_R(0) + \sum_{j=1}^{\infty} C_R(j) \quad . \qquad (1.4.6)$$

For large K, the correlation decays fairly fast and so it is sufficient to consider only short-term correlations. Then the diffusion coefficient is:

$$D_R = K^2/4 \cdot [1 - 2 J_2(K) + 2J_3^2(K) - 2J_1^2(K) + 2J_2^2(K) + \sigma(K^{-\infty})] \qquad (1.4.7)$$

where $J_n(x)$ is the Bessel function,

$$J_n(x) \simeq \sqrt{\frac{2}{\pi x}} \cdot \cos [x - (n + 1/2) \cdot \pi/2] \text{ for large } x,$$

$$C_R(0) = K^2/4, \; C_R(1) = 0 \; , \; C_R(2) = -\frac{K^2}{2} J_2 \; ,$$

$$C_R(3) = \frac{K^2}{2} (J_3^2 - J_1^2), \; C_R(4) = \frac{K^2}{2} (J_2^2 + \sigma(K^{-\infty})) \quad .$$

This result was first obtained by Rechester and White(1980) and later by Cary et al(1981) in a different way. Since the diffusion coefficient exists, one can see that there is an intrinsic stochasticity in the standard map for large K. But the stochastic motion is not purely random due to the short-term correlations. The result(1.4.7) agrees well to the result of a numerical simulation for K> 4 (Chirikov, 1979). But, in the parameter interval where an accelerator mode exist, one cannot neglect the effect of the accelerating island (Karney, 1983). In this case, the diffusion coefficient becomes very large. For 1< K < 4, by a numerical simulation, Chirikov(1979) obtained :

$$D(K) \sim (K - 1)^{2.55} \quad . \qquad (1.4.8)$$

Also, Dana and Fishman(1985) obtained :

$$D(K) \sim (K - 1)^3 \quad , \qquad (1.4.9)$$

for $1 < K < 2.5$, by a numerical simulation.

Now, let us see the statistical behavior of the motion in the separatrix map. The diffusion in w becomes inhomogeneous since D(K) in the standard map turns into $D(\lambda \cdot \zeta/\hat{w})$ by (1.4.3). Roughly speaking, there are two distinctive regions in the stochastic layer:

1) near the layer center, a fast diffusion takes place and the correlation may be neglected.
2) near the layer border, a slow diffusion takes place,

$$D(w) \sim (w_s / |w| - 1)^{2.55} \quad . \qquad (1.4.10)$$

Finally, I would like to mention long-time correlations of stochastic orbits in the stochastic layer. Chirikov and Shepelyansky(1984) followed a single trajectory while it crosses successively the line w = 0 in the separatrix map. Note that for $w > 0$, the trajectory is in the rotation region and for $w < 0$, it is in the vibration region. The motion time interval between two successive crossings was recorded. This time is called a trapping time or a recurrence time. Define $P(\tau)$ as the survival probability for a recurrence to occur later than τ. The asymptotic behavior of $P(\tau)$ as $\tau \to \infty$ is related to the structure of the layer border. For various λ, they obtained :

$$P(\tau) \sim \tau^{-\gamma} \quad . \qquad (1.4.11)$$

Note that as λ varies, the boundary is also changed. So, the survival probability distribution decays asymptotically as a power law , which is roughly independent of boundary circles , and thus the motion in the stochastic layer exhibits long-time correlations.

CHAPTER 2. Critical behavior in area-preserving maps

§ 2.1 Introduction

The phase space of a generic area-preserving map is devided into regular components and stochastic components : periodic, quasi-periodic, and stochastic orbits coexist and interact .

Let us see the roles of the above three kinds of orbits in the DeVogelaere map (1.1.3.5). Figure 2.1.1 is the phase flow near the main fixed point of the DeVogelaere map when the parameter p is 0.24. Near the main fixed point, vibrational invariant circles and a daughter island of rotation number 1/5 are visible. In fact, since the residue defined in (1.2.1.8) of the main fixed point is 0.38, m/n-bifurcations where $m/n<0.2114\cdots$ have already occurred (see § 1.2.4). So, in fact, many islands exist. But only one has the appropriate scale to be visible in the figure. Also many unstable orbits exist. Near these unstable periodic orbits, stochastic layers are formed due to the separatrix-splitting (see § 1.4) .

Figure 2.1.2 and figure 2.1.3 are the enlarged figure of the phase flow near an unstable periodic point of rotation number 1/5. Notice that the dark part of the picture is a single orbit. The orbit are very sensitive to initial conditions and appears to be area-filling . So, it is called an apparently area-filling stochastic orbit.

Looking at the picture in detail, there exist the boundary circles of the stochastic layer and near the boundary

circles, islands exist in the stochastic layer. The rotation number of a boundary circle on the left of the figure is [0,5,12,1,1,1,1,1,···] in the continued fraction representation. Two large islands near the boundary circle are visible. The rotation number of the left one outside the stochastic layer is 12/61 and that of the right one inside the stochastic layer is 13/66. Also, in the stochastic layer , two smaller islands are visible and their rotation number are 14/71 and 15/76, respectively.

If one follow the periodic orbits of rotation number [0,5,m], then one can approach the broken separatrix as $m \longrightarrow \infty$. Thus, one can obtain the residues of the periodic orbits and expect the phase flow near the periodic orbits.

The residues of the periodic orbit of rotation number 12/61 and 13/66 are roughly 0.20 and 0.28, respectively. Note that 12/61 and 13/66 are [0,5,12] and [0,5,13], respectively. As m increases further, the residues of the periodic orbits increase. So, the size of that island gets smaller as m increases, and all periodic orbits are unstable when m>16. So, in the central part of the stochastic layer , many unstable periodic orbits are embedded , and thus stochastic orbits are scattered by them . Therefore, a stochastic orbit has a short-term correlation in this region .

By Greene's residue criterion (see § 1.3.2), all the invariant circles whose rotation numbers are between 13/66 and 1/5 are broken, and thus a stochastic orbit wanders about inside this stochastic layer bounded by boundary invariant circles . But the stochastic orbit can not penetrate the bound-

ary circles . Therefore, invariant circles play the role of a complete barrier to transport of stochastic orbits .

The dark part of figure 2.1.2 and figure 2.1.3 are formed from an orbit of a point (-0.375,0). The times of the map iteration are $2X10^5$ and $1.5X10^6$, respectively. In the figure 2.1.2 , the orbit has approached a region near the island of rotation number 15/76, and it has been trapped for a long time near islands of rotation number 14/71 and 13/65 , as shown in the figure 2.1.3 . So, the region near islands of rotation number 14/71 and 13/65 has become darker in the figure. In fact, Channon and Lebowitz (1980) showed, quantitatively, that the stochastic orbits have a long-time correlation in this stochastic layer. Shepelyansky and Chirikov (1984) also showed the long-time correlations of stochastic orbits inside the stochastic layer in the separatrix map (see § 1.4).

Also, notice that the main fixed point has the outmost boundary circle in the figure 2.1.1. The rotation number ν_b of the boundary circle is [0,5,4,2,1,3,1,···] in the continued fraction representation. So, all the invariant circles whose rotation numbers are less than ν_b are broken. Hence, if one iterates the map with an appropriate initial point outside the boundary circle, then the orbit of the point wanders about outside that boundary circle. Sometime, the orbit approaches the region near the boundary circle , where the stochastic orbit spends much time. This is because small islands exist in the region as shown in the figure 2.1.1. That is, the

orbit has a long-time correlation in the region. In fact, Karney(1983) showed ,quantitatively, a long-time correlation of stochastic orbits near the outmost boundary circle when the parameter p in (1.1.3.5) is 0.3675....

We have not yet arrived at the full structure of the phase flow. In fact, the daughter islands have their own vibrational invariant circles and island chains around them , and so on. So, each island is a microcosm of the whole. In other words, each island has the infinitely nested structure (Arnold and Avez,1968).

In the way stated above, periodic, quasi-periodic and stochastic orbits coexist and play their own roles in the phase space : unstable periodic orbits play the role of 'scatterer' of stochastic orbits like the pins in a pin ball game, islands play the role of 'trap' of stochastic orbits , and invariant circles play the role of 'dam'.

In this thesis , we study the critical phenomena related to periodic and quasi-periodic orbits .

In § 2.2 , we describe generic bifurcations in reversible area-preserving maps in furthur details than in § 1.2.4. Particularly, we describe the relations between symmetric periodic orbits and symmetry half-lines in details . This relation play a very important role in understanding the critical phenomena. The role is described in § 2.3 and § 2.5 .

The first phenomenon we studied is the infinitely nested structure of islands which play the role of 'trap'. In § 2.3 , We show that at a certain parameter value, the

so-called accumulation point, island chains of all classes of a particular bifurcation exist and they have a self-similar nested structure asymptotically. We found that their limiting self-similar behaviors appear to be universal and calculated scaling factors for 1/n-bifurcation sequence, with n=3 to 6. We have also observed that the pattern of periodic orbits repeats itself asymptotically from one bifurcation to the next for even n and to every other for odd n. In fact, even more asymptotically self-similar behavior exists near the accumulation point. When we rescale not only dynamical variables but also the parameter with appropriate rescaling factors, the pattern of periodic orbits also exhibits the limiting self-similar hehavior.

Recently, Meiss(1986) also studied the infinitely nested island-structure for higher multifurcations than those studied by us. However, he did not obtain scaling factors of dynamic variables separately. Instead, he obtained the area-scaling factor directly by calculating Mather's action difference between the minimaximizing and the minimizing periodic orbit of each class. Of course, it is sufficient to obtain only the area-scaling factor if one is concerned about the transport of stochastic orbits near islands, since here the transport is the transport of the phase area. Actually, Meiss and Ott(1985) constructed a self-similar Markov tree model which describes the motion of stochastic orbits near islands,in which the transition probabilities are directly related to the self-similar scaling behavior of the infinitely nested structure of

islands and critical invariant circles. Thus, they obtained an algebraically decaying recurrence-time distribution of stochastic orbits near islands. In this way, the long-time behavior of a stochastic orbit near islands can be described only if one knows the self- similar scaling behavior of the infinitely nested structure of islands and critical invariant circles.

In § 2.4, we also study these asymptotically self-similar island structures by a simple approximate renormalization method.

The self-similarity of island structures is an asymptotic long-time behavior of a map T. Therefore , the short timescale behavior can be removed by considering a higher iterate T^n of the map. As a next step, an appropriate coordinate change to smaller spatial scales makes it look almost the same as T. The operation of iterating n times and rescaling is a renormalization. Under the renormalization, T converges to a fixed point of the renormalization. This fixed point is called the universal map of 1/n-bifurcation. Thus, T has asymptotically self-similar behavior on longer timescales and smaller spacescales. Since it is the same for all maps converging to the universal map, the behavior is said to be universal.

The approximate renormalization method used in this thesis may be called the method of quadratic approximants. Since the self-similarity is an asymptotically smaller spacescale behavior,it may be sufficient to retain upto quadratic terms in the Taylor expansion of the iterated maps.

So, the quadratic approximant is formed by keeping the terms to the second order in the Taylor expansion of T^n. Comparision of successive approximants gives the accumulation point p^*, the bifurcation ratio δ, the rescaling factors α and β, and the universal residue value. By looking at the recurrence relation between $T^{n^{\ell}}$ and $T^{n^{\ell+1}}$ with large ℓ, one can make better approximations. Furthermore, we also obtain the approximate universal map T^* and thus show approximately that the limiting self-similar behavior is universal.

The second phenomenon we studied is the break-up of invariant circles which play the role of 'dam' under a rough perturbation

Consider a boundary circle whose rotation number ν_b is [0,5,12,1,1,1,1,1,...] in the figure 2.1.2 . Then, if one follows periodic orbits of rotation number r_n which is the nth rational approximant of ν_b, then one can approach the boundary circle and study the behaviors of phase flow near it. For example, islands of rotation number 12/61 and 13/66 in the figure 2.1.2 are those of rotation numbers corresponding to rational approximants r_2 and r_3, respectively. The residues of periodic orbits of rotation number corresponding to the rational approximants of ν_b are roughly 1/4, asymptotically. This implies the self-similarity of the infinitely nested structure near the boundary circle locally since one can see the property of linearized flow in terms of residues. In fact, Shenker and Kadanoff(1982) and Mackay(1982) showed that the boundary circle has an infinitely nested self-similar structure in an analytic

map. When the map parameter is increased slightly, periodic orbits of rotation number corresponding to higher rational approximants become unstable and residues of periodic orbits of rotation number corresponding to lower rational approximants lie roughly between 1/4 and 1. In such a situation, the most important thing to happen is that the boundary circle which has separated islands is broken, and thus the width of the stochastic layer has widened. Therefore , it is important to study the critical invariant circles.

In the final section(§ 2.5), we study the persistence of a noble invariant circle in an integrable map under a C^2-perturbation.

First of all,it is worth while to notice that the persistence of an invariant circle depends on the quality and strength of perturbation and the robustness of the invariant circle . For example, intuitively, rough systems are likely to be chaotic (Wightman, 1981). There is a mathematical theorem called Moser's twist theorem(1973) which gives some answers about the question of persistence of invariant circles under perturbation. The theorem says that a sufficiently robust invariant circle persists under sufficiently small and smooth perturbation. Here, the sufficient smoothness is now $C^r (r>3)$. Then, the natural question is whether or not invariant circles persist under C^r($r \leq 3$)-perturbation. So, in this thesis, we study a C^2-map .

Following Greene's residue criterion and Mather's criterion, we show numerically that a noble invariant circle

persists below a critical parameter value in a map of class C^2. Therefore, the invariant circle plays the role of complete barrier to transport of stochastic orbits below the critical parameter value. Furthermore, we also observed that the critical behavior of that invariant circle seems to be the same as that in analytic maps within numerical accuracy. So, they seems to be in the same universal class .

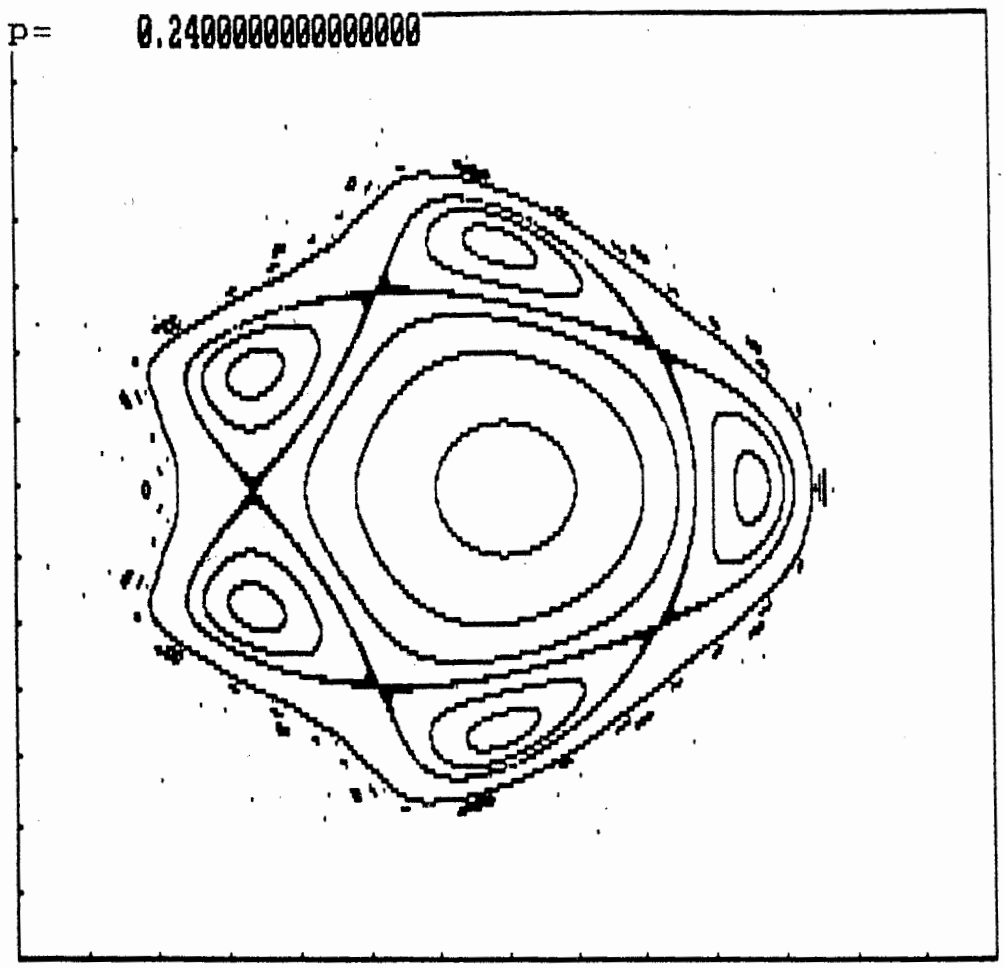
p= 0.2400000000000000
DEV. MAP
WINDOW
X1= -0.7000
Y1= -0.7000
X2= 0.7000
Y2= 0.7000
TICX= 0.1000
TICY= 0.1000

Figure 2.1.1

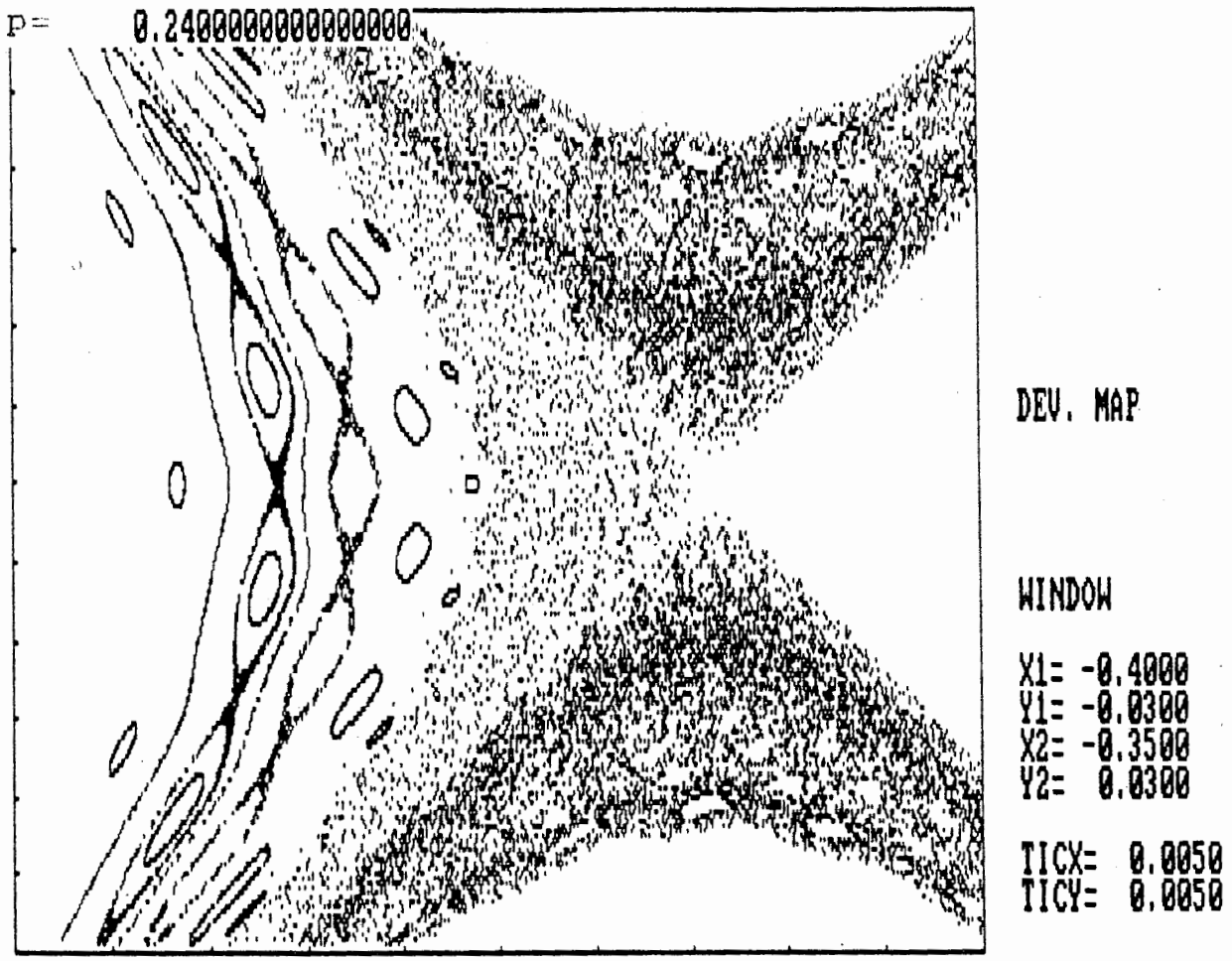
p= 0.2400000000000000
DEV. MAP
WINDOW
X1= -0.4000
Y1= -0.0300
X2= -0.3500
Y2= 0.0300
TICX= 0.0050
TICY= 0.0050

Figure 2.1.2

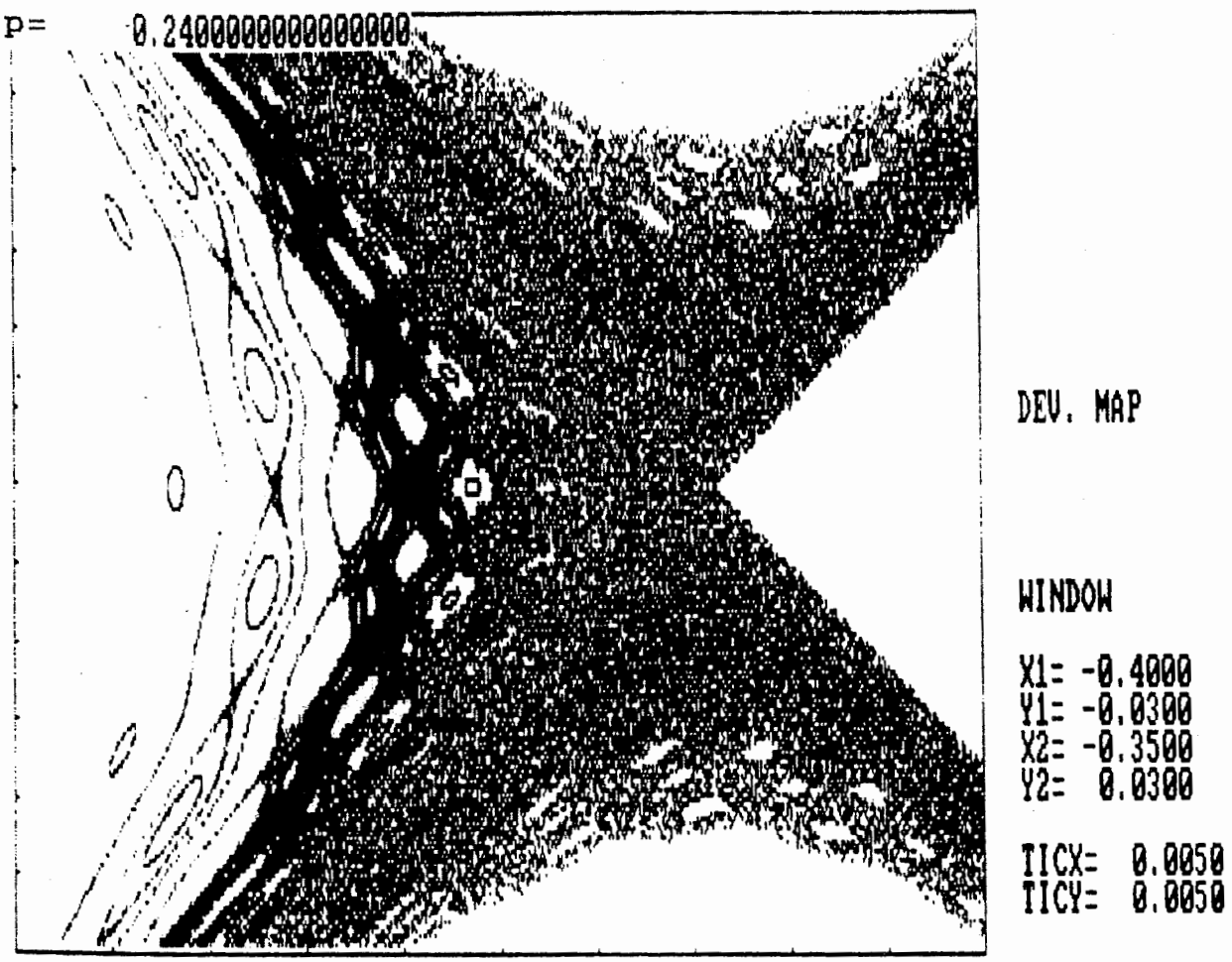
p= 0.2400000000000000
DEV. MAP
WINDOW
X1= -0.4000
Y1= -0.0300
X2= -0.3500
Y2= 0.0300
TICX= 0.0050
TICY= 0.0050

Figure 2.1.3

§ 2.2 Generic bifurcations in reversible area-preserving twist maps

In this thesis, we consider the DeVogelaere quadratic map since the map is represented in terms of symmetry coordinates (see (1.1.3.4)). The map is:

$$T_p:\begin{bmatrix} x \\ y \end{bmatrix}\rightarrow\begin{bmatrix} x' = -y + f_p(x) \\ y' = x - f_p(x') \end{bmatrix} , \qquad (2.2.1)$$

where $f_p(x)= px - (1-p)x^2$.

The map is an area-preserving map with unit Jacobian ($\det(DT)= 1$). Here DT is the Jacobian matrix which is the two by two matrix of partial derivatives of x' and y' with respect to x and y.

The stability of a periodic orbit of period n is determined by the Jacobian matrix M of T_p^n about the orbit (see § 1.2.1). The residue R of the periodic orbit is:

$$R = (2-\mathrm{Tr}M)/4 .$$

When $R<0$, the orbit is hyperbolic, when $0<R<1$ it is elliptic, and when $R>1$ it is hyperbolic with reflection. For an elliptic orbit the residue can be represented as $R=\sin^2(\pi\nu)$, since the eigenvalues λ of M are on the unit circle ($\lambda = e^{\pm i 2\pi\nu}$). Here ν is the central rotation frequency about a point on the orbit.

The map has the elliptic fixed point at the origin when $-1<p<1$. The residue of the fixed point is : $R=(1-p)/2$.

Hence the central frequency ν_0 about the fixed point is given by an equation :

$$p = \cos 2\pi\nu_0 \quad ,$$

and the eigenvalues λ of M are $e^{\pm i 2\pi\nu_0}$.

If $\lambda^k \neq 1$ for $k=1,2,\ldots, q(q\geq 4)$, then there exists a canonical transformation$(x,y)\rightarrow(\theta,I)$ such that

$$I = \frac{1}{2}(x^2+y^2), \quad \theta = \tan^{-1} y/x \quad ,$$

and the transformation takes the map (2.2.1) into a map:

$$\begin{aligned} I' &= I + \sigma(I^{(q+1)/2}) \quad , \\ \theta' &= \theta + \alpha(I) + \sigma(I^{(q-1)/2}) \quad , \end{aligned} \qquad (2.2.3)$$

where $\alpha(I)= 2\pi\nu_0 + \alpha_1 I + \cdots + \alpha_s \cdot I^s$,

$s = q/2 - 1$ (Arnold, 1978) .

Near the elliptic fixed point, typically, the map is a twist map (Mackay, 1982), since it satisfies the twist condition:

$$\left.\frac{\partial\theta'}{\partial I}\right|_{\theta} \neq 0 \qquad \text{for any } \theta \quad . \qquad (2.2.4)$$

So, near the elliptic fixed point, the map has typically rotation shear.

The rotation number of an orbit in a twist map is defined as the average rotation rate:

$$\nu = \lim \theta_n/(2\pi n) \quad ,$$

if the limit exists.

The range of twist defines the possible range of rotation numbers:

$$0 < \nu < \nu_0 \quad .$$

For example, in the figure 2.1.1, the possible range of rotation number is : $0 < \nu < 0.2114\cdots$.

A twist map can always be obtained from a generating function $L(\theta,\theta')$ such that

$$I = -\partial L(\theta,\theta') / \partial\theta \ , \qquad I' = \partial L(\theta,\theta') / \partial\theta' \ , \tag{2.2.5}$$

since it satisfies the twist condition (2.2.4).

If θ, θ' and θ'' are three successive points of θ on an orbit, then

$$\frac{\partial}{\partial\theta'} [L(\theta,\theta') + L(\theta',\theta'')] = 0 \ . \tag{2.2.6}$$

For integers r and s with $r+1 < s$, let $\{\theta_t,\ r \leq t \leq s\}$ be an arbitrary sequence of real values of θ subject to fixed initial θ_r and final θ_t. Then, from (2.2.4), this sequence gives an orbit-segment if and only if the action:

$$A = \sum_{t=r}^{s-1} L(\theta_t,\theta_{t+1})$$

is stationary with respect to arbitrary variations of intermediate point θ_t . So, an infinite sequence gives an orbit if and only if every finite segment has stationary action. Particularly, a periodic orbit can be obtained as follows. Let us consider a periodic sequence of type-(p,q), $\{\theta_0, \theta_1, \cdots, \theta_q = \theta_0 + 2\pi p\}$. Then, the action of the periodic sequence is:

$$A(\{\theta_i\}) = \sum_{i=0}^{q-1} L(\theta_i, \theta_{i+1}) \quad . \qquad (2.2.7)$$

A periodic sequence of type(p,q) gives an periodic orbit of type(p,q) if and only if its action is stationary with respect to variations keeping $\theta_q = \theta_0 + 2\pi p$.

By the Poincare-Birkhoff theorem(see § 1.2.2), in area-preserving twist maps, there exist at least a pair of periodic orbits in each rational ν in the range of twist. For the DeVogelaere map, one pair of periodic orbits exist , e.g. , in the figure 2.1.1 , a pair of periodic orbits of type(1,5) . One of these orbits minimizes the action (2.2.5) and the other is a minimaximizing periodic orbits(see § 1.2.2). The minimizing orbit has a negative residue and the minimaximizing one a positive residue (see § 1.2.2.). Also, the difference in the actions between the minimizing and minimaximizing orbits can be interpreted as the area transported between the minimizing and minimaximizing orbits per iteration of the map (see § 1.2.2.). So, computing the difference in the actions, one can obtain the area scaling factor (Meiss, 1986).

Finally, the map is reversible since it can be factored into the product $(T_p \cdot S) \cdot S$ of two orientation-reversing involutions:

$$S: \begin{bmatrix} x \\ y \end{bmatrix} \rightarrow \begin{bmatrix} x' = x \\ y' = -y \end{bmatrix} \quad ,$$

$$T_p S: \begin{bmatrix} x \\ y \end{bmatrix} \rightarrow \begin{bmatrix} x' = y + f_p(x) \\ y' = x - f_p(x') \end{bmatrix} \quad , \qquad (2.2.8)$$

$$S^2 = I(\text{identity}) = (T_p \cdot S)^2,$$

$$\det(DS) = -1 = \det(D(T_p S)) \quad .$$

If $\{ (x_i, y_i),\ i \in Z \}$ is an orbit of T_p, then $\{ S(x_i, y_i),\ i \in Z \}$ is an orbit of T_p^{-1} which is the inverse map of T_p, where $T_p^{-1} = S \cdot T_p S$. A symmetric orbit which is its own time reversal is an invariant set under S.

Two symmetry lines formed from the points invariant under S and $T_p \cdot S$ are the line $y=0$ and the line $y = x - f_p(x)$. Then, a symmetric periodic orbit must have two symmetric points on the symmetry lines(see §1.2.3); a periodic orbit of even period has two points on one symmetry line and none on the other, and a periodic orbit of odd period has one on each symmetry line. It may be helpful to see the figures 2.2.1, 2.2.2, 2.2.3. Two symmetry lines are shown in the pictures. They intersect at the elliptic fixed point. Since we are interested in the phase flow near the elliptic fixed point, we divide the two symmetry lines into four half-lines which meet at the elliptic fixed point. These half-lines point away from the fixed point and are assigned an orientation as follows. Positive orientation,denoted by the subscript "+", corresponds to pointing in the positive x direction. Similarly negative orientation is denoted by the subscript "-". Then, one can easily determine the rule for which points of the symmetric orbits of rotation number p/q lie on which half-lines. This depends on whether p and/or q are even or odd, as shown in the table 2.2.1. An obserbation, but not mathemathically proved, is that all the minimaximizing orbits tend

to have a point on one of the four half-lines denoted by E_1^1 (see § 1.2.3). This half-line E_1^1 is called the dominant half-line. For the map T_p , the dominant half-line is S_+. We denote the second elliptic line by E_2^1 , and the two hyperbolic lines by H_1^1 and H_2^1 . Figures 2.2.1, 2.2.2, and 2.2.3 correspond to each case shown in the table 2.2.1. These relations between symmetric periodic orbits and symmetry half-lines can be used usefully in locating symmetric orbits : a symmetric periodic point can be evaluated by going only halfway round the orbit (see § 1.2.3).

In fact, periodic orbits of type(p,q) have been born from the elliptic fixed point of T by generic bifurcations as the map-parameter p is varied (see § 1.2.4). In this section, we explain generic bifurcations with figures.

As stated above, for an elliptic orbit, the residue can be represented as $R = \sin^2(\pi\nu)$. A generic m/n-bifurcation occurs when ν is m/n, where m and n are coprime integers, $n \geq 1$ and $0 \leq m/n \leq 1/2$ (see § 1.2.4).

As an example, let us consider generic bifurcations of the elliptic fixed point of the Devogelaere map, when $p>1$. The residue of the elliptic fixed point is: $R= (1-p)/2$, and the central frequency ν_0 about the fixed point is given by an equation: $p=\cos 2\pi\nu_0$. As explained in § 1.2.4, when ν is $m/n(n \geq 5)$, a pair of stable and unstable orbits of rotation number m/n stable and unstable orbits of rotation number m/n are born. In the figure 2.2.1, a pair of stable and unstable orbits of rotation number 1/6 born from the fixed

point are visible and a pair of stable and unstable orbits of rotation number 1/5 and 2/5 are also visible in the figures 2.2.2 and 2.2.3, respectively. When ν_0 is 1/4, two types of generic 1/4-bifurcation exist (see §1.2.4). The 1st type is shown in the figure 2.2.4. At the resonance value, a pair of stable and unstable orbits of rotation number 1/4 are born. This case correspond to the case of a generic m/n($n \geq 5$) bifurcation. The 2nd type is shown in the figures 2.2.5 and 2.2.6. The figures shows a generic 1/4-bifurcation from the elliptic orbit of rotation number 1/4 born from the elliptic fixed point by a generic bifurcation of the 1st type. Let ν be the-central frequency about a point of the elliptic orbit of rotation number 1/4. Then, below the resonance value ($\nu<1/4$), a pair of stable and unstable orbits of rotation number 1/16 pop up. This is called a tangent bifurcation. As ν approaches the resonance value 1/4, the unstable orbit approaches the elliptic orbit of rotation number 1/4 (see figure 2.2.5). When ν is 1/4, the unstable orbit is absorbed by the elliptic orbit and as ν increases further, the unstable orbit is emitted(see figure 2.2.6). Note that the elliptic orbit becomes unstable at the resonance value since it absorbs the unstable orbit. As explained in § 1.2.4, a generic 1/3-bifurcation corresponds to the case of a generic 1/4-bifurcation of the 2nd type. In the figures 2.2.7, 2.2.8, 2.2.9, a generic 1/3-bifurcation from the elliptic fixed point is shown. Also in this case, the elliptic fixed point loses its stability. Finally, as ν_0 passes 1/2, the

elliptic fixed point turns to the hyperbolic point with reflection and a new elliptic orbit of doubled period appear (see figures 2.2.10 and 2.2.11).

All the daughter orbits born from the symmetric mother fixed point by a generic m/n($0< m/n \leq 1/2$)-bifurcation, are symmetric oribts (see § 1.2.4) . However, as explained in § 1.2.4, in a case of generic 0/1-bifurcation , daughter orbits are unsymmetric. The Devogelaere map has this example. But we do not consider the case in this thesis .

We call the mother elliptic fixed point the class-zero orbit(Meiss, 1986). So, the daughter orbits are class-1 orbits and encircle the class-zero orbit. Furthermore, each class one elliptic orbit becomes a mother orbit of class two orbits encircling the class one orbit, and so on. In this way, there exists an infinitely nested island structure, i.e. islands around islands of all classes.

As stated above, for class one orbits, there exist a rule for which points of a class one orbit lie on which half-lines. Similarly, for higher class orbit, there exists a rule depending on the mother orbit. Let E_1^n and E_2^n be two elliptic half-lines for class n. Then, since the daughter class-(n+1) orbits encircle the mother orbit, the four half-lines E_1^{n+1}, E_2^{n+1} , H_1^{n+1} and H_2^{n+1} for class-(n+1) are obtained from E_1^n and E_2^n by dividing each into two half-lines which meet at the mother point. Like the case of class 1, each half line points away from the mother points and is assigned an orientation as follows. Orientation of a half-line is designated

poistive if the half line points in the same direction as that of the mother line. For example, E_1^n is divided into two half-lines E_{1+}^n and E_{1-}^n . It may be helpful to see the figure 2.2.12. Then, one can easily determine the rule for which points of the class (n+1)orbits lie on which half-lines. This rule is shown in the table 2.2.2. This rule is not yet proved mathemathically. Note that higher class orbits also have the dominant symmetry line. So, all elliptic class-(n+1) orbit have one point on that dominant symmetry E_{2+}^n : $E_1^{n+1} = E_{2+}^n$. We call the elliptic point on the dominant half-line the dominant elliptic point, and the elliptic point on one of the remaining three subdominant half-lines is called the subdominant elliptic point. Let ν be the central frequency about a point of an elliptic orbit of class n. A generic p/q-bifurcation occurs when ν is p/q, where p and q are coprime integers, $q \geq 1$ and $0 \leq p/q \leq 1/2$. The positions of symmetric daughter points depend on whether p and/or q are even or odd, as shown in the table 2.2.2. When p/q is odd/enen, the dominant and subdominant elliptic points of class n+1 are born from the subdominant elliptic point of class n. When q is odd, the dominant elliptic daughter point is born from the subdominant elliptic mother point and the subdominant elliptic daughter from the dominant elliptic mother point. But the position of the subdominant point depends on whether p is even or odd (see the table 2.2.2). This rule is very useful in locating the higher class orbits and explains why at the accumulation point 1/n-bifurcation

sequence exhibits 'period-1' or 'period-2' behavior, according as n is even or odd, as will be seen in the next section.

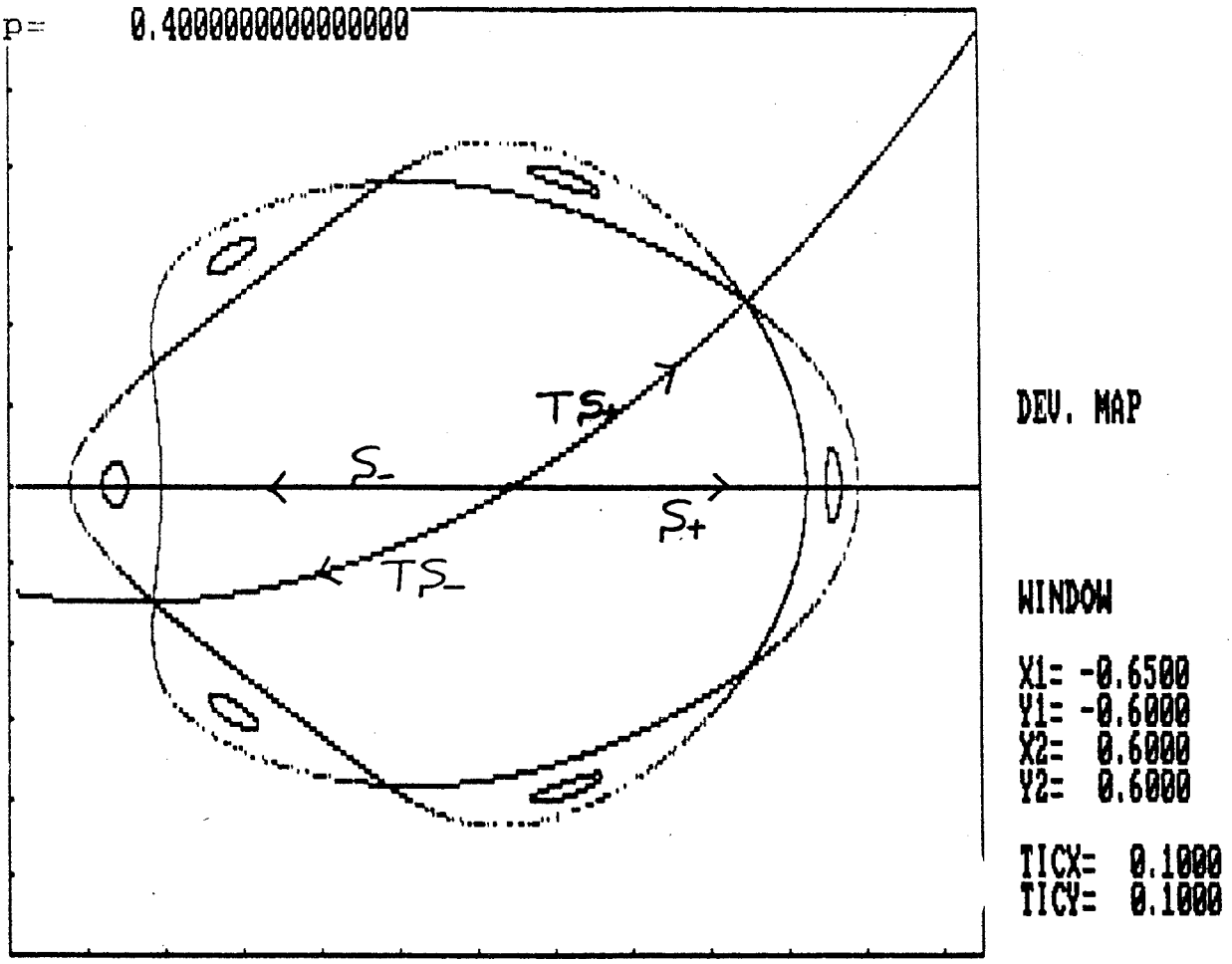

Figure 2.2.1 : A pair of periodic orbits of rotation number 1/6

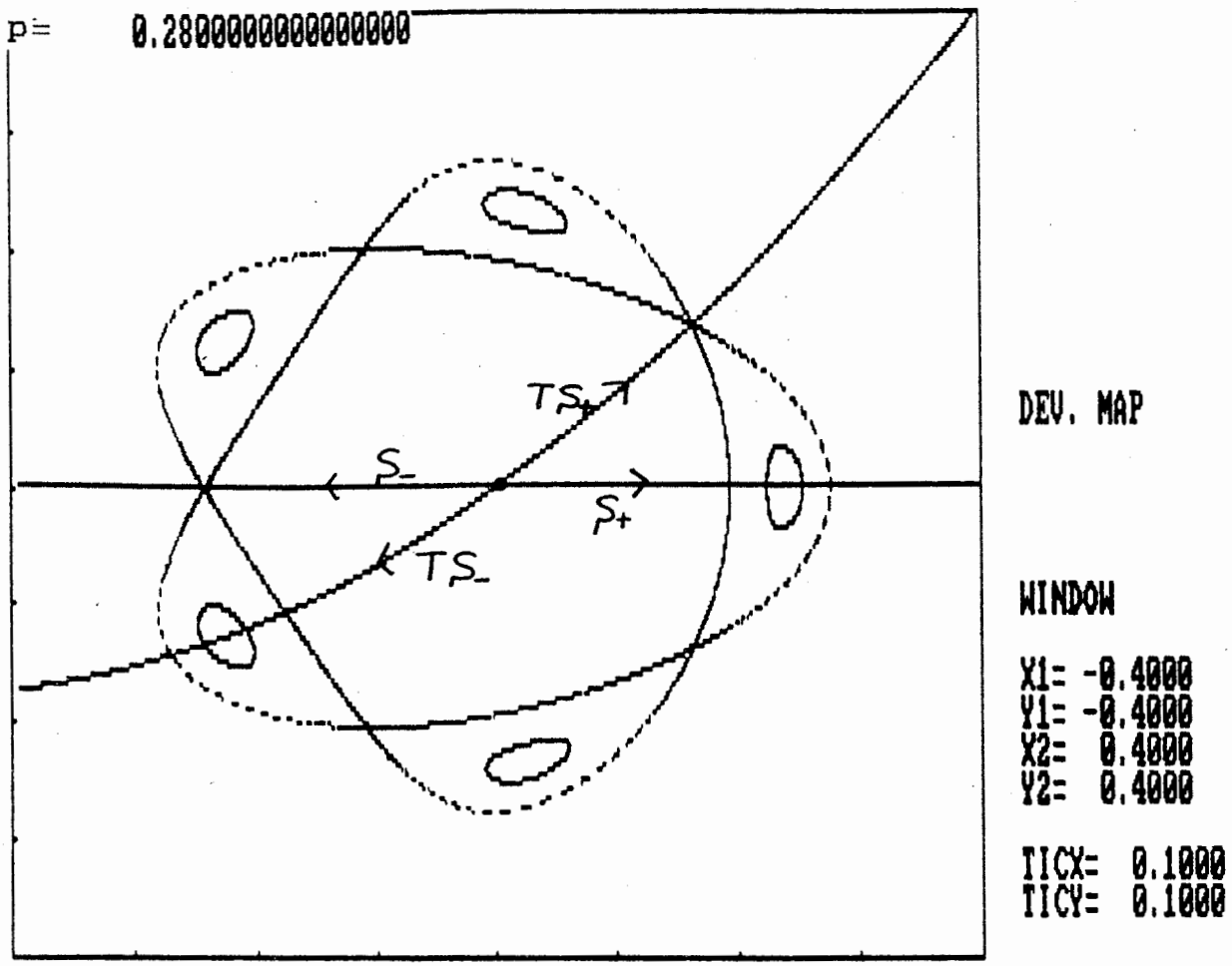

Figure 2.2.2 : A pair of periodic orbits of rotation number 1/5

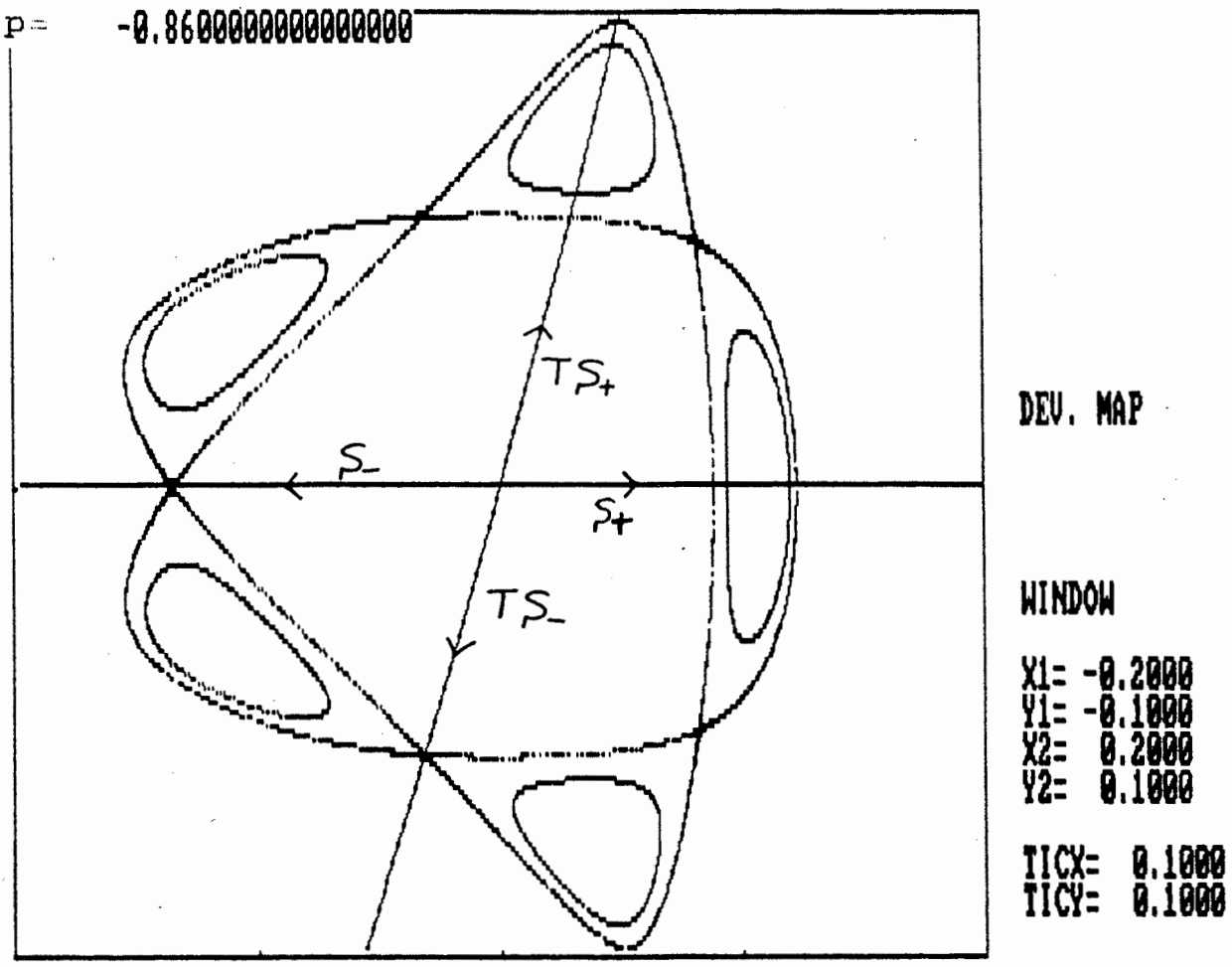

Figure 2.2.3 : A pair of periodic orbits of rotation number 2/5

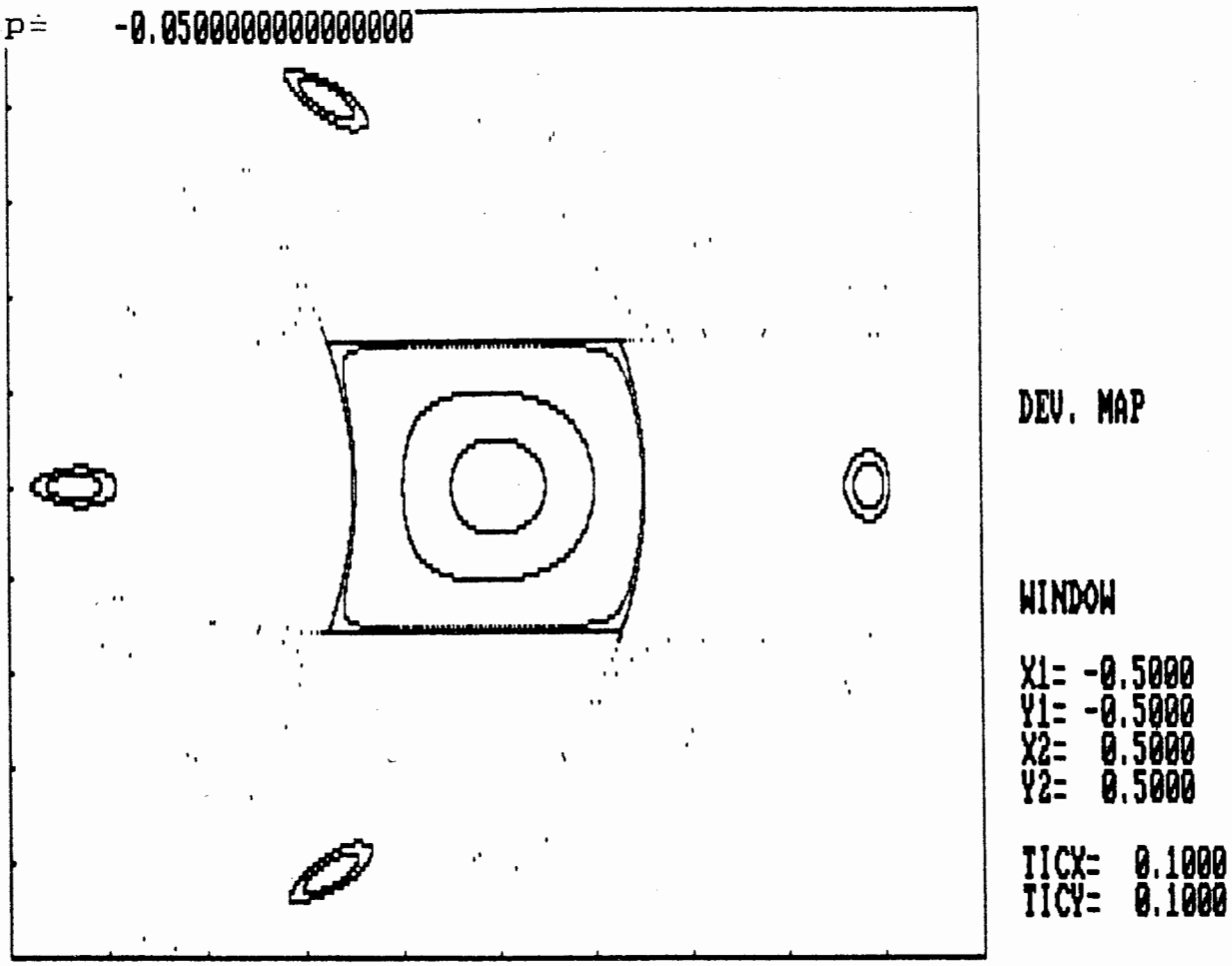

Figure 2.2.4 : A pair of periodic orbits of rotation number 1/4

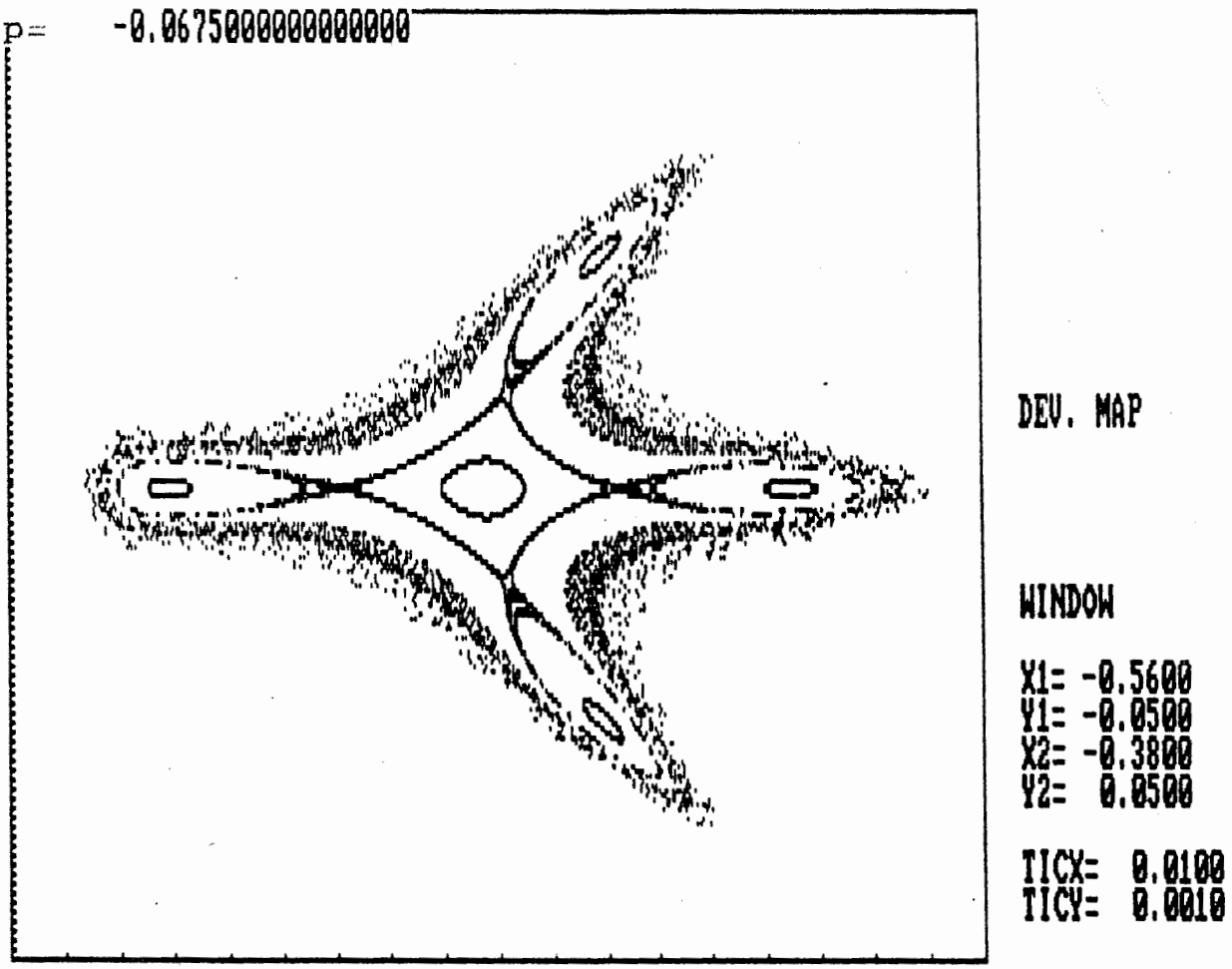

Figure 2.2.5 : A pair of periodic orbits of rotation number 1/16 when the central frequency is below 1/4

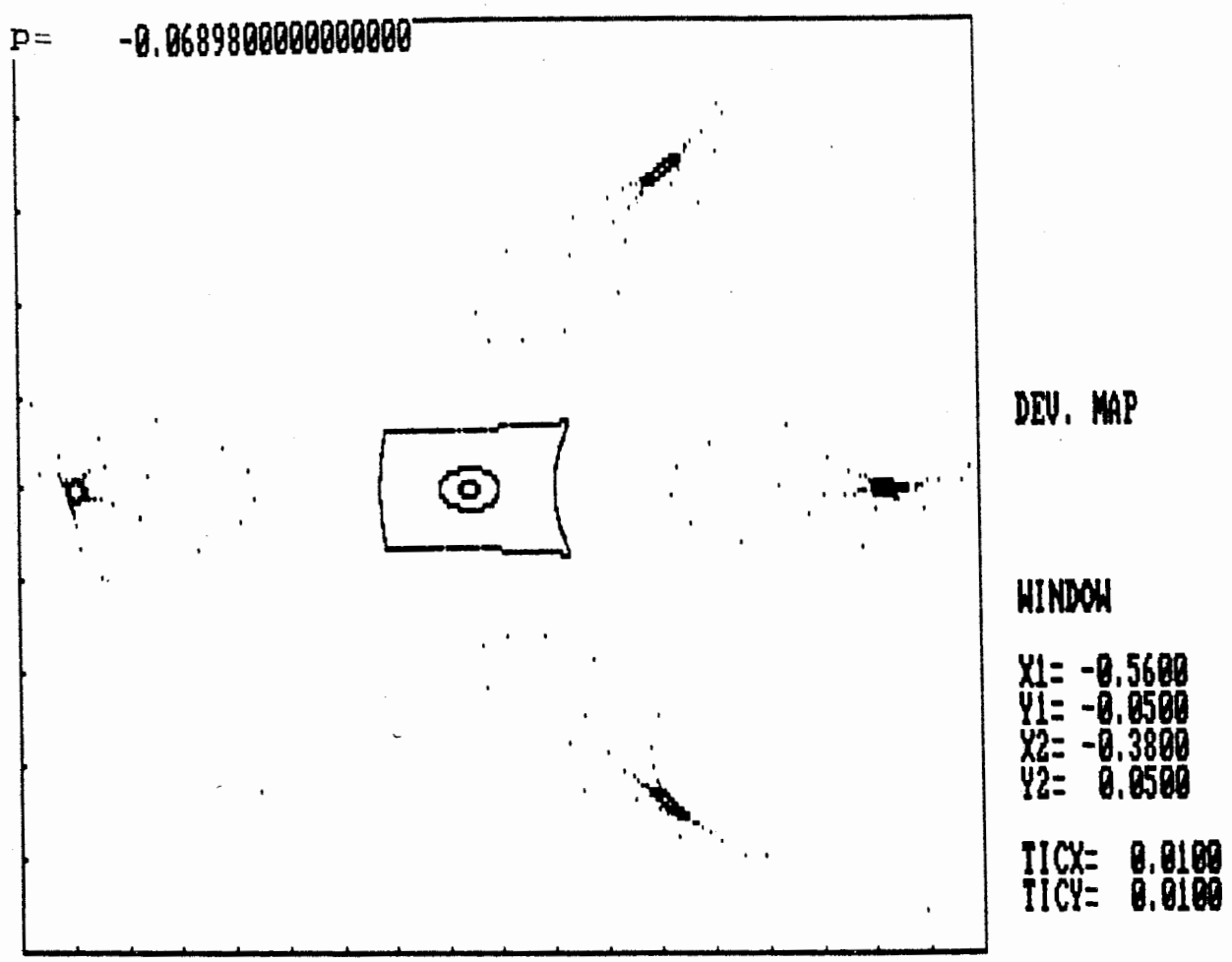

Figure 2.2.6 : A pair of periodic orbits of rotation number 1/16 when the central frequency is above 1/4

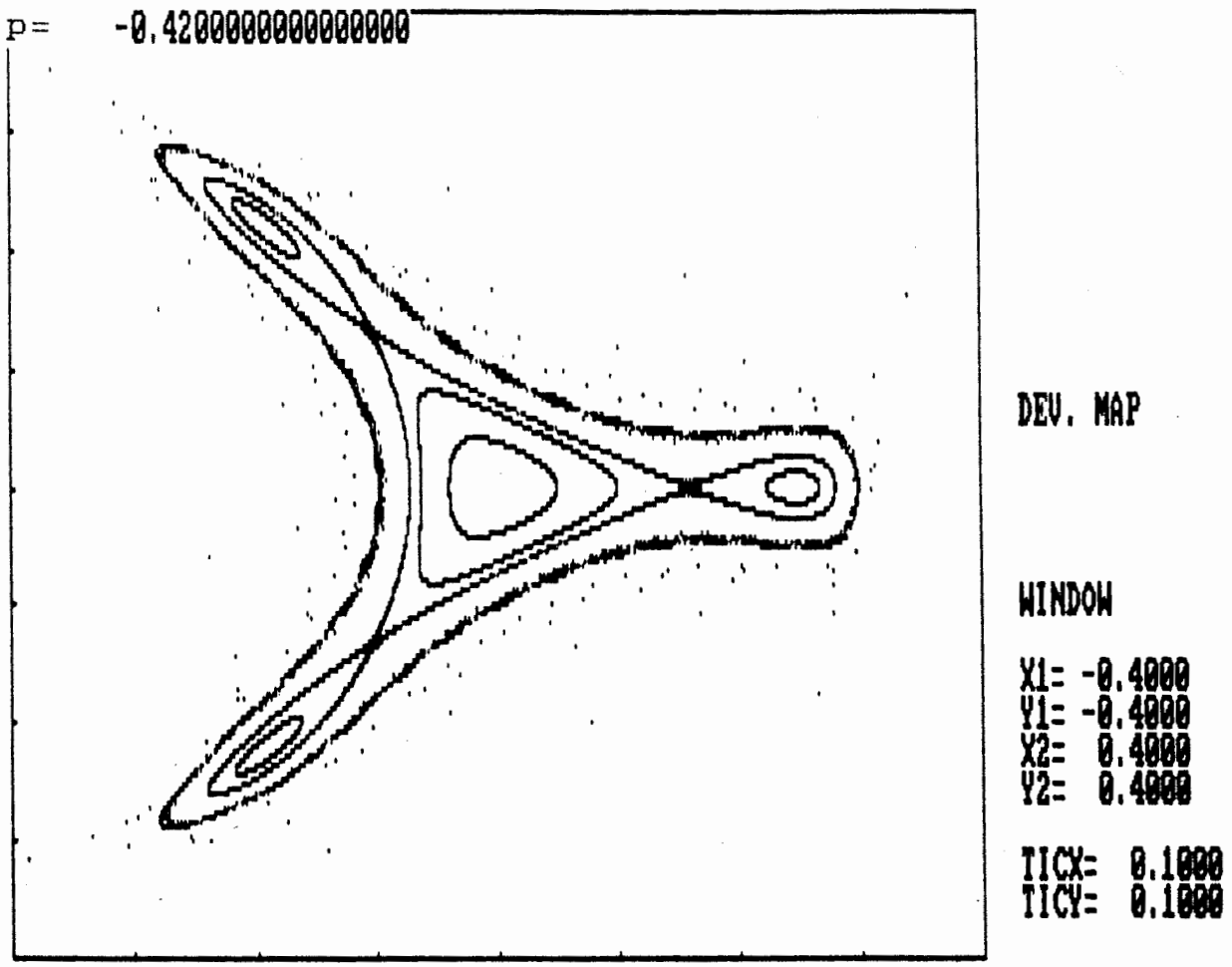

Figure 2.2.7 : A pair of periodic orbits of rotation number 1/3 pop up when the central rotation frequency is below 1/3

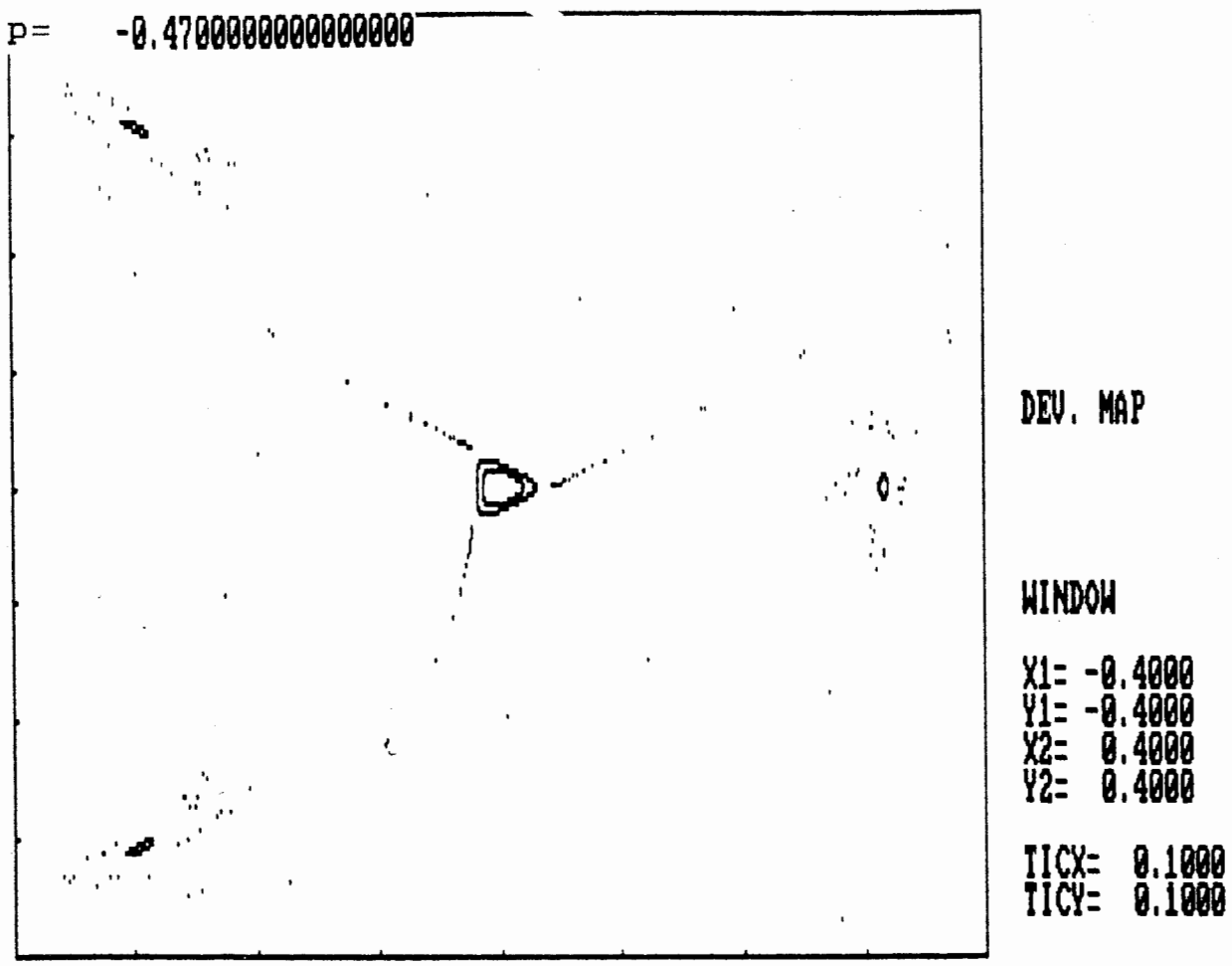

Figure 2.2.8 : The unstable orbit of rotation number 1/3 approaches the mother fixed point

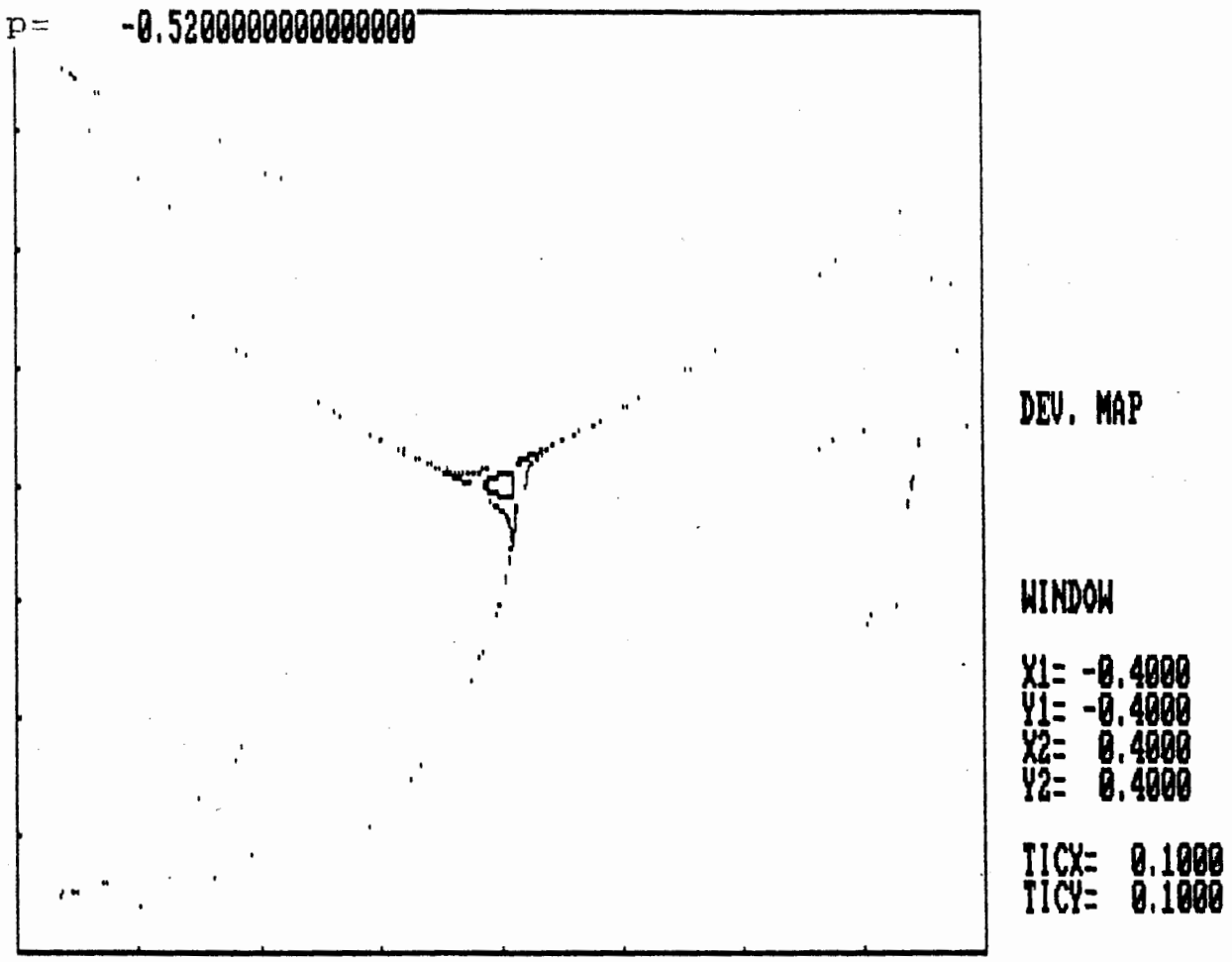

Figure 2.2.9 : The unstable orbit of rotation number 1/3 is emitted from the mother fixed point when the central frequency is above 1/3

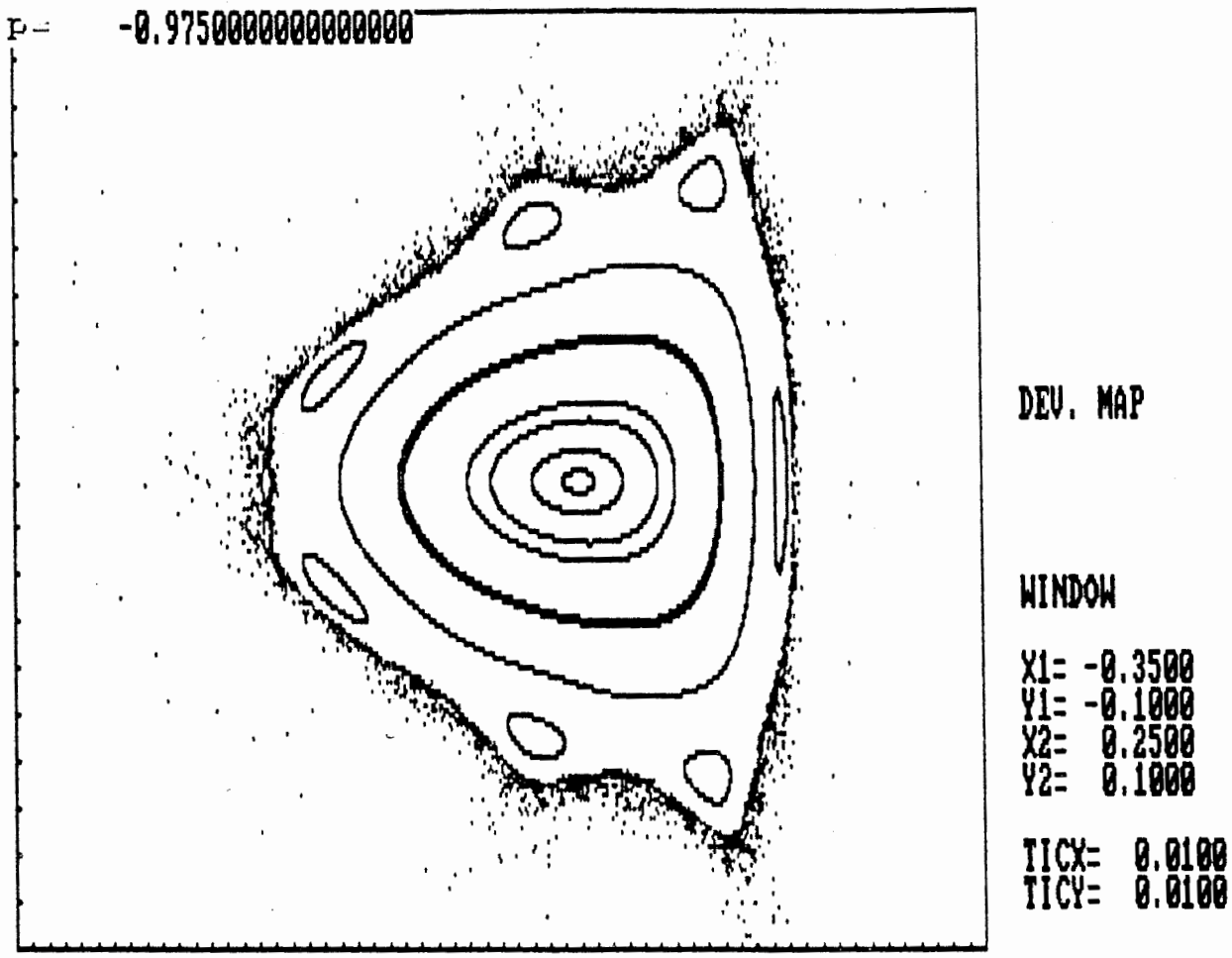

Figure 2.2.10 : The phase flow near the mother fixed point when the central frequency is 1/2

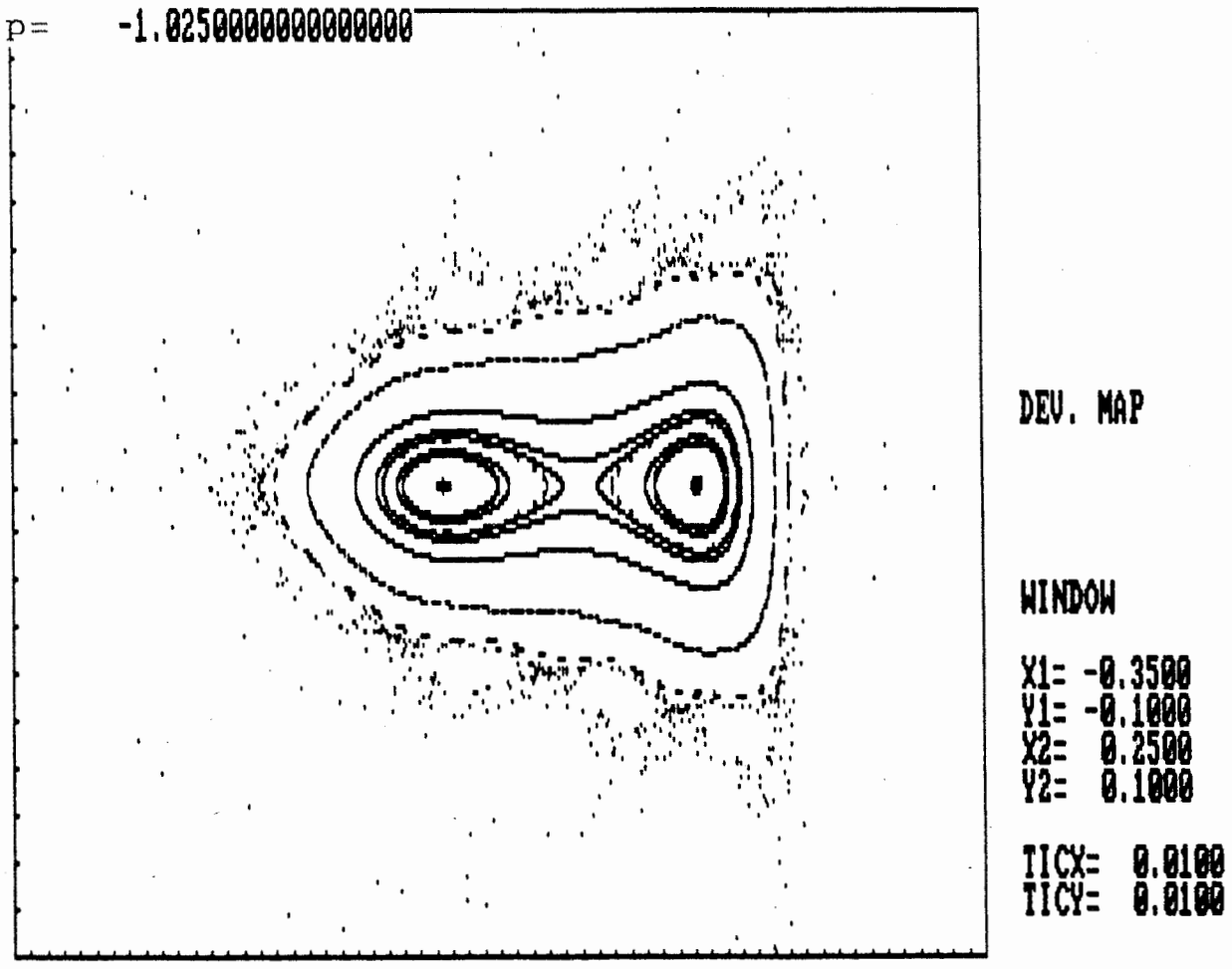

Figure 2.2.11 : A new elliptic orbit of doubled period is born from the mother fixed point

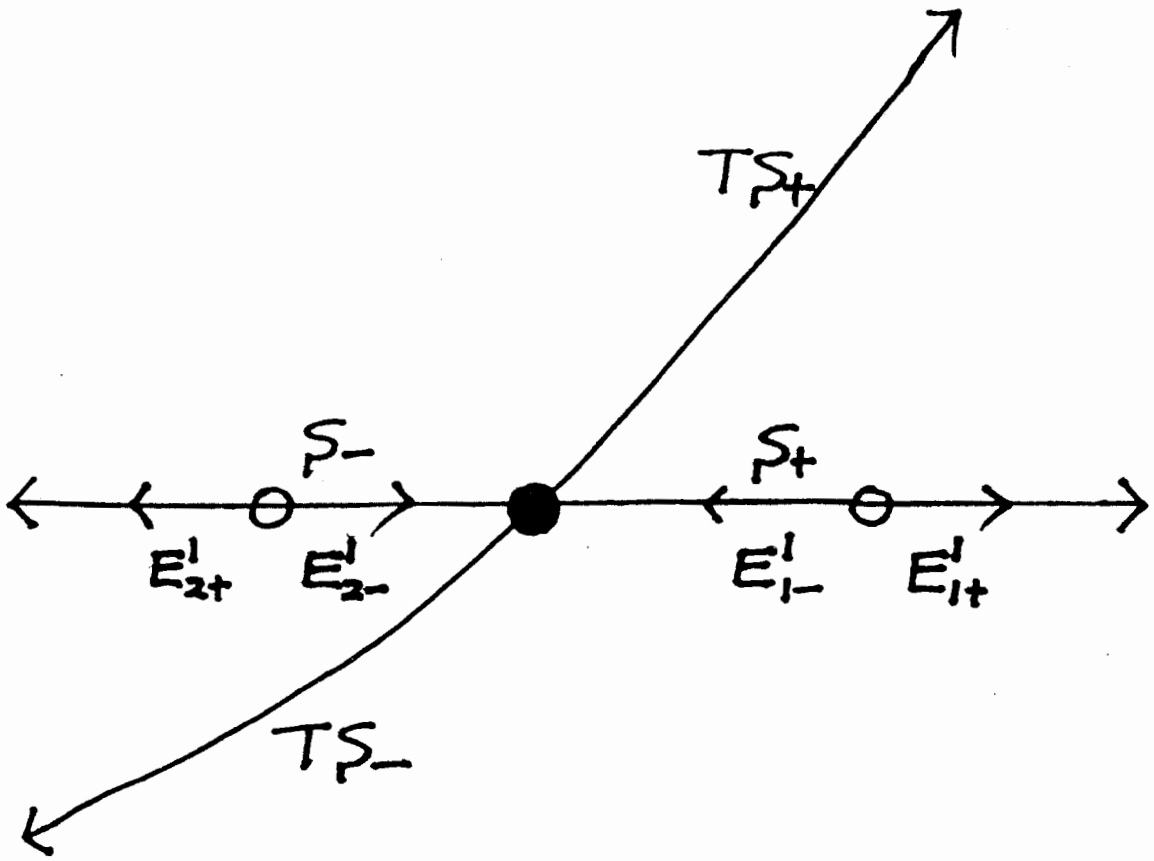

Figure 2.2.12 : A formation of four half-lines for class 1.

p/q	E_1^1	E_2^1	H_1^1	H_2^1
odd/even	S_+	S_-	TS_+	TS_-
odd/odd	S_+	TS_-	S_-	TS_+
even/odd	S_+	TS_+	S_-	TS_-

Tabel 2.2.1 : four symmetry half-lines for class one orbits

p/q	E_1^n	E_2^n	H_1^n	H_2^n
odd/even	E_{2+}^{n-1}	E_{2-}^{n-1}	E_{1+}^{n-1}	E_{1-}^{n-1}
odd/odd	E_{2+}^{n-1}	E_{1-}^{n-1}	E_{2-}^{n-1}	E_{1+}^{n-1}
even/odd	E_{2+}^{n-1}	E_{1+}^{n-1}	E_{2-}^{n-1}	E_{1-}^{n-1}

Table 2.2.2: four symmetry half-lines for higher class orbits ($n \geq 2$)

§2.2.3 Self-similar 1/n-bifurcation sequence

The remarkable discovery of universally self-similar period-doubling sequences in one dimensional noninvertible maps with one extremum by Feigenbaum (1978,1979) inspired several people (Benettin et al, 1980, Bountis, 1980, Greene et al, 1981) to look for period-doubling sequences in two dimensional area-preserving maps. They have found that there are infinite period-doubling sequences with asymptotic self-similarity and the limiting self-similar behaviors are different from those in one dim. noninvertible maps with one extremum .

In 1-dim. maps, there are only period-doubling bifurcations and tangent bifurcations, since the eigenvalues of the Jacobian matrix of a periodic orbit are real scalars. But, in 2-dim. area-preserving maps, there are generic m/n-bifurcations, where m and n are coprime integers, $n \geq 1$ and $0 \leq m/n \leq 1/2$.

A stable periodic orbit loses its stability by a period-doubling bifurcation and turns to a hyperbolic oribt with reflection (see figures 2.2.10 and 2.2.11) . As stated in §2.1, unstable orbits play the role of 'scatterer' of stochastic orbits like the pins in a pin ball game. On the other hand, a stable orbit does not lose its stability by a m/n-bifurcation($0< m/n <1/2$), apart from 1/3-bifurcation or sometimes 1/4-bifurcation. In this case, islands play the role of 'trap' of stochastic orbits. In other words, a stochastic orbit has a long-time correlation near these islands.

We (1984, 1985) have studied these island structures. We have found that at a certain parameter value, i.e. the so-called accumulation point, island chains of all classes of a 1/n-bifurcation, with n=3 to 6, exist and they have self-similar nested structures asymptotically. We have also observed that the pattern of periodic orbits repeats itself asymptotically from one bifurcation to the next for even n and to every other for odd n.

Firstly, I describe results for odd n-tupling bifurcations, with n=3,5.

Figure 2.2.7 shows a 1/3-bifurcation. One can follow as many triplings as one pleases. I have followed up to 10. Table 2.3.1 shows the parameter value at which by tangent bifurcation a pair of stable and unstable orbits of period 3^{n+1} are born and the residue of the stable orbit of period 3^n at the parameter value, Table 2.3.2 shows the parameter values at which the stable orbits of period 3^n become unstable, and Figure 2.3.1 shows the stable zones of orbits of period 3^n.

As shown in the table 2.3.1, a pair of stable and unstable orbits of period 3^{n+1} are born when the residue of the orbit of period 3^n is 0.7010815, asymptotically. The important thing to notice is that the successive parameter values in the table 2.3.2 accumulate at a finite value p^*. This point p^* is called the accumulation point of 1/3-bifurcation point. In this case,

$$p^* = -0.477013684274046437\ldots \quad . \qquad (2.3.1)$$

Also, note that given a residue value, the successive parameter values p_n converge asymptotically geometrically with ratio δ (see the table 2.3.2 and the figure 2.3.1) :

$$\delta_n = \frac{p_{n-1}-p_n}{p_n-p_{n+1}} \longrightarrow \delta \quad . \tag{2.3.2}$$

In this case, the bifurcation ratio is ;

$$\delta = 20.18468\cdots \quad . \tag{2.3.3}$$

So, given a residue, the successive parameter values obey a scaling law asymptotically :

$$p_n - p^* \sim \delta^{-n}. \tag{2.3.4}$$

At the accumulation point p^*, the orbits of all classes of 1/3-bifurcation exist and they have the same residue value asymptotically. The residues R_+^* and R_-^* of the stable and unstable orbit are :

$$\begin{aligned} R_+^* &= 0.7337096\cdots \ , \\ R_-^* &= -0.0092326\cdots \ . \end{aligned} \tag{2.3.5}$$

So, the parameter value of the accumulation point is below that of each 1/3-bifurcation point of stable periodic orbits of all classes, aymptotically.

n	p_{n+1}	R_n
0	-0.414213562	0.70710678
1	-0.474217896	0.69910465
2	-0.476873826	0.70112633
3	-0.477006766	0.70103844
4	-0.477013341	0.70108185
5	-0.477013667	0.70108055
6	-0.477013683	0.70108151
7	-0.477013684	0.70108150

Table 2.3.1: the parameter value p_{n+1} at which a pair of stable and unstable orbits of period 3^{n+1} are born and the residue R_n of the stable orbit of period 3^n at p_{n+1}

n	p_n	δ_n
1	-0.5	
2	-0.47815723	20.09
3	-0.47706996	20.31
4	-0.4770164737	20.1876
5	-0.4770138224	20.1878
6	-0.4770136911	20.1848
7	-0.4770136846	20.1847
8	-0.47701368429	20.184684
9	-0.47701368427 48	20.184686
10	-0.4770136842741	

Table 2.3.2: $\delta_n = (p_{n-1} - p_n)/(p_n - p_{n+1})$, where p_n is the parameter value at which a periodic orbit of period 3^n becomes a hyperbolic orbit with reflection.

Figure 2.3.1 : stable zones of peripheral orbitals of period 3rd

The next step is to fix the parameter value at the accumulation point at which islands of all classes of 1/3-bifurcation coexist and examine the infinitely nested structure. Figure 2.3.2 shows consecutively enlarged figures of the period-trebling bifurcation associated with two symmetric points on the symmetry lines. There are two symmetry lines $y=0$ and $y=x-f_p(x)$ corresponding to S-symmetry and its complementary T_pS-symmetry (see § 2.2). But it is more convenient to see the phase flows near the symmetric point on the complementary symmetry line in the Henon's quadratic map:

$$T_a : \begin{bmatrix} X \\ Y \end{bmatrix} \rightarrow \begin{bmatrix} X' = -Y + 2f_a(X) \\ Y' = X \end{bmatrix} , \qquad (2.3.6)$$

where $f_a(X) = \frac{1}{2}(1-aX^2)$,

since it has the complementary straight line $Y = X$ (1.1.3.10). In fact, the DeVogelaere map (2.2.1) can be transformed into the Henon's map (2.3.6) by a canonical coordinate change:

$$x = \frac{a}{2\sqrt{1+a}}(X-z) , \quad y = \frac{a}{2\sqrt{1+a}}(Y-z) - f_p(x) ,$$
$$p = 1-\sqrt{1+a} = -a \cdot z . \qquad (2.3.7)$$

So, we examine the infinitely nested structure in terms of two representations: S-symmetry is represented in terms of the DeVogelaere's coordinates ($y=0$) and TS-symmetry is represented in terms of the Henon's coordinates ($Y=X$) .

As explained in § 1.2.3, when one periodic point $P_n(0)$ of odd period ℓ is on the symmetry line of S, $y=0$, the $[(\ell+1)/2]$th point from that point ($P_n((\ell+1)/2)$) is on the

complementry line, Y=X ($P_n(m) = T^m \cdot P_n(0)$). It is important to notice that when one symmetric poit is the dominant elliptic point, the other one is the subdominant elliptic point. For example, in the figure 2.3.2, A_{n-1} is the subdominant elliptic point and A'_{n-1} is the dominant elliptic point. But, for the next higher periodic orbit A_n is the dominant elliptic point and A'_n is the subdominant elliptic point. In such a way, on each symmetry line, the dominant elliptic point and the subdominant elliptic point appear alternatively as n increases. So, as shown in the figure 2.3.2, the pattern of the periodic orbit of period 3^n is similar to that of the periodic orbit of period 3^{n+2}. That is, magnification of the region near the subdominant elliptic point of period 3^{n+1} by appropriate factors yields the same figure near the subdominant elliptic point of period 3^{n-1} .

On each symmetry line, symmetric elliptic points converge to a limit value in such a way as shown in the table 2.3.3. As expected, the sequence exhibits 'period-2' behavior. The limit value on the line y=0 is:

$$x^* = .2840928311\cdots ,$$

and the limit value on the line Y = X is : (2.3.7)

$$X^* = -0.488398124\cdots .$$

That is, on each symmetry dominant points or subdominant points converges asymptotically geometrically to the limit value with ratio α. Therefore, the scaling factor along the symmetry line is:

$$\alpha = -43.9807 .$$

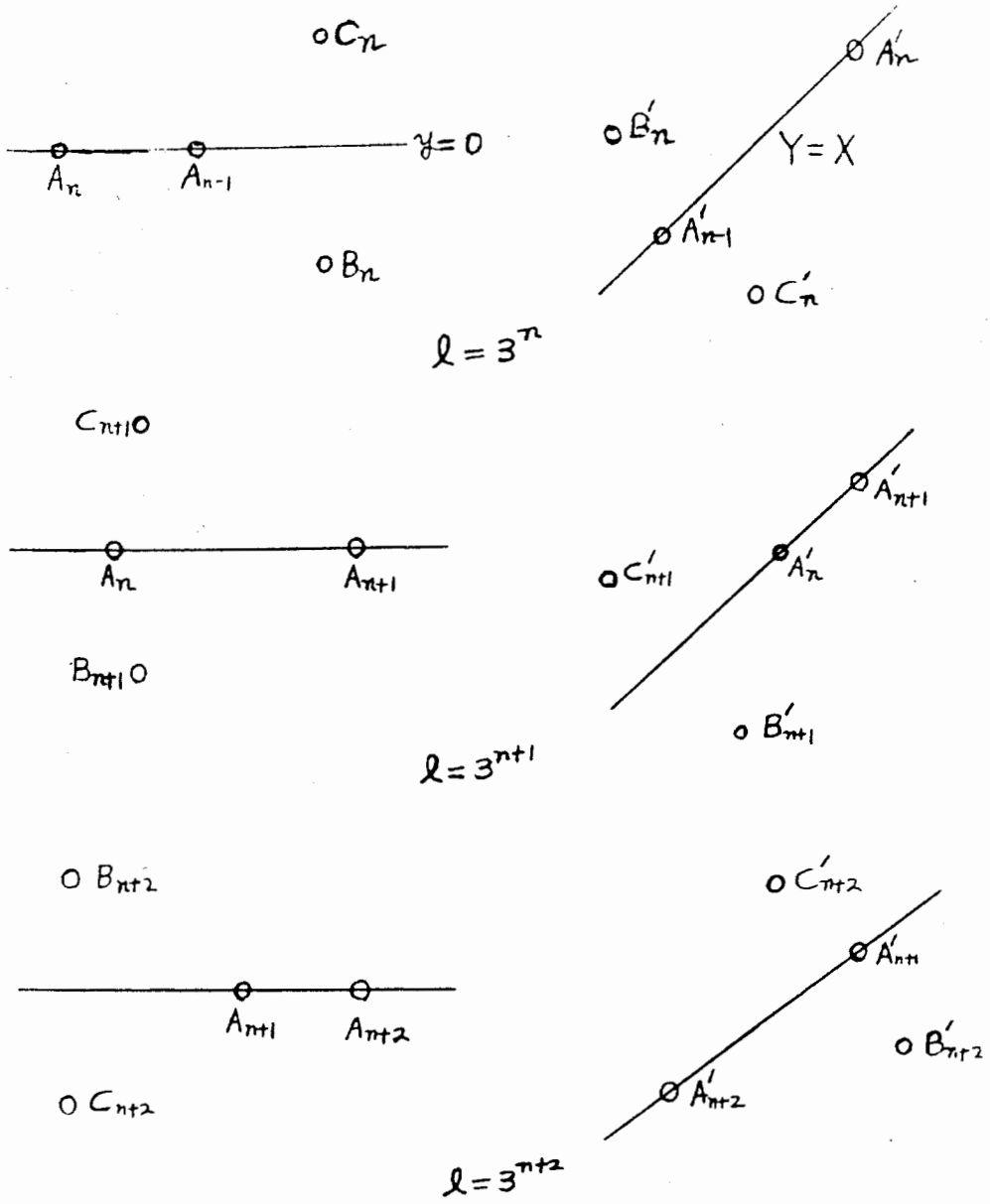

Figure 2.3.2 : Period-trebling bifurcations associated with two elliptic symmetric points on the symmetry lines y=0 and Y=X . A_n, B_n, C_n, A'_n, B'_n, and C'_n are ℓ-periodic points correspoding to $P_n(0)$, $P_n(\ell/3)$, $P_n(2\ell/3)$, $P_n((\ell+1)/2)$, $P_n((\ell+1)/2+\ell/3)$, and $P_n((\ell+1)/2-\ell/3)$ of the text with $\ell = 3^n$, respectively.

n	x_n	α_n
1	0.3213	
2	0.2898	4.77076
3	0.2832	-9.20728
4	0.28396	4.78659
5	0.28411	-9.18864
6	0.2840957	4.78665
7	0.28409239	-9.18816
8	0.28409276	4.786653
9	0.28409284	-9.188152
10	0.28409283	

Table 2.3.3: x_n is the x-component of the position of the symmetric elliptic point of period 3^n on the line $y=0$.

$\alpha_n=(x_{n-1} - x_n)/(x_n-x_{n+1})$

We also obtained scaling factors along and across the symmetry line by comparing the triangle with vertices A_n, B_n, C_n with the triangle with vertices A_{n+2}, B_{n+2} and C_{n+2} , as shown in the table 2.3.4. The scaling factors along and across the symmetry line are:

$$\alpha = -43.9807$$
$$\text{and} \qquad (2.3.8)$$
$$\beta = -186.723 \ .$$

In the way stated above, at the accumulation point p^*, the pattern of periodic orbits repeats itself from one bifurcation to every other one when magnified by the rescaling factor α and β.

We also studied two further trebling bifurcations of $2 \cdot 3^n$ and $6 \cdot 3^n$ and found the same results for both cases, except that symmetric points are on the same symmetry lines: the former is on the S-symmetry line(y=0)and the latter on the TS-symmetry line(Y=X) and thus there are two accumulation points on each symmetry line y=0 or Y=X. In the latter case, the orbit of the basic period 6 is one bifurcated of the mother orbit of period 3. So, these self-similar limiting behaviors appear to be universal.

Table 2.3.4 : Sequences of perioding-trebling bifurcation .

$$\alpha_n(1) = (A_n - B_n)_x \,/\, (A_{n+1} - B_{n+1})_x \ ,$$

$$\alpha_n(2) = (A'_n - D'_n)_X \,/\, (A'_{n+1} - B'_{n+1})_X \ ,$$

$$\beta_n(1) = (B_n - C_n)_y \,/\, (B_{n+1} - C_{n+1})_y \ , \quad \text{and}$$

$$\beta_n(2) = (B'_n - C'_n)_Y \,/\, (B'_{n+1} - C'_{n+1})_Y$$

are defined with respect to Figure 2.3.2 .

$(A_n - B_n)_x$ is the x-component of $(A_n - B_n)$ and $(B_n - C_r)_y$ the y-component of $(B_n - C_n)$. $D'_n = B'_n + C'_n$.

$(A'_n - D'_n)_X$ is the X-component of $(A'_n - D'_n)$ and $(B'_n - C'_n)_Y$ the Y-component of $(B'_n - C'_n)$

Table 2.3.4

n	$\alpha_n(1)$	$\alpha_n(2)$	$\beta_n(1)$	$\beta_n(2)$
2	2.39623	-17.9717	-32.1398	5.97879
3	-17.9389	2.46836	5.94564	-31.5555
4	2.45693	-17.8893	-31.4510	5.94589
5	-17.8954	2.45809	5.93983	-31.4376
6	2.45779	-17.8943	-31.4364	5.93983
7	-17.8942	2.45781	5.93982	-31.4360
8	2.45781	-17.8942	-31.4360	5.93982
9	-17.8942	2.45781	5.93981	-31.4360

The 1/5-bifrucation sequcnes also exhibit 'period-2' behaviors like the 1/3-bifurcation sequences. So, we describe our results briefly. Given a residue value, the successive parameter values p_n converge asymptotically geometrically to the accumulation point p^* with ratio δ :

$$p_n - p^* \sim \delta^{-n} \quad , \tag{2.3.9}$$

where $p^* = 0.17713742750981\cdots$.

As shown in the table 2.3.5, the bifurcation ratio is :

$$\delta = 20.0478 \quad . \tag{2.3.10}$$

At the accumulation point, the orbits of all classes of 1/5-bifurcation exist and they have the same resiude values asymptotically. The residues R_+^* and R_-^* of the stable and unstable orbits are:

$$R_+^* = 0.38915\cdots \quad , \tag{2.3.11}$$

$$R_-^* = -0.16083\cdots \quad .$$

Figure 2.3.3 shows consecutively enlarged figures of the 5-tupling bifurcations associated with two symmetric points on the symmetry lines y=0 and Y=X, when the parameter is fixed at the accumulation point p^*. On each symmetry line, symmetric elliptic points converge to a limit value: the limit value on the line y=0 is :

$$x^* = 0.4085718\cdots \quad ,$$

and the limit value on the line Y=X is:

$$X^* = 3.456924\cdots \quad . \tag{2.3.12}$$

As shown in the figure 2.3.3, the pattern of periodic orbits repeats itself from one bifurcation to every other when magnified by the scaling factors α and β along and across the symmetry lines, respectively. The scaling factors can be obtained by comparing the pentagon with vertices A_n , B_n , C_n , D_n and E_n with the pentagon with vertices A_{n+2} , B_{n+2} , C_{n+2} , D_{n+2} and E_{n+2} , as shown in the table 2.3.5. The scaling factors along and across the symmetry line are:

$$\alpha = -43.27$$

and (2.3.13)

$$\beta = -75.70$$

In summary, for odd n-tupling bifurcation with n=3 and 5, n-tupling bifurcation sequences exhibit 'period-2' behaviors at the accumulation point p^*. However, the bifurcation ratio δ, the scaling factors α and β depend on n. The reason why these sequences exhibit 'period-2' behaviors is that the dominant elliptic point and the subdominant point appear alternatively and converge to a limit value.

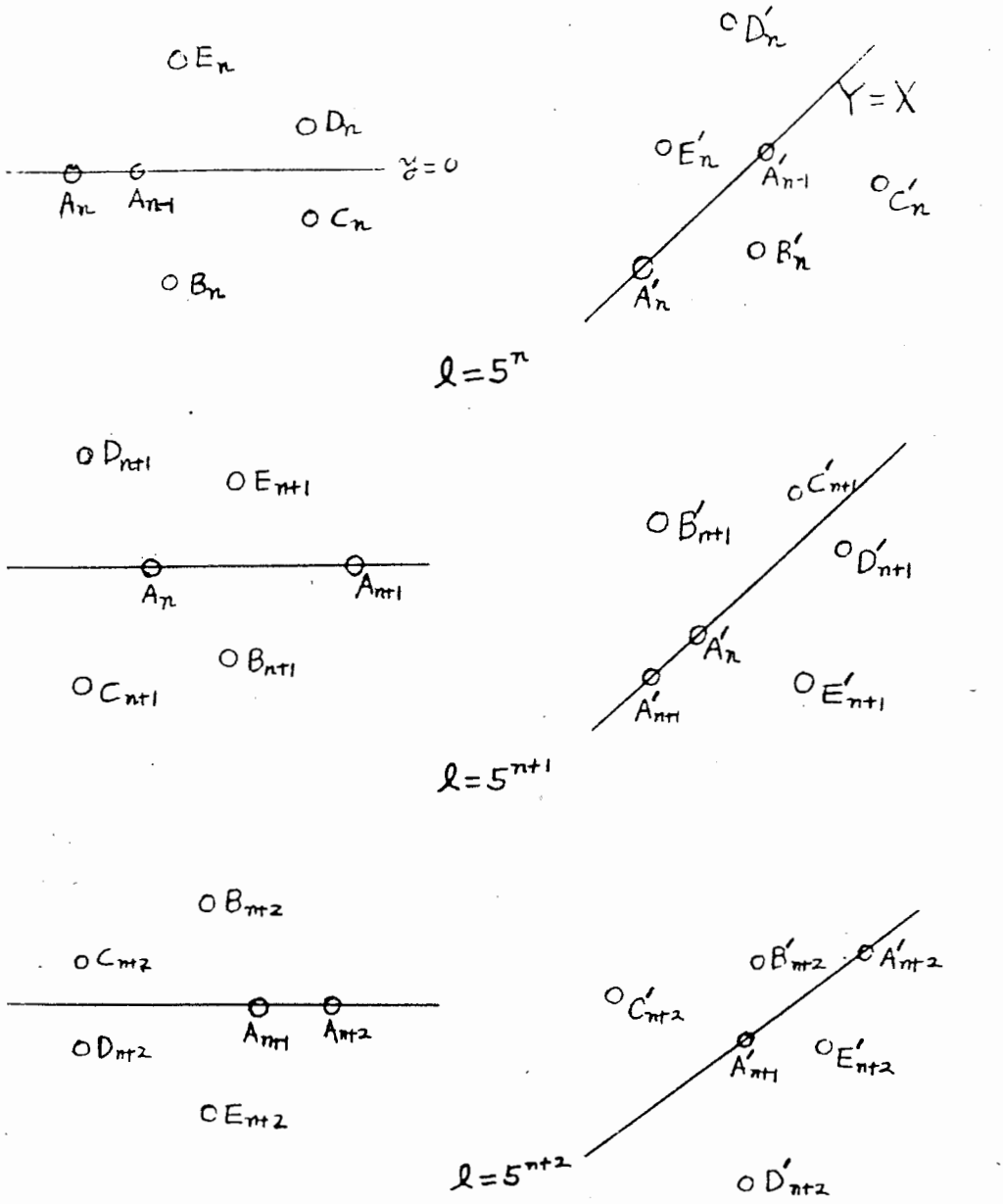

Figure 2.3.3 : Period 5-tupling bifurcations associated with two symmetric elliptic points on the two symmetry lines y=0 and Y=X . A_n, B_n, C_n, D_n, E_n, A'_n, B'_n, C'_n, D'_n and E'_n are ℓ-periodic points corresponding to $P_n(0)$, $P_n(\ell/5)$, $P_n(2\ell/5)$, $P_n(3\ell/5)$, $P_n(4\ell/5)$, $P_n((\ell+1)/2)$, $P_n((\ell+1)/2+\ell/5)$, $P_n((\ell+1)/2+2\ell/5)$, $P_n((\ell+1)/2+3\ell/5)$, and $P_n((\ell+1)/2+4\ell/5)$ with $\ell = 5^n$, respectively. $P_n(m) = T^m.P_n(0)$.

Table 2.3.5 : Period 5-tupling **sequences** .

$$\alpha_n(1) = (C_n-B_n)_x \;/\; (C_{n+1}-B_{n+1})_x \;,$$

$$\alpha_n(2) = (B_n-A_n)_x \;/\; (B_{n+1}-A_{n+1})_x \;,$$

$$\alpha'_n(1) = (A'_n-F'_n)_X \;/\; (A'_{n+1}-F'_{n+1})_X \;,$$

$$\alpha'_n(2) = (F'_n-G'_n)_X \;/\; (F'_{n+1}-G'_{n+1})_X \;,$$

$$\beta_n(1) = (C_n-D_n)_y \;/\; (C_{n+1}-D_{n+1})_y \;,$$

$$\beta_n(2) = (B_n-E_n)_y \;/\; (B_{n+1}-E_{n+1})_y \;,$$

$$\beta'_n(1) = (B'_n-E'_n)_Y \;/\; (B'_{n+1}-E'_{n+1})_Y \;, \quad \text{and}$$

$$\beta'_n(2) = (C'_n-D'_n)_Y \;/\; (C'_{n+1}-D'_{n+1})_Y$$

are defined with respect to Figure 2.3.3 . $(C_n-B_n)_x$ and $(B_n-A_n)_x$ are the x-components of (C_n-B_n) and (B_n-A_n), and $(C_n-D_n)_y$ and $(B_n-E_n)_y$ the y-components of (C_n-D_n) and (B_n-E_n) , respectively. $F'_n = B'_n + E'_n$. $G'_n = C'_n + D'_n$. $(A'_n-F'_n)_X$ and $(F'_n-G'_n)_X$ are the X-components of $(A'_n-F'_n)$ and $(F'_n-G'_n)$, and $(B'_n-E'_n)_Y$ and $(C'_n-D'_n)_Y$ the Y-components of $(B'_n-E'_n)$ and $(C'_n-D'_n)$, respectively. $\delta_n = (p_{n-1}-p_n) \;/\; (p_n-p_{n+1})$. p_n is the parameter value at which the residue of the stable orbit of period 5^n is $\sin(\pi/5)$.

Table 2.3.5

n	δ_n	$\alpha_n(1)$	$\alpha_n(2)$	$\alpha_n'(1)$	$\alpha_n'(2)$
2	19.9690	7.40849	0.831189	-29.2454	-5.59284
3	20.0877	-6.24997	-30.8353	1.41469	7.20745
4	20.0436	7.16292	1.40393	-30.8921	-6.04406
5	20.0479	-6.03398	-30.8830	1.40105	7.16761
6	20.0476	7.16827	1.40099	-30.8829	-6.03628
7	20.0478	-6.03657	-30.8834	1.40105	7.16804

n	$\beta_n(1)$	$\beta_n(2)$	$\beta_n'(1)$	$\beta_n'(2)$
2	-17.8562	-8.83636	8.77680	4.35194
3	3.73783	8.14048	-9.09062	-19.4407
4	-19.6196	-9.11968	8.29347	3.85777
5	3.86617	8.30441	-9.11740	-19.5907
6	-19.5885	-9.11757	8.30287	3.86455
7	3.86432	8.30272	-9.11786	-19.5900

Secondly, I describe results for even n-tupling bifurcations, with n=4 ,6 .

As explained in § 2.2, there are two types of 1/4-bifurcation. A pair of stable and unstable orbits of period 4 are born by a 1/4-bifurcation of the 1st type. On the other hand, for $4^n (n \geq 2)$, the 2nd type bifurcation is observed up to n=8. Like the case of 1/3-bifurcation, a pair of stable and unstable orbits of period 4^{n+1} are born when the residue of the orbit of period 4^n is 0.494..., asymptotically. Like the case of odd n-tupling bifurcation, given a residue, the successive parameter values p_n converge to the accumulation point p^* asymptotically geometrically with ratio δ :

$$p_n - p^* \sim \delta^{-n} , \qquad (2.3.14)$$

where $p^* = -0.0689824402834\cdots$,

and

$\delta = 24.45$.

These results are included in the table 2.3.6. So, at this accumulation point the orbits of all classes of 1/4-bifurcation coexist and also they have the same residue values asymptotically. The residues R_+^* and R_-^* of the stable and unstable orbits are:

$$R_+^* = 0.5178\cdots , \qquad (2.3.15)$$

$$R_-^* = -0.02777\cdots .$$

So, the parameter value of the accumulation point is above that of each 1/4-bifurcation point of stable orbits of all classes, asymptotically.

n	p_n	δ_n
1	-0.1	
2	-0.07	23.065
3	-0.06904	25.004
4	-0.06898	24.454
5	-0.0689825	24.478
6	-0.068982448	24.451
7	-0.0689824442	24.450
8	-0.0689824440	

Table 2.3.6: $\delta_n=(p_{n-1}- p_n)/(p_n-p_{n+1})$, where p_n is the parameter value at which a periodic orbit of period 4^n becomes a hyperbolic orbit with reflection.

Figure 2.3.4 shows consecutively enlarged figures of period-quadrupling bifurcations associated with two elliptic symmetric points on the symmetry line y=0. As explained in § 1.2.3, when one periodic point $P_n(0)$of even period ℓ is on the symmetry line y=0, the $(\ell/2)$-th point from that point $P_n(\ell/2)$ is also on the same symmetry line y=0 ($P_n(m)=T^m \cdot P_n(0)$). Unlike the odd n-tupling bifurcation, the dominant elliptic point and the subdominant point appear successively as n increases, respectively. In the figure 2.3.4, A_n is the subdominant point and C_n the dominant point. So, as shown in the figure 2.3.5, the pattern of orbits repeat itself from one bifurcation to the next one asymptotically when magnified by appropriate scaling factors.

Symmetric elliptic points on the line y=0 converge to a limit value x^* geometrically with ratio α :

$$x^* = -0.4086080643\cdots \quad , \qquad (2.3.16)$$
$$\alpha = -5.614 \quad .$$

The ratio α is just the scaling factor along the symmetry line.

We defined various sequences for scaling factors in the table 2.3.7 like the case of odd n-tupling bifurcation and computed them. The results are included in that table. As expected, unlike the case of odd n-tupling bifurcation sequences , these sequences exhibit 'period-1' behaviors, asymptotically. The scaling factors along and across the symmetry line y=0 are :

$$\alpha = -5.614$$

and (2.3.17)

$$\beta = 14.27 \quad .$$

We also studied one further quadrupling bifurcations of $6 \cdot 4^n$. Also, in this case, we obtained the same result. In this case, the orbit of basic period 6 is one bifurcated from the mother orbit of period 3 and so symmetric elliptic points on the line Y=X. Therefore, these self-similar limiting behaviors appear to be universal.

The 1/6-bifurcation sequences also exhibit 'period-1' behaviors like the 1/4-bifurcation sequences.

Given a residue value, the successive parameter values p_n converge to the accumulation point p^* asymptotically geometrically with ratio δ :

$$p_n - p^* \sim \delta^{-n} \quad , \qquad (2.3.18)$$

where $p^* = 0.33623839313\cdots$,

and as shown in the table 2.3.8, the bifurcation ratio δ is:

$$\delta = 13.85 \quad . \qquad (2.3.19)$$

At the accumulation point, the orbits of all classes of 1/6-bifurcation exist and they have the same residue value asymptotically. The residues R_+^* and R_-^* of the stable and unstable orbits are:

$$R_+^* = 0.3130 \quad ,$$

$$R^* = -0.2420 \quad . \qquad (2.3.20)$$

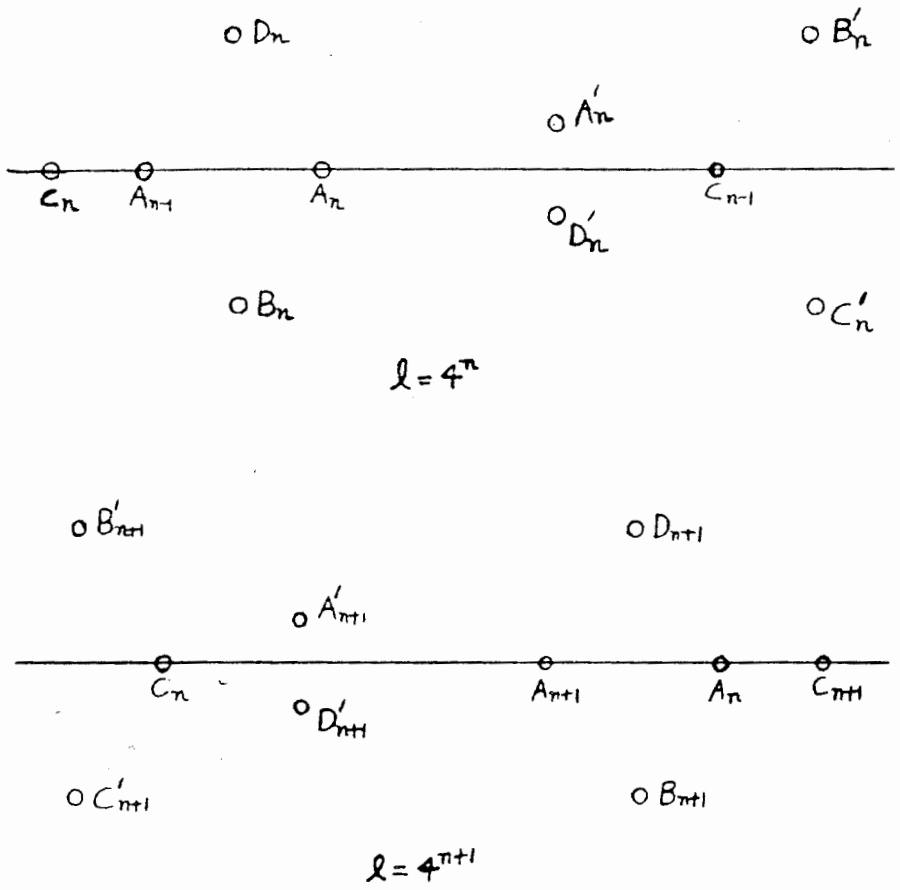

Figure 2.3.4 : Period-quadrupling bifurcations associated with two symmetric elliptic points on the symmetry line y=0 . A_n, B_n, C_n, D_n, A'_n, B'_n, C'_n, and D'_n are ℓ-periodic points corresponding to $P_n(0)$, $P_n(\ell/4)$, $P_n(\ell/2)$, $P_n(3\ell/4)$, $P_n(\ell/8)$, $P_n(3\ell/8)$, $P_n(5\ell/8)$, and $P_n(7\ell/8)$ of the text with $\ell = 4^n$, respectively.

Table 2.3.7 : Period-quadrupling sequences.

$$\alpha_n(1) = (A_n - B_n)_x \;/\; (A_{n+1} - B_{n+1})_x \;,$$

$$\alpha_n(2) = (B_n - C_n)_x \;/\; (B_{n+1} - C_{n+1})_x \;,$$

$$\alpha_n(3) = (A'_n - B'_n)_x \;/\; (A'_{n+1} - B'_{n+1})_x \;,$$

$$\beta_n(1) = (B_n - D_n)_y \;/\; (B_{n+1} - D_{n+1})_y \;,$$

$$\beta_n(2) = (A'_n - D'_n)_y \;/\; (A'_{n+1} - D'_{n+1})_y \;, \text{ and}$$

$$\beta_n(3) = (B'_n - C'_n)_y \;/\; (B'_{n+1} - C'_{n+1})_y \;,$$

are defined with respect to Figure 2.3.4 . $(A_n - B_n)_x$, $(B_n - C_n)_x$ and $(A'_n - B'_n)$ are x-components of $(A_n - B_n)$, $(B_n - C_n)$ and $(A'_n - B'_n)$, and $(B_n - D_n)_y$, $(A'_n - D'_n)_y$ and $(B'_n - C'_n)_y$ y-components of $(B_n - D_n)$, $(A'_n - D'_n)$ and $(B'_n - C'_n)$, respectively .

Table 2.3.7

n	$\alpha_n(1)$	$\alpha_n(2)$	$\alpha_n(3)$	$\beta_n(1)$	$\beta_n(2)$	$\beta_n(3)$
2	-5.6072	-5.8023	-4.7438	14.828	17.148	16.440
3	-5.6169	-5.5718	-5.9847	14.365	13.529	13.628
4	-5.6138	-5.6309	-5.4984	14.294	14.588	14.589
5	-5.6141	-5.6117	-5.6413	14.277	14.211	14.213
6	-5.6142	-5.6151	-5.6078	14.270	14.287	14.287
7	-5.6140	-5.6137	-5.6153	14.269	14.265	14.265

Figure 2.3.5 shows consecutively enlarged figures of the 6-tupling bifurcations associated with two symmetric elliptic points on the symmetry line y=0, when $p=p^*$. On that line, symmetric elliptic points converge to a limit value:

$$x^* = -0.578806968\cdots \quad . \tag{2.3.21}$$

We defined various sequences for scaling factors in the table 2.3.8 and computed them. The results are included in that table. Like the 1/4-bifurcation sequences, these sequences exhibit 'period-1' behaviors, asymptotically. The scaling factors along and across the symmetry line y=0 is:

$$\alpha = -8.25 \quad ,$$
$$\beta = 6.30 \quad . \tag{2.3.22}$$

In summary, for even n-tupling bifurcation with n=4 and 6, n-tupling bifurcation sequences exhibit 'period-1' behaviors at the accumulation point p^* . Period-doubling sequences also exhibit 'period-1' behaviors. But, the limiting self-similar behaviors depend upon n.

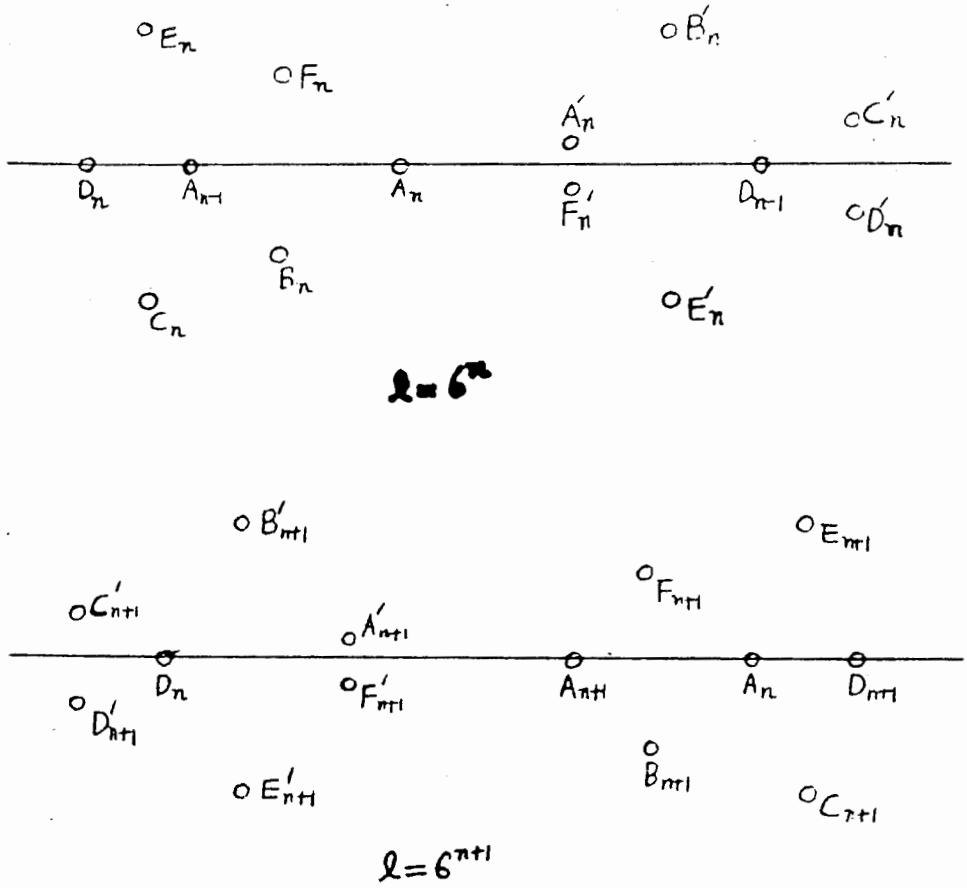

Figure 2.3.5 : Period 6-tupling bifurcations associated with two symmetric elliptic points on the symmetry line y=0 . A_n, B_n, C_n, D_n, E_n, F_n, A'_n, B'_n, C'_n, D'_n, E'_n, and F'_n are ℓ-periodic points corresponding to $P_n(0)$, $P_n(\ell/6)$, $P_n(2\ell/6)$, $P_n(3\ell/6)$, $P_n(4\ell/6)$, $P_n(5\ell/6)$, $P_n(3\ell/36)$, $P_n(9\ell/36)$, $P_n(15\ell/36)$, $P_n(21\ell/36)$, $P_n(27\ell/36)$ with $\ell=6^n$, respectively. $P_n(m) = T^m \cdot P_n(0)$.

Table 2.3.8 : Period 6-tupling sequences.

$$\alpha_n(1) = (A_n - B_n)_x \;/\; (A_{n+1} - B_{n+1})_x \;,$$

$$\alpha_n(2) = (B_n - C_n)_x \;/\; (B_{n+1} - C_{n+1})_x \;,$$

$$\alpha_n(3) = (C_n - D_n)_x \;/\; (C_{n+1} - D_{n+1})_x \;,$$

$$\alpha_n(4) = (A'_n - B'_n)_x \;/\; (A'_{n+1} - B'_{n+1})_x \;,$$

$$\alpha_n(5) = (B'_n - C'_n)_x \;/\; (B'_{n+1} - C'_{n+1})_x \;,$$

$$\beta_n(1) = (B_n - F_n)_y \;/\; (B_{n+1} - F_{n+1})_y \;,$$

$$\beta_n(2) = (C_n - E_n)_y \;/\; (C_{n+1} - E_{n+1})_y \;,$$

$$\beta_n(3) = (A'_n - F'_n)_y \;/\; (A'_{n+1} - F'_{n+1})_y \;,$$

$$\beta_n(4) = (B'_n - E'_n)_y \;/\; (B'_{n+1} - E'_{n+1})_y \;, \quad \text{and}$$

$$\beta_n(5) = (C'_n - D'_n)_y \;/\; (C'_{n+1} - D'_{n+1})_y$$

are defined with respect to Figure 2.3.5 .

$(A_n - B_n)_x$, $(B_n - C_n)_x$, $(C_n - D_n)_x$, $(A'_n - B'_n)_x$ and $(B'_n - C'_n)_x$ are x-components of $(A_n - B_n)$, $(B_n - C_n)$, $(C_n - D_n)$, $(A'_n - B'_n)$ and $(B'_n - C'_n)$, and $(B_n - F_n)_y$, $(C_n - E_n)_y$, $(A'_n - F'_n)_y$, $(B'_n - E'_n)_y$, and $(C'_n - D'_n)_y$ y-components of $(B_n - F_n)$, $(C_n - E_n)$, $(A'_n - F'_n)$, $(B'_n - E'_n)$, and $(C'_n - D'_n)$, respectively .

$\delta_n = (p_{n-1} - p_n) \;/\; (p_n - p_{n+1})$, where p_n is the parameter value at which the residue of the orbit of period 6^n is 1/4 .

Table 2.3.8

n	δ_n	$\alpha_n(1)$	$\alpha_n(2)$	$\alpha_n(3)$	$\alpha_n(4)$	$\alpha_n(5)$
2	13.91	-9.820	-9.099	-9.234	1.307	-5.298
3	13.82	-8.006	-8.206	-8.268	-10.36	-10.04
4	13.84	-8.340	-8.285	-8.260	-7.832	-8.094
5	13.85	-8.248	-8.257	-8.261	-8.281	-8.283
6	13.85	-8.257	-8.254	-8.252	-8.231	-8.254

n	$\beta_n(1)$	$\beta_n(2)$	$\beta_n(3)$	$\beta_n(4)$	$\beta_n(5)$
2	6.080	5.596	12.24	12.01	11.67
3	6.289	6.353	5.226	5.202	5.128
4	6.290	6.282	6.454	6.453	6.457
5	6.300	6.300	6.289	6.284	6.281
6	6.303	6.303	6.306	6.306	6.305

In the above, we show numerically that there exist limiting self-similar behaviors at the accumulation point ($p=p^*$) on smaller spatialscales. In fact, even more asymptotically self-similar behaviors exist near the accumulation point (Lee et al, 1984, 1985). Given a residue value R, let p_n be the parameter value at which periodic orbit of class-n has R. Then, asymptotically, the pattern of the periodic orbit of class-n when $p=p_n$ appears to be the same as that of the periodic orbit of class-m when $p=p_m$ on smaller spatial scales, where m is (n-1) for even n and (n-2) for odd n. So, when the parameter and the dynamic variables are rescaled with the rescaling factors δ, α and β , the pattern of periodic orbits also repeats itself from one bifurcation to the next for even n-tupling bifurcations and to every other for odd n-tupling bifurcations.

§ 2.4 Renormalization Analysis of Bifurcations

We(1986) also studied the asymptotically self-similar island structures described in the previous section by a simple approximate renormalization method.

The renormalization method was introduced into the dynamical system first by Feigenbaum(1978,1979) to study the Feigenbaum sequence in 1-dim. noninvertible maps with one extremum . The method soon extended to the 2-dim. area-preserving maps for the study of period-doubling sequences and critical invariant curves. Collet et al (1981), and Widom and Kadanoff (1982) solved directly the fixed point equation for the renormalization of 1/2-bifurcation in map and action space, respectively and obtained an approximate fixed point, the scaling factors and the bifurcation ratio. Using MACSYMA, Greene et al (1981) also obtained an approximate universal map, but they used the information of the accumulation point and the scaling factors obtained by directly following 1/2-bifurcation sequence. However, these methods of directly solving the fixed point equation for the renormalization of 1/n-bifurcation become rapidly intractable as n increases. Therefore, for higher n-tupling bifurcation, it is desirable to use an approximate renormalization method in which the difficulty of calculations does not increase significantly with n.

The approximate renormalization method used in this thesis may be called the method of quadratic approximants. Since the self-similarity is an asymptotic property valid

only in the immediate vicinity of symmetric elliptic point, we expect that it would be sufficient to retain upto quadratic terms in the Taylor expansion of the composed map. So, the quadratic approximant is formed by keeping the terms to the 2nd order in the Taylor expansion of the nth iterate of a map T, i.e. T^n. Then, comparison of successive approximants of a 1/n-bifurcation gives the accumulation point p^*, the bifurcation ratio δ, the scaling factors α and β, and the universal residue value R^*. Furthermore, by looking at the recurrence relation between $T^{n^{\ell}}$ and $T^{n^{\ell+1}}$ as ℓ increases, we can make better approximations and obtain the approximate universal map T^*:

$$T^* = \lim_{\ell \to \infty} A^{\ell} \cdot T_{p^*}^{n^{\ell}} \cdot A^{-\ell} \quad , \qquad A = \begin{bmatrix} \alpha & 0 \\ 0 & \beta \end{bmatrix} .$$

Actually Helleman(1980) and Helleman and Mackay(1983) used this method for 1/2-bifurcation. In their calculation they compare quadratic approximants for T and T^2, i.e. the lowest pair of approximants. We(1986) made better approximations analytically by comparing the next higher approximants for T^2 and T^4 . Although approximants for low order iterates can be handled analytically , it is imperative to resort to numerical method for quadratic approximants for high order iterates of T for 1/n-bifurcation with high n and high order calculations. So, by the numerical implementation of this simple method, we obtained universal maps, scaling factors, bifurcation ratios and universal residue values for 1/n-bifurcation, with n=2 to 6.

Recently Lichtenberg(1985) obtained accumulation points for higher n-tupling bifurcations(n>2)in the standard map by a simple method. He reconstitutes approximately a local standard map about a single island of period n (n>2). Through this procedure he obtains a recurrence relation between the old parameter of the original map and the new one of the local map, and calculates the accumulation point as the fixed point of the recurrence relation. However, in effect, his one-shot renormalization scheme amounts to our lowest $\ell(\ell=1)$ approximation.

As an example, we take 1/2-bifurcation and describe our method briefly. Let us denote the subdominont point of period 2^{ℓ} as $(\hat{x}_{\ell}, 0)$. Then, the idea of the renormalization method is to associate, for each p', a value p such that $T_p^{2^{\ell}}$ with origin $(\hat{x}_{\ell},0)$ looks the same as $T_{p'}^{2^{\ell-1}}$ on a small spatial scale:

$$T_{p'}^{2^{(\ell-1)}} = A \cdot T_p^{2^{\ell}} \cdot A^{-1} , \qquad (2.4.1)$$

where A is the geometric rescaling matrix:

$$A = \begin{bmatrix} \alpha & 0 \\ 0 & \beta \end{bmatrix} .$$

If we denote $T_p^{2^{\ell}}$ as

$$T_p^{2^{\ell}} : \begin{bmatrix} x \\ y \end{bmatrix} \rightarrow \begin{bmatrix} x' = F_p^{(\ell)}(x,y) \\ y' = G_p^{(\ell)}(x,y) \end{bmatrix} ,$$

then $F_p^{(\ell)}(\hat{x}_\ell, 0) = 0$ and $G_p^{(\ell)}(\hat{x}_\ell, 0) = 0$.

Let us first make Taylor-expansions of $F_p^{(\ell)}$ and $G_p^{(\ell)}$ about $(\hat{x}_\ell, 0)$. Then,

$$F_p^{(\ell)}(x,y) = \hat{x}_\ell + A_\ell(p)\cdot(x-\hat{x}_\ell) + B_\ell(p)\cdot y + U_\ell(p)\cdot(x-\hat{x}_\ell)^2 + V_\ell(p)\cdot(x-\hat{x}_\ell)\cdot y + W_\ell(p)\cdot y^2 + \cdots ,$$

$$G_p^{(\ell)}(x,y) = C_\ell(p)\cdot(x-\hat{x}_\ell) + D_\ell(p)\cdot y + Q_\ell(p)\cdot(x-\hat{x}_\ell)^2 + R_\ell(p)\cdot(x-\hat{x}_\ell)\cdot y + S_\ell(p)\cdot y^2 + \cdots .$$

Since the self-similarity holds in the vicinity of the periodic point, we expect that it would be sufficient to keep the terms to the 2nd order in Taylor-expansion.

Let us define the linearized map $M_p^{(\ell)}(x,y)$ of $T_p^{2^\ell}(x,y)$ as

$$M_p^{(\ell)}(x,y) = DT_p^{2^\ell}(x,y) = \begin{bmatrix} H_p^{(\ell)}(x,y) & I_p^{(\ell)}(x,y) \\ J_p^{(\ell)}(x,y) & K_p^{(\ell)}(x,y) \end{bmatrix} , \qquad (2.4.2)$$

by introducing four functions $H_p^{(\ell)}$, $I_p^{(\ell)}$, $J_p^{(\ell)}$ and $K_p^{(\ell)}$.

Here the area-preserving condition is given by

$$H_p^{(\ell)}\cdot K_p^{(\ell)} - I_p^{(\ell)}\cdot J_p^{(\ell)} = 1 \quad \text{for any } (x,y). \qquad (2.4.3)$$

Then, the coefficients of linear terms of Taylor-expansions can be represented by :

$$A_{\ell}(p) = H_p^{(\ell)}(\hat{x}_{\ell}\ ,\ 0),\ B_{\ell}(p) = I_p^{(\ell)}(\hat{x}_{\ell}\ ,\ 0),$$

$$C_{\ell}(p) = J_p^{(\ell)}(\hat{x}_{\ell}\ ,\ 0) \text{ and} \qquad (2.4.4)$$

$$D_{\ell}(p) = K_p^{(\ell)}(\hat{x}_{\ell}\ ,\ 0) = (1+B_{\ell}\cdot C_{\ell})/A_{\ell}\ .$$

On the other hand, in symmetry coordinates, $A_{\ell}=D_{\ell}$ (Mackay, 1982). So, the trace of the Jacobian matrix of $T_p^{2^{\ell}}$ about $(\hat{x}_{\ell}\ ,0)$ is:

$$\mathrm{Tr}M_{\ell}(p) = 2A_{\ell}(p) \qquad (2.4.5)$$

The coefficients of quadratic terms are also represented by the derivatives of the above four functions:

$$U_{\ell}(p) = \frac{1}{2}\cdot\frac{\partial H_p^{(\ell)}}{\partial x}\bigg|_{(\hat{x}_{\ell},0)},\quad V_{\ell}(p) = \frac{\partial I_p^{(\ell)}}{\partial x}\bigg|_{(\hat{x}_{\ell},0)},$$

$$Q_{\ell}(p) = \frac{1}{2}\cdot\frac{\partial J_p^{(\ell)}}{\partial x}\bigg|_{(\hat{x}_{\ell},0)},\quad W_{\ell}(p) = \frac{1}{2}\cdot\frac{\partial I_p^{(\ell)}}{\partial y}\bigg|_{(\hat{x}_{\ell},0)},$$

$$R_{\ell}(p) = \frac{\partial K_p^{(\ell)}}{\partial x}\bigg|_{(\hat{x}_{\ell},0)} = (2B_{\ell}\cdot Q_{\ell}+C_{\ell}\cdot V_{\ell}-2D_{\ell}\cdot U_{\ell})/D_{\ell}\ , \qquad (2.4.6)$$

and

$$S_{\ell}(p) = \frac{1}{2}\cdot\frac{\partial K_p^{(\ell)}}{\partial x}\bigg|_{(\hat{x}_{\ell},0)} = (B_{\ell}\cdot R_{\ell}+2C_{\ell}\cdot W_{\ell}-D_{\ell}\cdot V_{\ell})/(2D_{\ell})\ .$$

In (2.4.4) and (2.4.6), the area-preserving condition (2.4.3) is used to express D_{ℓ}, R_{ℓ} and S_{ℓ} in terms of the other coefficients. In such a way, the quadratic approximant of $T^{2^{\ell}}$ is formed to keep the terms to the 2nd order of the Taylor-expansion of $T_p^{2^{\ell}}$ about the subdominant point. Then,

substituting the quadratic approximants of $T_{p'}^{2^{l-1}}$ and $T_p^{2^l}$ into(2.4.1) , we have

$$A_{l-1}(p')=A_l(p) , \qquad D_{l-1}(p')=D_l(p) ,$$

$$B_{l-1}(p')= \frac{\alpha}{\beta} B_l(p) , \qquad C_{l-1}(p')= \frac{\beta}{\alpha} C_l(p) ,$$

$$U_{l-1}(p')= \frac{1}{\alpha} U_l(p) , \qquad V_{l-1}(p')= \frac{1}{\beta} V_l(p) ,$$

$$W_{l-1}(p')= \frac{\alpha}{\beta^2} W_l(p) , \qquad Q_{l-1}(p')= \frac{\beta}{\alpha^2} Q_l(p) ,$$

$$R_{l-1}(p')= \frac{1}{\alpha} R_l(p) , \text{ and } \quad S_{l-1}(p')= \frac{1}{\beta} S_l(p) . \qquad (2.4.7)$$

Comparing the diagonal coefficients of the linear terms of $T_p^{2^l}$ with origin$(\hat{x}_l ,0)$ and $T_{p'}^{2^{l-1}}$ with origin $(\hat{x}_{l-1} ,0)$, we can obtain the accumulation point p^* and the bifurcation ratio δ as follows. By (2.4.5) and (2.4.7) , we have :

$$\text{Tr } M_{l-1}(p') = \text{Tr } M_l(p) . \qquad (2.4.8)$$

This recurrence relation (2.4.8) can be also obtained by the method of Derrida and Pomeau(1980). The fixed point of the recurrence relation gives the accumulation point p^*:

$$\text{Tr } M_{l-1}(p^*) = \text{Tr } M_l(p^*) , \qquad (2.4.9)$$

and the bifurcation ratio is given by an equation :

$$\delta = \frac{dp'}{dp}\Big|_{p^*} = \frac{d(\text{Tr } M_l(p))/dp \,|_{p^*}}{d(\text{Tr } M_{l-1}(p'))/dp' \,|_{p^*}} . \qquad (2.4.10)$$

As l increases, naturally one can obtain more accurate values.

For the first two-orders, explict analytic recurrence relations can be easily derived, and thus Derrida and Pomeau(1980) obtained p and δ to the second order. We extend the calculations to higher orders. Our method is as follows. For any given (x_1, y_1), the function values of $H_p^{(k)}$, $I_p^{(k)}$, $J_p^{(k)}$ and $K_p^{(k)}$ in (2.4.2) are easily calculated from

$$m_p^{(k)}(x_1,y_1)=\begin{bmatrix} H_p^{(k)}(x_1,y_1) & I_p^{(k)}(x_1,y_1) \\ J_p^{(k)}(x_1,y_1) & K_p^{(k)}(x_1,y_1) \end{bmatrix} = \prod_{i=1}^{2^k} m_i \ , \tag{2.4.11}$$

where

$$m_i = DT_p = \begin{bmatrix} f_p'(x_i) & -1 \\ 1-f_p'(x_{i+1})\cdot f_p'(x_i) & f_p'(x_{i+1}) \end{bmatrix} ,$$

$$f_p'(x_i) = p - 2\cdot(1-p)\cdot x_i \quad \text{and} \quad \begin{bmatrix} x_{i+1} \\ y_{i+1} \end{bmatrix} = T_p \begin{bmatrix} x_i \\ y_i \end{bmatrix} .$$

Therefore, Tr $M_k(p)$is readily calculated after finding the periodic orbit of period 2^k. That is,

$$\text{Tr } M_k(p) = 2\cdot H_p^{(k)}(\hat{x}_k, 0) \ . \tag{2.4.12}$$

The equation for p to be solved is given by :

$$F(p)= \text{Tr } M_k(p) - \text{Tr } M_{k-1}(p) = 0 \ . \tag{2.4.13}$$

The root of F(p)=0 is just the accumulation point p^* and the universal residue R^* is (2-Tr $M_k(p^*)$)/4. Also, the bifurcation ratio δ is the ratio of the slopes of Tr $M_k(p)$and Tr $M_{k-1}(p')$ at the accumulation point(see (2.4.10)). At $p=p^*$, the derivatives of Tr $M_k(p)$ and Tr $M_{k-1}(p')$ are calculated by ordinary differen-

tiation routine. We numerically solve (2.4.13) and (2.4.10), and obtain p^* and δ to the 6th order (see the table 2.4.1). As shown in that table, we have more accurate values as ℓ increases.

Once we have p^*, we can obtain the scaling factors α and β through (2.4.7). At the accumulation point p^*, we first find the subdominot point of period 2^ℓ and calculate the function values of $H_p^{(\ell)}$, $I_p^{(\ell)}$, $J_p^{(\ell)}$ and $K_p^{(\ell)}$ at $(\hat{x}_\ell, 0)$ through (2.4.11). Next, we calculate the derivative values of them at $(\hat{x}_\ell, 0)$ by ordinary differentiation routine. Thus, at $p=p^*$, we obtain the quadratic approximants of $T_{p*}^{2^{\ell-1}}$ and $T_{p*}^{2^\ell}$. Then, by (2.4.7), when $p=p^*=p'$, we obtain not only the ratio of the scaling factors α/β comparing the off-diagonal coefficients of the linear terms, but also the scaling factors α and β, separately comparaing the quadratic coefficients. As shown in the table 2.4.1, we obtain more accurate values of α and β as ℓ increases.

Finally, we obtain an approximate universal map of 1/2-bifurcation as follows. We define a renormalization transformation N :

$$T' = N(T) = A\, T^2\, A^{-1} \quad ,$$

where $A = \begin{bmatrix} \alpha & 0 \\ 0 & \beta \end{bmatrix}$ and the subdominant point of period 2 in T lies at the origin. Let us define T_ℓ as the ℓ-times renormalized map. That is, $T_\ell = N^\ell(T_0) = A^\ell \cdot T_0^{2^\ell} \cdot A^{-\ell}$ with origin $(\hat{x}_\ell, 0)$. If we put $T_0 = T_{p*}$, then $\lim_{\ell\to\infty} T_\ell = T^*$,

as shown in the figure 2.4.1. Then, we have approximately $T^* \simeq A^{\ell} \cdot T^{2^{\ell}} \cdot A^{-\ell}$ for large ℓ. Thus, we have an approximate universal map T^* of 1/2-bifurcation:

$$T^* \simeq A^{\delta} \cdot T_{p*}^{2^{\delta}} \cdot A^{-\delta}$$

$$= \begin{bmatrix} x' = -1.27176x - 1.01322y - 2.31933x^2 + 0.334822xy + \cdots \\ y' = -.609305x - 1.27176y + .793849x^2 + 5.91963xy + \cdots \end{bmatrix}$$

and thus the universal residue R^* is :

$$R^* = 1.13588 \quad .$$

Consider the linearization of N, dN, in the neighborhood of T^*. Then, it has one relevant eigenvalue δ outside the unit circle which is coordinate independent. Of course, there exist coordinate dependent unstable eigenvalues (Mackay, 1982). However, it is possible to choose coordinates for a system in order that it have no components in those unstable directions(Mackay,1982). These coordinates are called scaling coordinates. Maps in the figure 2.4.1 are represented in terms of scaling coordinates. So, only one relevant eigenvalue δ exist. The horizontal line in that figure represents maps in which the parameters are fixed at the accumulation points. This is called the critical surface of maps. So, all maps in this surface converge to T^* under the renormalization N. In such a sense, the limiting self-similar behaviors are universal. The vertical line in that figure represents a universal 1-parameter family. This unviersal 1-parameter satisfies :

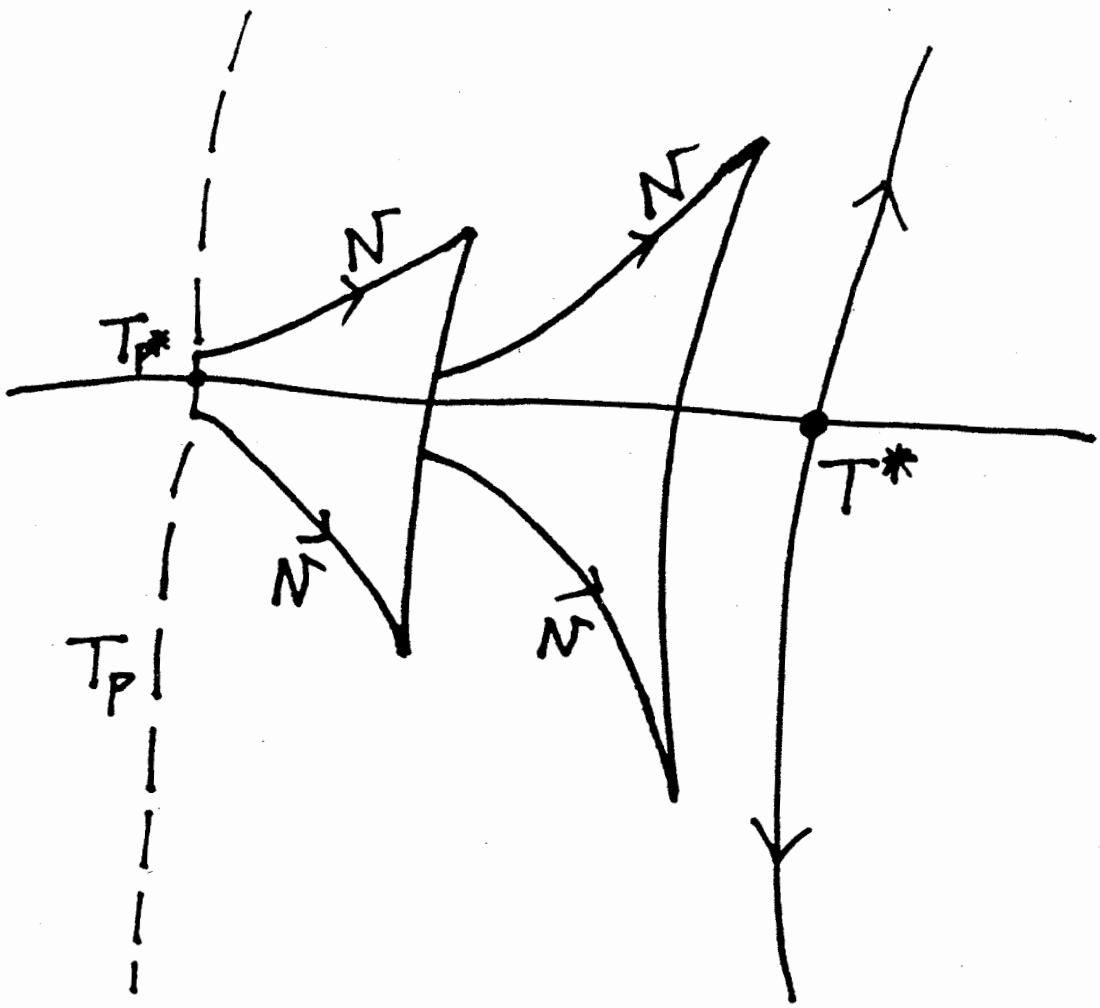

Figure 2.4.1 : A sketch of flow produced by the renormalization operator N in the infinite dim. function space. The dashed line represents a 1-parameter family.

$$T^*_{\mu\cdot\delta} = N(T^*_\mu) \quad ,$$

where μ is the scaling parameter and thus at $\mu=0$, the map is T^*. As shown in the figure, a 1-parameter family of maps near the accumulation point converges to the universal 1-parameter under the renormalization.

The renormalization method can be also applied to 1/3-, 1/4-, 1/5- and 1/6-bifurcations. However, since 1/3- and 1/5-bifurcation sequences exhibit 'period-2' behaviors, the renormalization transformation N now must be:

$$T' = N(T) = A\cdot T^{n^2}\cdot A^{-1} \quad ,$$

where n=3 and 5. Let T_0 be the initial map. We define T_ℓ by:

$$T_\ell = N^\ell(T_0) = A^\ell\cdot T_0^{n^{2\ell}}\cdot A^{-\ell} \quad .$$

Then, for $T_0 = T_{p*}$ we have :

$$\lim_{\ell\to\infty} A^\ell\cdot T_{p*}^{n^{2\ell}}\cdot A^{-\ell} = T^*$$

and for $T_0 = T^n_{p*}$ we have:

$$\lim_{\ell\to\infty} A^\ell\cdot T_{p*}^{n^{(2\ell+1)}}\cdot A^{-\ell} = T^{**} \quad .$$

Therefore, unlike even n-tupling bifurcation, we have two fixed T^* and T^{**} : T^* and T^{**} are the universal maps which describe the phase flows near the subdominant and dominant elliptic points, respectively. However, the linearization of N, dN, near these two fixed points has the same relevant eigenvalue δ.

Using this method, we have performed the calculations to higher order for 1/3-,1/4-,1/5- and 1/6-bifurcations. The results of p^*, δ, α and β are listed in the table 2.4.2.

For 1/4- and 1/6-bifurcations, like 1/2-bifurcation, we obtained a single approximate universal map. For 1/4-bifurcation, we have :

$$T^* \propto A^5 . T_{p*}^{4^5} . A^{-5}$$

$$= \begin{bmatrix} x' = -0.03561x-1.0114y-1.251x^2-0.3308xy+\cdots \\ y' = 0.9874x-0.03561y-0.1982x^2+0.4157xy+\cdots \end{bmatrix}$$

with $R^* = .51781$

and for 1/6-bifurcation, we have :

$$T^* \propto A^5 . T_{p*}^{6^5} . A^{-5}$$

$$= \begin{bmatrix} x' = 0.374x-1.129y-0.764x^2-0.623xy+\cdots \\ y' = 0.7617x+0.374y+0.0588x^2-0.0967xy+\cdots \end{bmatrix} .$$

As explained above, for 1/3- and 1/5-bifurcations, there exist two universal maps. For 1/3-bifurcation, they are:

$$T^* \propto A^3 . T_{p*}^{3^6} . A^{-3}$$

$$= \begin{bmatrix} x' = -0.46742x-0.908416-1.737x^2-0.23725xy+\cdots \\ y' = 0.86032x-0.46742y-0.58538x^2+1.8279xy+\cdots \end{bmatrix}$$

and

$$T^{**} \propto A^{3}.T_{p*}^{3^{7}} .A^{-3}$$

$$= \begin{bmatrix} x' = -0.46742x+0.28035y-17.773x^2-18.059xy+\cdots \\ y' = -2.7877x-0.46742y'-32.037x^2-33.728xy+\cdots \end{bmatrix}$$

with $R^* = 0.73371$,

and for 1/5-bifurcation, they are :

$$T^* \propto A^{2}.T_{p*}^{5^{4}} .A^{-2}$$

$$= \begin{bmatrix} x'=.2217x-.46y-1.4x^2-.377xy+\cdots \\ y'= 2.07x+.2217y-.215x^2 + .162xy\cdots \end{bmatrix}$$

and

$$T^{**} \propto A^{2}.T_{p*}^{5^{5}} .A^{-2}$$

$$= \begin{bmatrix} x'=.2217x+.27y-15.9x^2-3.21xy+\cdots \\ y'= -3.52x+.2217y-41.4x^2-18.3xy+\cdots \end{bmatrix}$$

with $R^*=.3892$.

ℓ	p^*	δ	α	β
1	-1.265564	9.0623	-4.1204	17.012
2	-1.266321	8.6845	-4.0059	16.294
3	-1.26631115	8.72541	-4.01992	16.3729
4	-1.2663112786	8.720596	-4.01775	16.3627
5	-1.266311276899	8.721156	-4.01814	16.3641
6	-1.2663112769223	8.721090	-4.01806	16.36386
known best values	-1.2663112769221	8.721097	-4.0180767	16.363897

Table 2.4.1: The various quantities obtained by an approximate renormalization method for 1/2-bifurcation. Known best values are those obtained by Greene et al(1981) by following 1/2-sequence.

m/n-bifurcation	ℓ	p^*	δ	α	β
1/3	3	-.477013684274045	407.4254	-43.9794	-186.723
Known best values		-.477013684274048	407.422	-43.9807	-186.7
1/4	5	-.0689824440291	24.4616	-5.6119	14.2824
Known best values		-.0689824440286	24.45	-5.6141	14.269
1/5	2	.177137427506	401.75	-43.34	-76.09
Known best values		.177137427510	401.92	-43.27	-75.70
1/6	5	.3362383932	13.83	-8.248	6.032
Known best values		.3362383931	13.85	-8.25	6.30

Table 2.4.2: The various quantities obtained by an approximate renormalization method for 1/n-bifurcation, with n=3 to 6. Known best values are those obtained by following 1/n-sequence in our works(1984, 1985).

§ 2.5 Critical behavior of an invariant circle in a C^2-map

In this section, we study whether or not invariant circles exist in a map of class-C^2. In this case, persistence of invarinat circles is not guaranteed by Moser's twist theorem, since the sufficient critical smoothness of a map is now class-$C^r(r>3)$in that theorem (§ 1.3.1).

Following Greene's residue criterion (see § 1.3.2), we show numerically that a nobel invariant circle persists below a critical parameter value. Therefore, below the critical parameter value, the invariant cirlce plays the role of a complete barrier to the trnasport of stochastic orbits. We also observed that the critical behavior of that invariant circle appears to be the same as that in analytic maps. On the other hand, Herman(1983) has $C^r(r<\tau)$-counterexamples to Moser's twist theorem. So, for a map of class-$C^r(r<3)$ invariant circles may or may not exist, depending on the map.

In this section, we study an area-preserving map of class-C^2, T which has a unit Jacobian (det(DT)=1) :

$$T:\begin{cases} I' = I + \epsilon F(\theta) \\ \theta' = \theta + I' \end{cases}, \qquad (2.5.1)$$

$$\text{where } F(\theta) = \begin{cases} 4\theta^3 - 3\theta/4 , & 0 \le \theta \le 1/4 \\ -4(\theta-\tfrac{1}{2})^3 + \frac{3}{4}\cdot(\theta-\tfrac{1}{2}) , & 1/4 \le \theta \le 3/4 \\ 4(\theta-1)^3 - \frac{3}{4}\cdot(\theta-1) , & 3/4 \le \theta \le 1 , \end{cases}$$

$$\int_0^1 F(\theta)\cdot d\theta = 0 .$$

Since the map T has a rotational shear ($\left(\frac{\partial\theta'}{\partial I}\right|_{\theta} > 0$), T is a twist map(see § 1.1.2). So, the map can be obtained from a generating function L such that $I=-\partial L(\theta,\theta')/\partial\theta$ and $I'=\partial L(\theta,\theta')/\partial\theta'$,

where $L(\theta,\theta') = \frac{1}{2}\cdot(\theta,\theta')^2 - \epsilon\cdot V(\theta)$ (2.5.2)

and

$F(\theta) = - V'(\theta)$.

From the stationary action principle (see § 1.2.2) a periodic sequence$\{\theta_t\}$ with $\theta_{t+q}=\theta_t+p$ yields a periodic orbit of rotation number p/q if its action:

$$A = \sum_{t=0}^{q-1} L(\theta_t, \theta_{t+1}) \qquad (2.5.3)$$

is stationary with respect to variations keeping $\theta_q=\theta_0+p$.

T is also reversible, since T can be factored into the product (TS)·S of two orientation-reversing involutions, where

$$S:\begin{bmatrix} \theta' = -\theta \\ I' = I + \epsilon\, F(\theta) \end{bmatrix} \quad . \qquad (2.5.4)$$

The four symmetry half-lines formed from the invariant points under S and TS are the lines $\theta=0$, $\theta=\frac{1}{2}$, $I=2\theta$ and $I=2\theta-1$.

We study the most robust invariant circle. The most robust invariant circle is one that is the farthest from nearby islands(see § 1.3.2). The continued fraction representation of the rotation number of that invariant circle is :

$$\nu = [m_0, m_1, m_2, \cdots] = [0, 2, (1,)^{\infty}] = \gamma^{-2}, \qquad (2.5.5)$$

$$\gamma = (1+\sqrt{5})/2 \ ,$$

and the rational approximant r_n of ν is:

$$r_n = p_n/q_n = [m_0, m_1, \cdots, m_n] \ ,$$

$$p_{n+1} = m_{n+1} \cdot p_n + p_{n-1} \ , \quad p_{-2} = 0 \ , \ p_{-1} = 1 \ , \qquad (2.5.6)$$

$$q_{n+1} = m_{n+1} \cdot q_n + q_{n-1} \ , \quad q_{-2} = 1 \ , \ q_{-1} = 0 \ .$$

Following Greene's residue criterion, we show that the invariant circle of rotation number γ^{-2} persists under a critical parameter value ϵ^*. Near ϵ^*, it is observed that given a rotation number p_n/q_n, a pair of periodic orbits of the rotation number exist. As explained in § 1.2.2, one is a minimizing orbit , the other is minimaximizing one , and the differences in the actions F_n between the two orbits can be interpreted as the area that is transported between the two orbits per iteration. Mather (referred to by Mackay 1982) has shown that given a sequence of rational approximants $p_n/q_n \to \nu$, there exists an invariant circle of rotation ν if and only if $F_\nu = \lim_{n\to\infty} F_n = 0$. When F_ν is nonzero , Mather (referred to by Mackay, 1982), Aubry and Daeron(1983), and Katok(1982) has shown that a hyperbolic invariant set of rotation number ν, i.e. the so-called cantorus, exists. The cantorus can be regarded as a circle with a dense set of countably infinite gaps caused by overlap of nearby island chains.

The critical parameter value ϵ^* can be obtained as follows. We follow the parameter values ϵ_n such that the minimaximizing periodic orbit of rotation number p_n/q_n corresponding to the nth rational approximant to γ^{-2} has some given residue, e.g. 1. The limit value of (ϵ_n)-sequence is just the critical parameter value ϵ^*. The convergence ratio δ is the limit value of (δ_n)-sequence defined by $\delta_n=(\epsilon_{n-1}-\epsilon_n)/(\epsilon_n - \epsilon_{n+1})$. These sequences are shown in the table 2.5.1. By superconverging the results, we obtained ϵ^* and δ:

$$\epsilon^* = 1.3630577 \text{ and } \delta = 1.628 \quad . \qquad (2.5.7)$$

Thus, the parameter value ϵ_n converges to the critical parameter value geometrically, asymptotically:

$$\epsilon_n - \epsilon^* \sim \delta^{-n} \quad . \qquad (2.5.8)$$

In the subcritical, critical and supercritical cases, we calculated the residues R_n^- and R_n^+ of the minimizing and minimaximizing periodic orbits of rotation number p_n/q_n, their action difference F_n and the θ-coordinate θ_n of the nearest minimizing periodic point to the dominant symmetry line(θ=0). Near ϵ^*, all the minimaximizing periodic point tend to have a point on the dominant symmetry line and the relations between periodic points and the other three sub-dominant half-lines are shown in the table 1.1.3.1.

As shown in the figures 2.5.1 and 2.5.2, when $\epsilon<\epsilon^*$ $R_n^{\pm}$ approaches to zero and when $\epsilon>\epsilon^*$ $R_n^{\pm}$ diverge to $\pm\infty$. The results are shown in the tables 2.5.2 and 2.5.3 in details.

For the critical case, $R_n^{\pm}$ approaches to some finite value:

$$R_+^* = 0.250 \qquad (2.5.9)$$

and

$$R_-^* = -0.255 \ .$$

Therefore, when the residues of nearby minimaximizing orbits are nearly 1/4, the invariant circle of rotation number γ^{-2} is on the edge of disappearence.

Figure 2.5.3 shows the flux F_n. In the critical case, as shown in the table 2.5.5, the ratio F_n/F_{n+1} approaches to some value ξ. Here ξ is the area-scaling factor of nearby islands and the observed value of ξ is :

$$\xi = 4.3390 \ . \qquad (2.5.10)$$

Therefore, F_n obeys a power law decay :

$$F_n \sim q_n^{-d} \ , \ d_o = \log_\gamma \xi \simeq 3.0499 \ . \qquad (2.5.11)$$

In the subcritical case, as shown in the figure 2.5.3 and the table 2.5.4, F_n approaches to zero at a rate faster than that in the critical case. On the other hand, when $\epsilon > \epsilon^*$, F_n approaches to some nonzero value. In this case, the invariant circle is broken into a cantorus. As shown in the table 2.5.4, at $\epsilon = \epsilon^* + 10^{-3}$, the observed flux through the cantorus is 1.23×10^{-11}.

The θ-coordinate θ_n of the nearest minimizing periodic point to the dominant symmetry line approaches to zero when $\epsilon \leq \epsilon^*$, as shown in the figure 2.5.4 and the table 2.5.5. In

the critical case, θ_n obeys a power law decay(see the table 2.5.6):

$$\theta_n \sim q_n^{-x_0} \quad , \qquad x_0 = 0.7211 \quad . \qquad (2.5.12)$$

Therefore, the critical invariant circle is not differentiably but topologically conjugate to uniform rotation. On the other hand, when $\epsilon=\epsilon^* + 10^{-3}$, the observed limiting value of θ_n is 2.22×10^{-3}. This is the half-width of the gap lying on the dominant symmetry. Since the forward and backward images of this gap are also gaps, the invariant circle is broken into the cantorus with an infinity of gaps.

Figure 2.5.5 shown orbits near the Golden Mean invariant circle at ϵ^*. That invariant cirlce plays the role of a complete barrier. For example, with an initial condition: $(\theta,I)=(0.5,0.05)$ in the figure 2.5.6, we have iterated the map 10^6 times. As shown in that figure, the orbit with that initial condition is confined by the Golden Mean invariant circle. On the other hand, when $\epsilon>\epsilon^*$, extended chaos occurs, as shown in the figure 2.5.7. The dark part in the figure is formed by iterating the map $2\cdot10^5$ times with an initial condition : $(\theta,I)=(0.5,0.1)$.

To sum up, the Golden-Mean invariant circle persists below the critical parameter value in the map T (2.5.1) of class-C^2.

n	ϵ_n	δ_n
3	1.72791753	
4	1.56942565	1.94941
5	1.48812316	1.59105
6	1.43702338	1.78782
7	1.40844114	1.58694
8	1.39043019	1.71734
9	1.37994250	1.59142
10	1.37335234	1.66866
11	1.36940298	1.60707
12	1.36694548	1.64267
13	1.36544944	1.61811
14	1.36452488	1.63471
15	1.36395930	1.62591
16	1.36361144	1.62855
17	1.36339784	1.62802
18	1.36326664	1.62793
19	1.36318605	1.62815
20	1.36313655	1.62791
21	1.36310614	

Table 2.5.1 : Parameter values ϵ_n for the nth convergent minimaximizing periodic orbit to have residue 1 and the convergence ratio δ_n

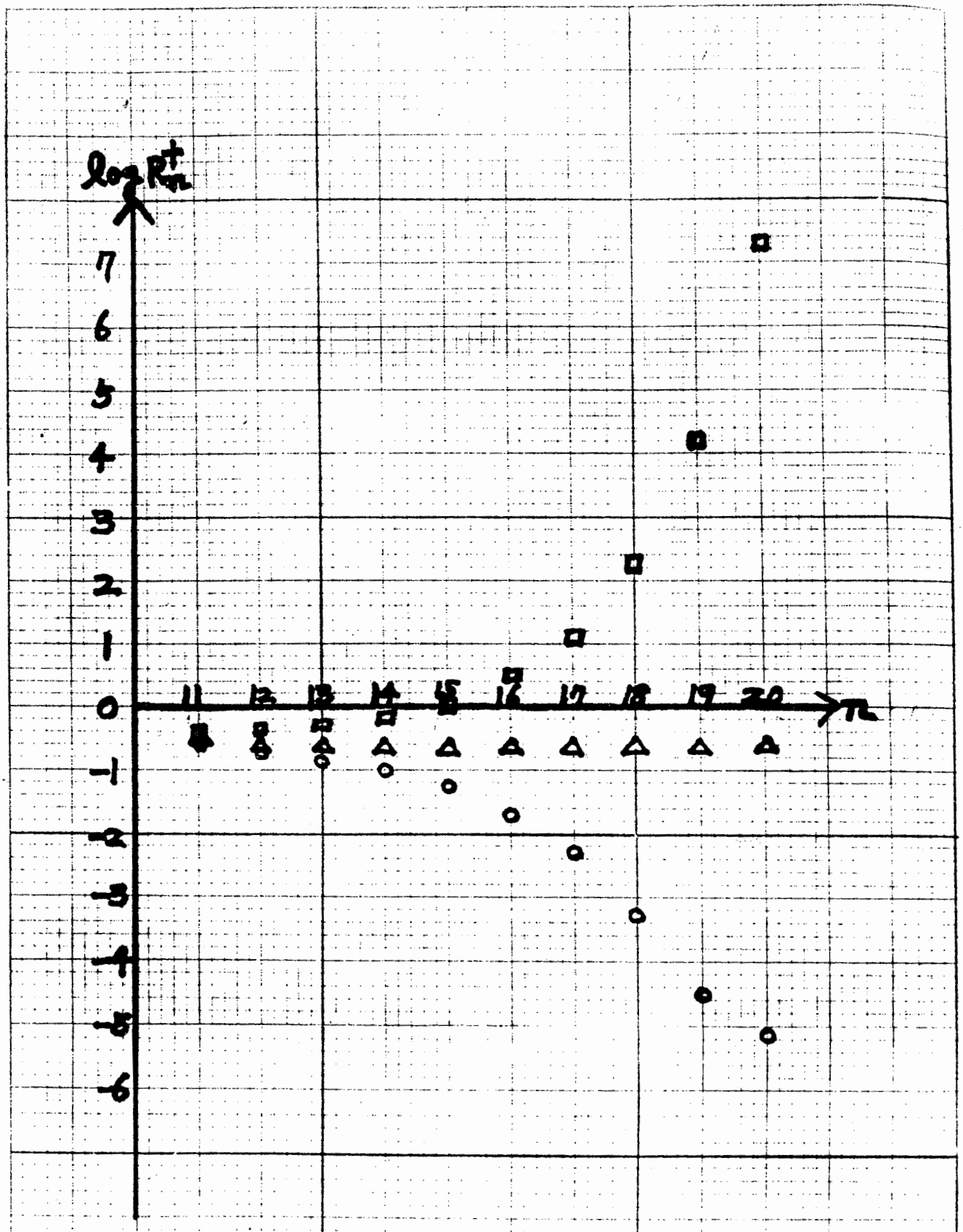

Figure 2.5.1: Residue values R_n^+ of the nth ~~convergent~~ minimaximizing periodic orbits when $\varepsilon = \varepsilon^* - \Delta\varepsilon$, ε^*, $\varepsilon^* + \Delta\varepsilon$, respectively denoted by $\circ, \Delta, \square$; $\Delta\varepsilon = 10^{-3}$

n		$\epsilon^*-\Delta\epsilon$	ϵ^*	$\epsilon^*+\Delta\epsilon$
3		2.4275×10^{-1}	.24383	2.4490×10^{-1}
4		2.5281×10^{-1}	.25468	2.5656×10^{-1}
5		2.4077×10^{-1}	.24370	2.4667×10^{-1}
6		2.4931×10^{-1}	.25409	2.5896×10^{-1}
7		2.3767×10^{-1}	.24531	2.5319×10^{-1}
8		2.3974×10^{-1}	.25216	2.6523×10^{-1}
9		2.2855×10^{-1}	.24819	2.6953×10^{-1}
10	R_n^+	2.1946×10^{-1}	.25084	2.8675×10^{-1}
11		2.0079×10^{-1}	.24949	3.1015×10^{-1}
12		1.7606×10^{-1}	.25059	3.5711×10^{-1}
13		1.4061×10^{-1}	.24996	4.4539×10^{-1}
14		9.7913×10^{-2}	.25002	6.4207×10^{-1}
15		5.4693×10^{-2}	.25009	1.1646
16		2.1251×10^{-2}	.25010	3.0983
17		4.5081×10^{-3}	.25008	1.5553×10^{1}
18		4.2434×10^{-4}	.24005	2.2475×10^{2}
19		3.3628×10^{-5}	.25005	1.8266×10^{4}
20		7.1529×10^{-6}	.24999	2.3227×10^{7}

Table 2.5.2 : Residue values R_n^+ of the nth convergent mini-maximizing periodic orbits when $\epsilon = \epsilon^* - \Delta\epsilon$, ϵ^* , $\epsilon^* + \Delta\epsilon$; $\Delta\epsilon = 10^{-3}$

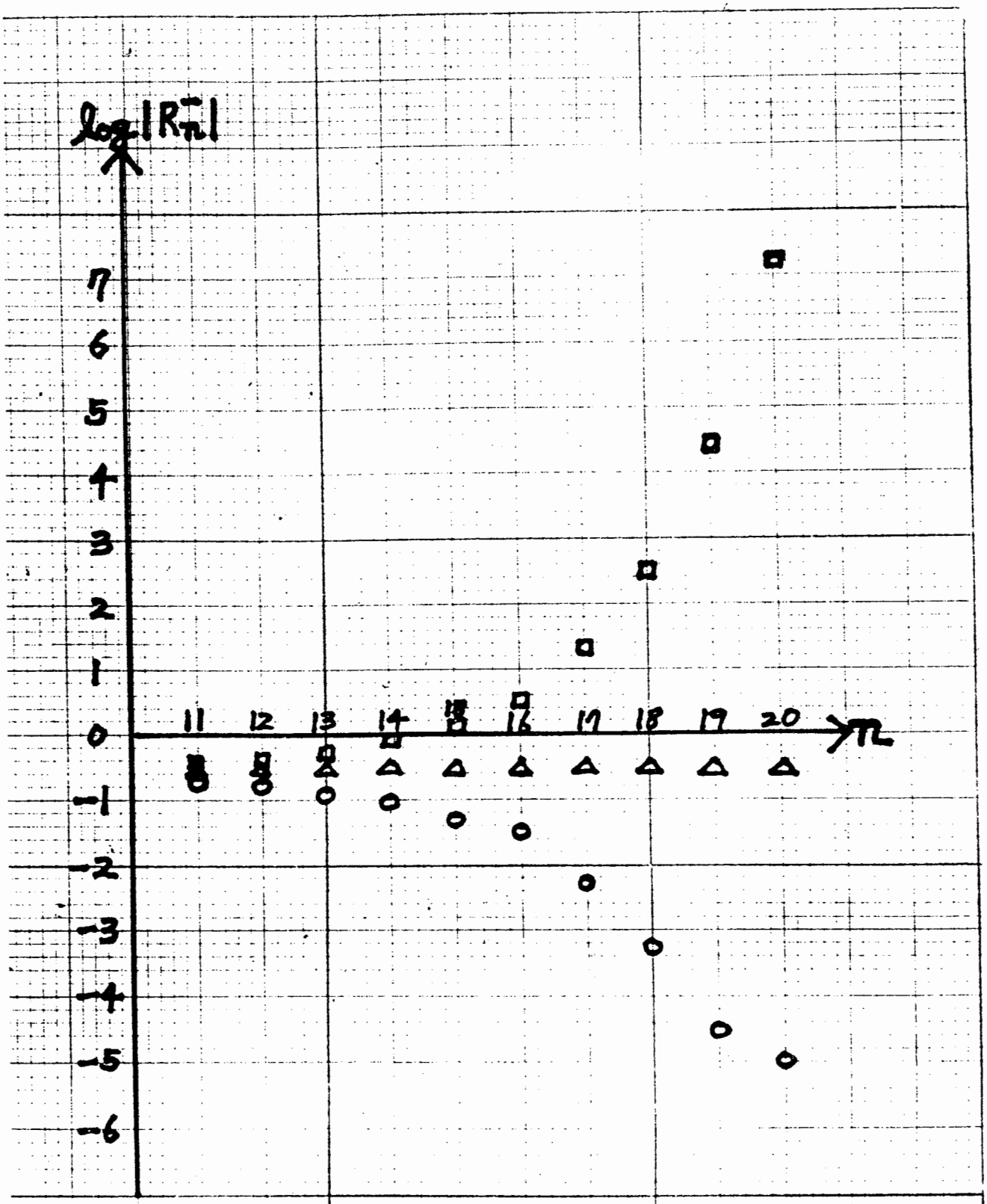

Figure 2.5.2: Residue values $\bar{R}_n$ of the nth convergent minimizing periodic orbits when $\varepsilon = \varepsilon^* - \Delta\varepsilon, \varepsilon^*, \varepsilon^* + \Delta\varepsilon$, respectively denoted by $\circ, \triangle, \square$; $\Delta\varepsilon = 10^{-3}$.

n	$\epsilon^* - \Delta\epsilon$	ϵ^*	$\epsilon^* + \Delta\epsilon$
3	-2.4742×10^{-1}	-.24854	-2.4965×10^{-1}
4	-2.5107×10^{-1}	-.25301	-2.5496×10^{-1}
5	-2.3960×10^{-1}	-.24263	-2.4570×10^{-1}
6	-2.5674×10^{-1}	-.26173	-2.6682×10^{-1}
7	-2.4286×10^{-1}	-.25078	-2.5897×10^{-1}
8	-2.4444×10^{-1}	-.25737	-2.7099×10^{-1}
9	-2.3254×10^{-1}	-.25296	-2.7521×10^{-1}
10 R_n^-	-2.2321×10^{-1}	-.25577	-2.9321×10^{-1}
11	-2.0410×10^{-1}	-.25455	-3.1787×10^{-1}
12	-1.7914×10^{-1}	-.25631	-3.6793×10^{-1}
13	-1.4235×10^{-1}	-.25556	-4.6206×10^{-1}
14	-9.8819×10^{-1}	-.25529	-6.7336×10^{-1}
15	-5.4992×10^{-2}	-.25553	-1.2565
16	-2.1332×10^{-2}	-.25545	-3.5658
17	-4.5270×10^{-3}	-.25544	-2.0119×10^{1}
18	-4.2689×10^{-4}	-.25537	-3.1750×10^{2}
19	-2.7293×10^{-5}	-.25539	-2.6190×10^{4}
20	-1.1374×10^{-5}	-.25533	-1.6148×10^{7}

Table 2.5.3: Residue values R_n^- of the nth convergent minimizing periodic orbits when $\epsilon=\epsilon^* - \Delta\epsilon$, ϵ^* , $\epsilon^* + \Delta\epsilon$; $\Delta\epsilon = 10^{-3}$.

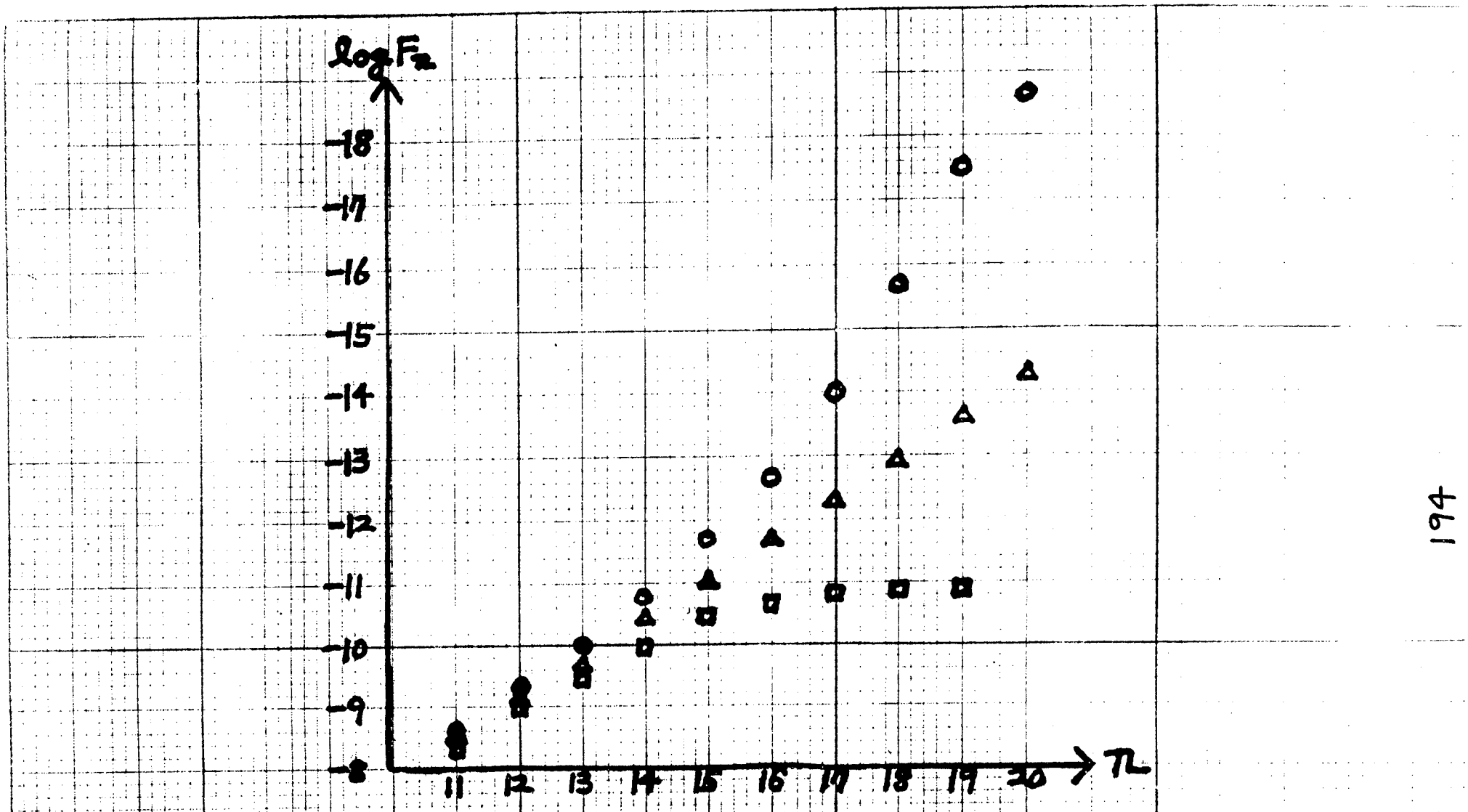

Figure 2.5.3: Action differences F_n between the nth convergent minimaxmizing and minimizing periodic orbits when $\varepsilon = \varepsilon^* - \Delta\varepsilon, \varepsilon^*, \varepsilon^* + \Delta\varepsilon$, respectively denoted by ○, ▲, □ ; $\Delta\varepsilon = 10^{-3}$.

n		$\epsilon^* - \Delta\epsilon$	ϵ^*	$\epsilon^* + \Delta\epsilon$
3		3.5759×10^{-4}	3.5910×10^{-4}	3.6061×10^{-4}
4		8.7155×10^{-5}	8.7771×10^{-5}	8.8391×10^{-5}
5		1.9044×10^{-5}	1.9267×10^{-5}	1.9492×10^{-5}
6		4.6220×10^{-6}	4.7054×10^{-6}	4.7902×10^{-6}
7		1.0143×10^{-6}	1.0451×10^{-6}	1.0768×10^{-6}
8		2.3514×10^{-7}	2.4664×10^{-7}	2.5868×10^{-7}
9		5.1822×10^{-8}	5.6032×10^{-8}	6.0572×10^{-8}
10	F_n	1.1489×10^{-8}	1.3037×10^{-8}	1.4788×10^{-8}
11		2.4374×10^{-9}	2.9936×10^{-9}	3.6737×10^{-9}
12		4.9606×10^{-10}	6.9317×10^{-10}	9.6625×10^{-10}
13		9.2165×10^{-11}	1.5936×10^{-10}	2.7351×10^{-10}
14		1.4998×10^{-11}	3.6692×10^{-11}	8.8038×10^{-11}
15		1.9669×10^{-12}	8.4643×10^{-12}	3.4528×10^{-11}
16		1.8020×10^{-13}	1.9504×10^{-12}	1.8067×10^{-11}
17		9.0380×10^{-15}	4.4945×10^{-13}	1.3281×10^{-11}
18		2.0163×10^{-16}	1.0356×10^{-13}	1.2377×10^{-11}
19		3.3880×10^{-18}	2.3868×10^{-14}	1.2316×10^{-11}
20		2.2246×10^{-19}	5.5006×10^{-15}	

Table 2.5.4 : Action difference F_n between the nth convergent minimaximizing and minimizing periodic orbits when $\epsilon = \epsilon^* - \Delta\epsilon$, ϵ^* , $\epsilon^* + \Delta\epsilon$; $\Delta\epsilon = 10^{-3}$

n	F_n/F_{n+1}
3	4.0913
4	4.5555
5	4.0946
6	4.5023
7	4.2374
8	4.4018
9	4.2980
10	4.3548
11	4.3188
12	4.3496
13	4.3433
14	4.3349
15	4.3397
16	4.3396
17	4.3400
18	4.3390
19	4.3391

Table 2.5.5 : Ratio of the fluxes F_n/F_{n+1} in the critical case

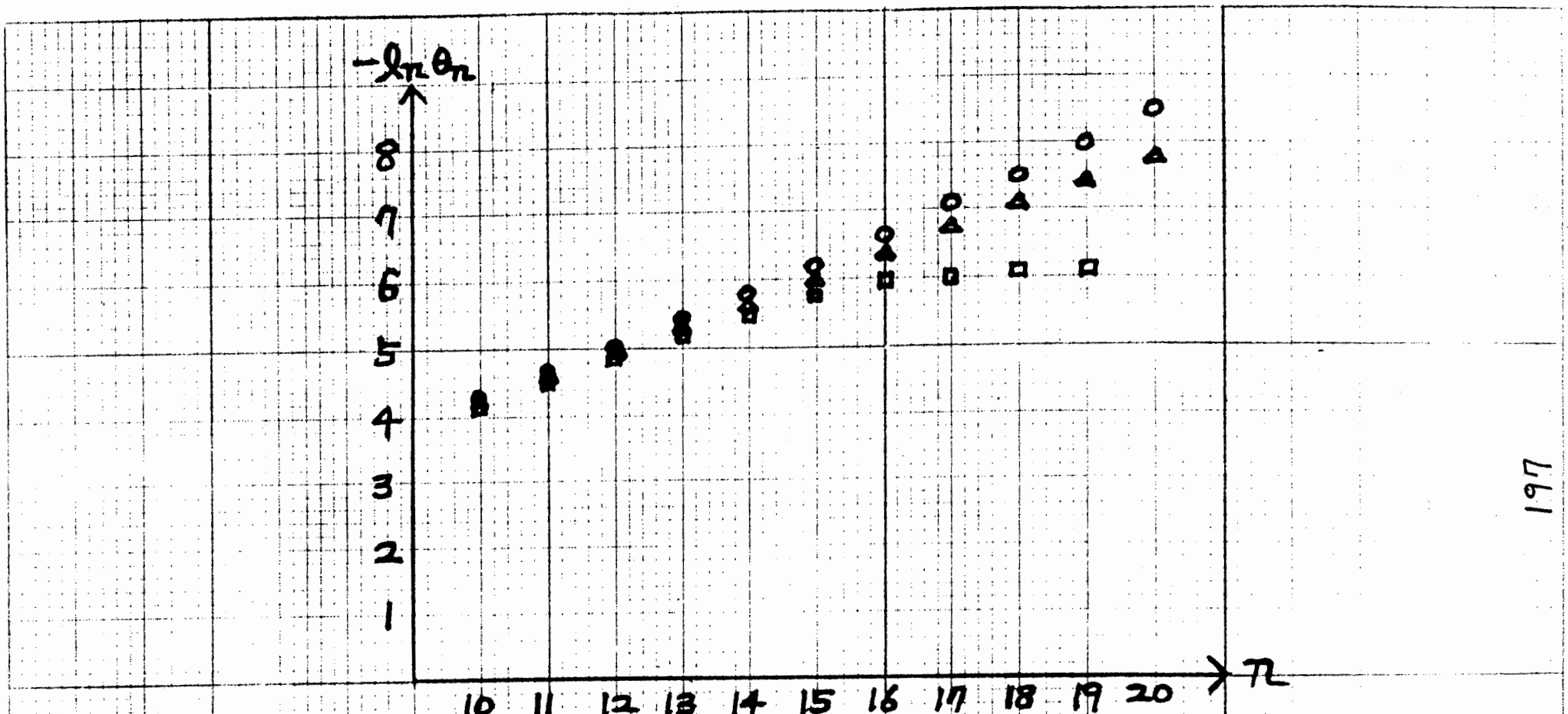

Figure 2.5.4 : θ-coordinate θ_n of the nth convergent minimizing periodic point nearest to the dominant symmetry line when $\varepsilon = \varepsilon^* - \Delta\varepsilon$, ε^*, $\varepsilon^* + \Delta\varepsilon$, respectively denoted by $\circ, \triangle, \square$: $\Delta\varepsilon = 10^{-3}$.

n		$\epsilon^* - \Delta\epsilon$	ϵ^*	$\epsilon^* + \Delta\epsilon$
3		1.5271×10^{-1}	1.5277×10^{-1}	1.5284×10^{-1}
4		1.0956×10^{-1}	1.0965×10^{-1}	1.0973×10^{-1}
5		7.6817×10^{-2}	7.6921×10^{-2}	7.7025×10^{-2}
6		5.4429×10^{-2}	5.4555×10^{-2}	5.4682×10^{-2}
7		3.8269×10^{-2}	3.8417×10^{-2}	3.8566×10^{-2}
8		2.7049×10^{-2}	2.7221×10^{-2}	2.7396×10^{-2}
9		1.8993×10^{-2}	1.9192×10^{-2}	1.9395×10^{-2}
10	θ_n	1.3353×10^{-2}	1.3580×10^{-2}	1.3817×10^{-2}
11		9.3276×10^{-3}	9.5852×10^{-3}	9.8617×10^{-3}
12		6.4878×10^{-3}	6.7778×10^{-3}	7.1033×10^{-3}
13		4.4667×10^{-3}	4.7885×10^{-3}	5.1768×10^{-3}
14		3.0354×10^{-3}	3.3856×10^{-3}	3.8602×10^{-3}
15		2.0235×10^{-3}	2.3926×10^{-3}	2.9934×10^{-3}
16		1.3191×10^{-3}	1.6911×10^{-3}	2.4869×10^{-3}
17		8.4100×10^{-4}	1.1953×10^{-3}	2.2715×10^{-3}
18		5.2738×10^{-4}	8.4480×10^{-4}	2.2258×10^{-3}
19		3.2790×10^{-4}	5.9709×10^{-4}	2.2227×10^{-3}
20		2.0318×10^{-4}	4.2201×10^{-4}	

Table 2.5.6 : θ-coordinate θ_n of the nth convergent minimizing periodic point nearest to the dominant symmetry line when $\epsilon=\epsilon^*-\Delta\epsilon, \epsilon^*, \epsilon^*+\Delta\epsilon$; $\Delta\epsilon=10^{-3}$

n		$\epsilon^*-\Delta\epsilon$	ϵ^*	$\epsilon^*+\Delta\epsilon$
3		.69001	.68928	.68854
4		.73787	.73668	.73548
5		.71595	.71396	.71195
6		.73204	.72883	.72560
7		.72106	.71590	.71066
8		.73472	.72633	.71771
9		.73223	.71877	.70473
10	x_o^n	.74553	.72395	.70080
11		.75447	.72020	.68183
12		.77568	.72199	.65746
13		.80278	.72044	.60986
14		.84270	.72145	.52845
15		.88913	.72108	.38526
16		.93543	.72112	.18828
17		.96976	.72113	$.42202 \times 10^{-2}$
18		.98576	.72114	2.8981×10^{-3}
19		.99455	.72117	

Table 2.5.7 : Exponent x_o^n when $\epsilon=\epsilon^*-\Delta\epsilon$, ϵ^*, $\epsilon^*+\Delta\epsilon$.

$x_o^n = \ell n(\theta_n/\theta_{n+1})/\ell n\gamma$; $\gamma=(1+5^{1/2})/2$,

$\Delta\epsilon=10^{-3}$.

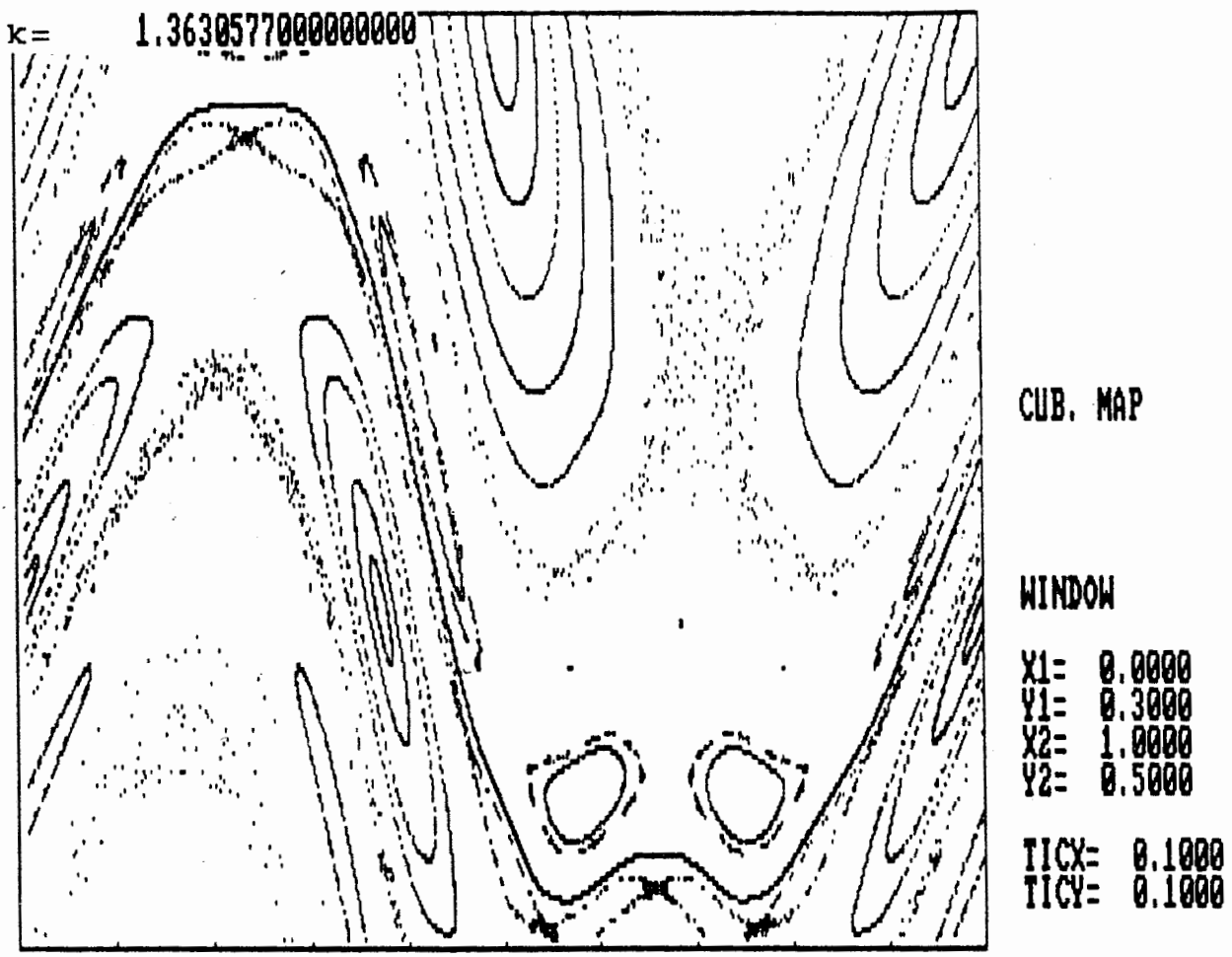

Figure 2.5.5 : Orbits near the Golden-Mean invariant circle when $\epsilon = \epsilon^*$

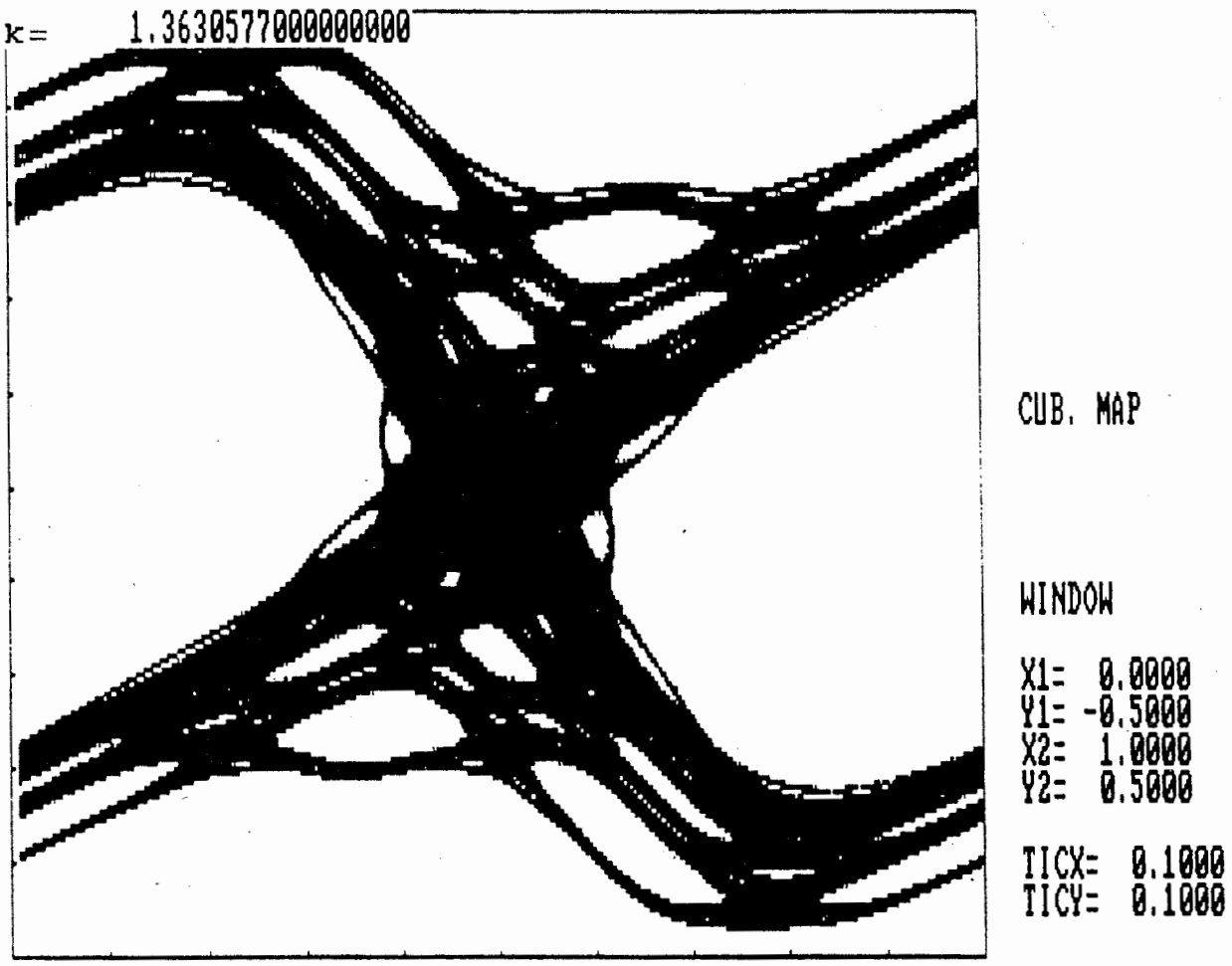

Figure 2.5.6 : A single orbit when $\epsilon = \epsilon^*$

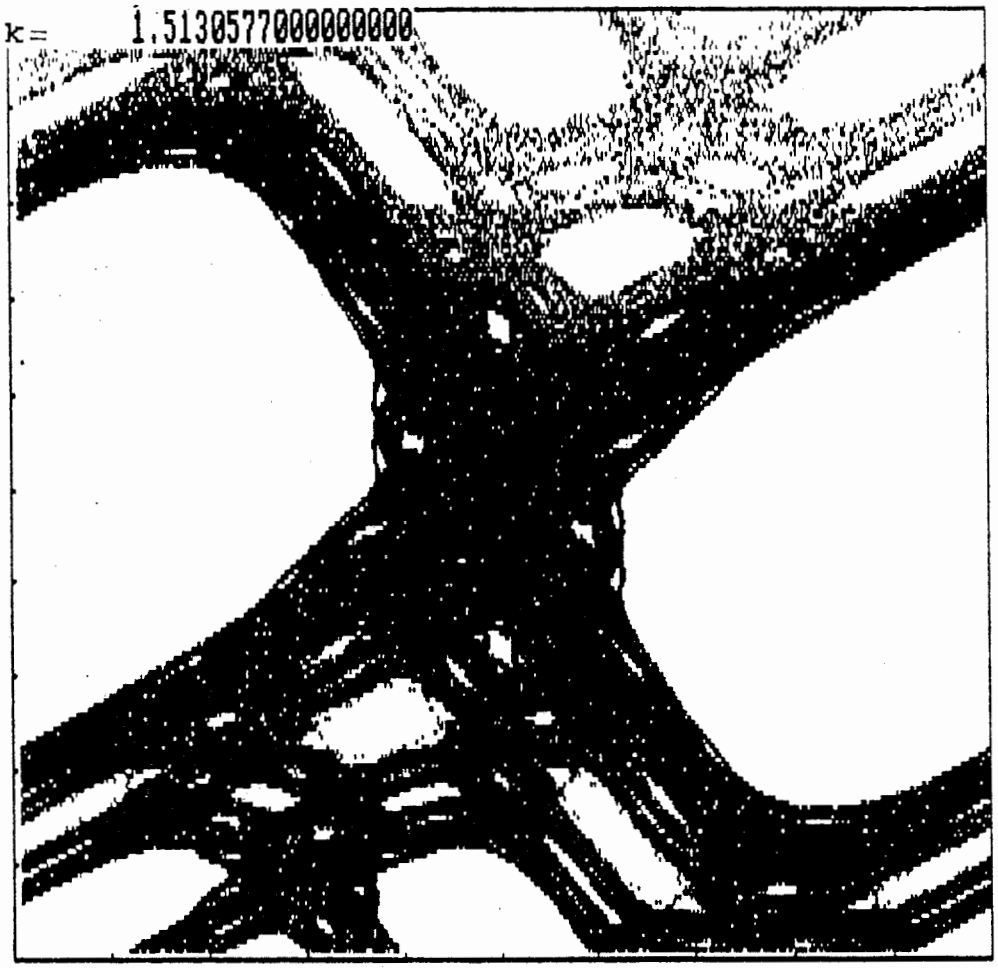

Figure 2.5.7 : A single orbit when $\epsilon = \epsilon^*$

The next question is whether or not the critical behavior of the invariant circle is the same as that of the Golden -Mean invariant circle of class C^r $(r>3)$.

We describe the scaling along and across the symmetry lines for the critical invariant circle. We use symmetry coordinates (X,Y). For S-symmetry, symmetry coordinates are : $X=\theta$ and $Y=I+\epsilon/2\cdot F(\theta)$, and for TS-symmetry symmetry coordinates are : $X=\theta-I/2$, $Y=I$. In the symmetry coordinates ,the symmetries are represented as $(X,Y) \to (X',Y') = (-X+n,Y), n\in Z$.

Firstly, we describe the scaling behavior near the dominant half-line. We call the periodic point $(0,Y_n)$ on the dominant half-line the dominant point. We measured the position Y_n of the dominant point. (Y_n)-sequence converges geometrically to the invariant circle with ratio β. Here the limit value of (Y_n)-sequence is :

$$Y^* = 0.405611110478107 \ , \qquad (2.5.13)$$

and the convergence ratio β is the limit value of (β_n)-sequence defined by $\beta_n=(Y_{n-1}-Y_n)/(Y_n-Y_{n+1})$. This sequence is shown in the table 2.5.8. The observed scaling factor β along the dominant half-line is :

$$\beta = - 3.0668 \ . \qquad (2.5.14)$$

Therefore, Y_n approaches to the invariant circle in a nonanalytic fashion:

$$\left| \frac{Y_{n+1}-Y_n}{Y_n-Y_{n+1}} \right| \sim \gamma^{-y_0} \ , \qquad (2.5.15)$$

$$y_0 = \log_\gamma |\beta| = 2.3288 \ .$$

This is consistent with :

$$|Y_n - Y^*| \sim q_n^{-y_o} \quad . \tag{2.5.16}$$

The scaling bahavior across the dominant symmetry line can be also studied by measuring the positions (X_n, Y_n) of the nearest point of the periodic orbit to the dominant half-line. The convergence ratio α is the limit value of (α_n)-sequence defined by $\alpha_n = X_n / X_{n+1}$. This sequence is included in the table 2.5.9. The observed scaling factor α across the dominant half-line is :

$$\alpha = -1.4148 \ . \tag{2.5.17}$$

This is consistent with :

$$|X_n| \sim q_n^{-x_o} \ , \ x_o = \log_\gamma |\alpha| \quad . \tag{2.5.18}$$

Secondly, we describe the scaling behaviors near the three subdominant half-lines. We call the periodic point on the subdominanf half-line the subdominant point. In a similar way, by measuring the positions of the subdominant point and the nearest point to it, the scaling behaviors can be studied. However the scalings exhibit 'period-3' behaviors unlike the scaling behaviors near the dominant symmetry line. These behaviors are shown in the tables 2.5.9 and 2.5.10. This 'period-3' scaling behavior is directly related to the fact that periodic points on each subdominant symmetry line have a 'period-3' routing pattern as shown in the table 1.1.3.1. The 3-step scaling factors β_3 and α_3 along and across the dominant half-lines are :

$$\beta_3 = -16.859, \qquad \alpha_3 = -4.8458 \ . \qquad (2.5.19)$$

Note that $\beta_3 \neq \beta^3$, $\alpha_3 \neq \alpha^3$ and $\alpha_3 \cdot \beta_3 = (\alpha \cdot \beta)^3$. Hence, though the scalings along and across the symmetry half-lines exhibit different behaviors, the area-scalings exhibit the same behaviors. This is consistent with the fact that the ratio of the fluxes F_n/F_{n+1} approach to some value ξ: $\xi = |\alpha \cdot \beta|$.

Finally, note that these critical behaviors are the same as those of the Golden KAM circle in the analytic standard map within numerical error(Shenker and Kadanoff, 1982, Mackay, 1982).

To sum up, we show numerically that in a map of class-C^2, the Golden KAM circle persists below the critical parameter value and the critical behaviros appear to be the same as those in analytic maps. But, Herman(1983)has C^r ($r<3$)-counterexamples to Moser's twist theorem. So, for a map of class-C^r($r<3$), KAM circles may or may not exist, depending on the map. It may be helpful to recall that a Denjoy's theorem on a circle map $f: S^1 \to S^1$ requires that f has first derivatives of bounded variations (Moser, 1973):

$$\exists C > 0 \quad \text{s.t.} \quad \sum_{i=1}^{n} | f'(\theta_i) - f'(\theta_{i-1}) | \leq C$$

for all finite sequences $0 \leq \theta_0 \leq \cdots \leq \theta_n \leq 1$.
Then, f is topologically conjugate to uniform rotation on S^1. So, we guess that like the case of circle maps some additional detailed conditions on the quality of perturbation should be required in the case of 2-dim. area-preserving maps.

n	β_n	α_n
4	-3.0326	-1.4232
5	-3.0725	-1.4082
6	-3.0469	-1.4191
7	-3.0735	-1.4128
8	-3.0630	-1.4174
9	-3.0658	-1.4138
10	-3.0660	-1.4164
11	-3.0651	-1.4146
12	-3.0669	-1.4157
13	-3.0673	-1.4147
14	-3.0680	-1.4150
15	-3.0661	-1.4148
16	-3.0670	-1.4149
17	-3.0670	-1.4148
18	-3.0669	-1.4148
19	-3.0668	-1.4149
20	-3.0668	-1.4149

Table 2.5.8 : Scaling factors β_n and α_n along and across the dominant symmetry line when $\epsilon=\epsilon^*$.

n		θ=1/2	I=2θ	I=2θ-1
4		-2.0485	-3.3367	-2.4447
5		-3.3876	-2.4215	-2.0625
6		-2.4459	-2.0686	-3.3489
7		-2.0577	-3.3795	-2.4165
8		-3.3542	-2.4396	-2.0643
9		-2.4254	-2.0584	-3.3714
10	β_n	-2.0621	-3.3625	-2.4345
11		-3.3692	-2.4285	-2.0594
12		-2.4318	-2.0604	-3.3673
13		-2.0589	-3.3698	-2.4291
14		-3.3678	-2.4305	-2.0597
15		-2.4306	-2.0596	-3.3678
16		-2.0596	-3.3684	-2.4302
17		-3.3682	-2.4303	-2.0596
18		-2.4303	-2.0597	-3.3681
19		-2.0597	-3.3679	-2.4304
20		-3.3679	-2.4303	-2.0597

Table 2.5.9 : Scaling factors β_n along the three subdominant half-lines when $\epsilon = \epsilon^*$

n		θ=1/2	I=2θ	I=2θ-1
4		-1.7835	-1.6283	-1.7055
5		-1.6101	-1.7087	-1.7706
6		-1.6966	-1.7734	-1.6075
7		-1.7729	-1.6005	-1.7067
8		-1.6022	-1.6980	-1.7748
9		-1.7065	-1.7722	-1.6038
10	α_n	-1.7747	-1.6029	-1.7013
11		-1.6039	-1.7042	-1.7735
12		-1.7025	-1.7745	-1.6030
13		-1.7743	-1.6033	-1.7037
14		-1.6032	-1.7030	-1.7746
15		-1.7034	-1.7741	-1.6037
16		-1.7743	-1.6034	-1.7033
17		-1.6034	-1.7032	-1.7744
18		-1.7033	-1.7743	-1.6035
19		-1.7743	-1.6034	-1.7033
20		-1.6034	-1.7033	-1.7743

Table 2.5.10 : Scaling factors across the three subdominant half-lines when $\epsilon = \epsilon^*$.

CHAPTER 3. Summary and Discussion

We have studied two phenomena related to periodic and quasi-periodic orbits in area-preserving maps.

The first phenomenon is the infinitely nested structure of islands which play the role of 'trap'. We show that at the accumulation point island chains of all classes exist and they have a self-similar structure asymptotically for 1/n-bifurcation, with n=3 to 6. It is also observed that the limiting self-similar behaviors depend on n. For even n, the pattern of periodic orbits repeats itself from one bifurcation to the next one, while for odd n to every other one. These observations are related to the following observations. For even n, the subdominant elliptic point and the dominant elliptic point appear successively as the class C increases,respectively , while for odd n they appear alternatively as C increases. However, these observations are not proved mathematically. Indeed, even more limiting self-similar behaviors exist near the accumulation point. When we rescale not only the dynamical variables but also the parameter with the rescaling factors of dynamic variables α and β , and the parameter rescaling factor δ , the pattern of periodic orbits also exhibits the limiting self-similar behavior .

It may be worth while to compare the period-doubling bifurcation with higher n-tupling bifurcations(n>2). The residue values R^* for higher n-tupling bifurcation are less than 1, while R^* in the period-doubling bifurcation is 1.13588(Greene et al, 1981). So, for higher n-tupling

bifurcation, infinitely nested islands exist and near these islands a stochastic orbit has a long-time correlations. That is, these islands play the role of 'trap' of a stochastic orbit. On the other hand, at the accumulation point of 1/2-bifurcation, no islands exist and thus the unstable orbits play the role of 'scatterer' of stochastic orbits.

We also studied the limiting self-similar structure by a simple approximate renormalization method. The method we employed is essentially a generalization of Helleman's original idea(1980,1983) which was used for 1/2-bifurcation to the lowest order. As explained in § 2.4, comparison to the quadratic approximants of $T^{n\ell}$ and $T^{n\ell+1}$ yields the accumulation point p^*, the scaling factor α and β, the bifurcation ratio δ and the universal residue value R^*. Naturally, as ℓ increases, the higher order approximation gives better values. Thus, the results obtained by this method agree well with those obtained by directly following bifurcation-sequences. We can also obtain an approximate universal map since at the accumulation point, in the limit $\ell \to \infty$, $A^{\ell} \cdot T^{n} \cdot A^{-\ell} \to T^{*}$; $A = \begin{bmatrix} \alpha & 0 \\ 0 & \beta \end{bmatrix}$.

So, we show approximately that the limiting self-similar behaviors are universal. Hence, all maps lying on the critical surface converge to the universal map T^* under the renormalization transformation N, and thus they exhibit the same limiting self-similar behaviors on longer time scales and smaller spatial scales. Also, note that the linearization of the renormalization transformation N, dN , has one essentially relevant

eigenvalue δ. That is just the bifurcation ratio. So,only if the residues R of a periodic orbit is computed, then one can say whether the map describing the phase flow near the periodic orbit lies above or below the critical surface in the figure 2.4.1 as follows. The map lies above or below that critical surface according as R is larger or smaller than R^*. For higher n-tupling bifurcation (n > 2), in the subcritical case periodic orbits of higher period are not born yet, and in the supercritical case periodic orbits of higher period have become unstable already. In this way, one information of R^* yields a lot of information.

The second phenomenon we studied is the break-up of invariant circles which play the role of 'dam' under a rough perturbation .

We studied whether or not invariant circles exist in a map of class-C^2. In this case, persistence of invariant circles is not guaranteed by Moser' twist theorem, since the sufficient critical smoothness of a map in the theorem is now class-C^r(r > 3).

We showed numerically that a noble invariant circle of rotation number γ^{-2} ($\gamma=(1+5^{1/2})/2$) persists below a critical parameter value. So, the invariant circle plays the role of a complete barrier to transport of stochastic orbits below the critical parameter value. We also observed that the critical behavior appears to be the same as that in analytic maps. So, they seem to be in the same universality class. However, Herman(1983) has C^r(r<3)-counterexample to Moser's twist

theorem. So , for a map of class-C ($r < 3$) invariant circles may or may not exist, depending on the map. A similar phenomenon exists in circle maps. A theorem of Denjoy (referred to by Mackay , 1982) on a circle map requires the map to bave first derivatives of bounded variations for the map to be topologically conjugate to uniform rotation on S^1, but it is false for C^1-maps. So, we guess that for invariant circles in a map of class-C^r($r<3$) to exist, some additional detailed conditions on the quality of perturbtion should be required like the case of circle maps.

Like the cases of bifurcations, the information of the universal residue R^* gives us much information concerning the phase flow. In order to use this, we first define neighboring periodic orbits in terms of their rotation numbers as follows. We define two rational rotation numbers, ν_1 and ν_2 , to be neighboring if they are expressed as

$$\nu_1 = [\ m_0\ ,\ m_1\ ,\ \cdots\ ,\ m_n\ ] = p_1/q_1\ ,$$

and

$$\nu_2 = [\ m_0\ ,\ m_1\ ,\ \cdots\ ,\ m_n + 1\ ] = p_2/q_2\ .$$

The first question is whether an invariant circle exists between two neighboring periodic orbits. We expect that the most robust invariant circle in the frequency interval between ν_1 and ν_2 may have the rotation number :

$\nu = [\ m_0,\ m_1\ ,\ \cdots\ ,\ m_n\ ,\ (1,)^{\infty}\ ] = (p_2\cdot\gamma + p_1)/(q_2\cdot\gamma + q_1)$,
where $\gamma = (1 + 5^{1/2})/2$.

Then , the invariant circle may or may not exist according as the average residue R of the residues R_1 and R_2 of the two

periodic orbits is larger or smaller than R^* which is roughly 1/4. In this way, we obtained the rotation numbers of boundary circles in the figure 2.1.2 (see § 2.1).

In the way stated above, the universal residue values R^* of bifurcations and noble invariant circles give us much information concerning the phase flow in 2-dim. area-preserving maps. Also, one can expect naturally that the long-time behavior of stochastic orbits near islands may be governed by the self-similar behavior of the infinitely nested structure of islands and the critical boundary circle. Actually, the self-similar behavior is directly related to the transition probabilities in a self-similar Markov tree model which describes the transport of stochastic orbits near islands (Meiss and Ott , 1985), and a long-time correlation of stochastic orbits near islands is obtained in the model. In this way, the universal residue value R^*, the parameter rescaling factor δ , and the rescaling factors of dynamic variables , α and β give much information of the phase flow in area-preserving maps.

References

Abraham, R and Marsden, J., 1978, Foundations of Mechanics (Benjamin, New York)

Apostol, T.M., 1973, Mathematical Analysis (Addison-Wesley, London)

Arnod, V.I., 1978, Mathemathical Methods of Classical Mechanics (Springer, New York)

Arnold, V.I. and Avez, A., 1968, Ergodic Problems of Classical Mechanics (Springer, New York)

Aubry, S., 1983, Physica 7D, 240

Aubry, S. and Le Daeron, P.Y., 1983, Physica 8D, 381

Benettin, G., Cercignani, C., Galgani,L. and Giorgilli, A., 1980, Lettere Nuovo Cimento 28, 1

Benettin, G., Cercignani, C., Galgani, L. and Giorgilli,A., 1980, Lettere Nuovo Cimento 29, 163

Birkhoff, G. D., 1927, Dynamical systems (AMS Colloq. Publ., vol. 9)

Bountis, T. C., 1981, Physica 3D, 577

Channon, S. and Lebowitz, J. L., 1980, Ann. N. Y. Acad. Sci. 357, 108

Cary, J. R. and Meiss, J. D., 1981, Phys. Rev. 24A, 2664

Chirikov, B.V., 1979, Phys. Reports 52, 263

Chirikov, B. V. and Shepelyansky, D.L., 1984, Physica 13D, 395

Collet, P., Eckmann, J. P. and Koch, H., 1981, Physica 3D, 457

Dana, I. and Fishman, S., 1985, Physica 17D, 63

Derrida, B. and Pomeau, Y., 1981, Phys. Lett. 80A, 217

Devaney, R., 1976, Trans. AMS 218, 89

DeVogelaere, R., 1958, in Contributions to the Theory of Nonlinear Oscillations, vol. IV, ed. S. Lefschtz, p.53

Finn, J.M., 1974, Ph.D. Thesis (Univ. of Maryland)

Feigenbaum, M.J., 1978, J. Stat. Phys. 19, 25

Feigenbaum, 1979, J. Stat. Phys. 21, 669

Greene, J. M., 1968, J. Math. Phys. 9, 760

Greene, J. M., 1979, J. Math. Phys. 20, 1183

Greene, J. M., Mackay, R.S., Vivaldi, F. and Feigenbaum, M.J., 1981, Physica 3D, 457

Henon, M., 1969, Quart. App. Math. 27, 291

Helleman, R. H. G., 1980, in Fundamental Problems in Statistical Mechanics, vol. 5, ed. E. G. D. Cohen, p.165 (North-Holland, Amsterdam)

Helleman, R. H. G. and Mackay, R. S., in Long-Time Prediction in Dynamics, eds. C. W. Horton, L.E. Reichl and V.G. Szebehely, p.95 (Wiley, New York)

Herman, M. R., 1983, Asterisque 103-104, 47

Karney, C.F.F., Rechester, A. B., white, R. B., 1982, Physica 4D, 425

Karney, C.F.F., 1983, Physica 8D, 360

Katok, A., 1982, Ergodic Theory and Dyn. Sys. 2, 185

Lee,K.C., 1983, J.Phys. 16A, L137

Lee, K. C., Kim, S. Y. and Choi, D. I., 1984, Phys. Lett. 103A, 225

Lee, K. C., Kim, S. Y. and Choi, D. I., 1985, J. Korean Phys. Soc. 18, 243

Lee, K. C., Kim, S. Y. and Choi, D. I., 1986, in Proceedings of 14th ICGTMP, e.d. Y.M. Cho, p.425(World Scientific, Singapore), to appear in J. Korean Phys. Soc.

Liebermann, M.A. and Lichtenberg, A.J., 1972 Phys. Rev. A5, 1852

Lichtenberg,A.J. and Liebermann,M.A., 1982, Regular and stochasic Motion (Springer-Verlag, New York)

Lichtenberg, A.J., 1985, Physica 14D, 387

Mackay, R. S., 1982, Ph.D. Thesis (Princeton Univ.)

Mackay, R.S. and Meiss, J.D., 1983, Phys. Lett. 98A, 92

Mackay, R.S., Meiss, J.D. and Percival I.C., 1984, Physica 13D, 55

Mackay, R.S. and Percival, I.C., 1985, Commu.Math. Phys. 98, 469

Mather, J. N., 1982, Topology 21, 457

McMillan, E.M., 1971, in Topics in Modern Physics(Colo.Ass. U.P., Boulder, CO), p.219

Meiss, J.D. and Ott, E., 1985, Phys. Rev. Lett. 55. 2741

Meiss, J.D., 1986, 'Class Renormalization:Islands around islands' , Preprint(Univ. of Texas)

Meyer, K.R., 1970, Trans. AMS 149,95

Moser, J.K., 1973, Stable and Random Motions in Dynamical Systems (Princeton Univ. Press)

Nering, E.D., 1969, Linear Algebra and Matrix Theory (Wiley, New York)

Niven, I., 1963, Irrational Numbers(Carus Math. Monographs, no.11, Wiley)

Percival, I.C., 1979, in Nonlinear Dynamics and the Beam-Beam Interactions, eds. M. Month and J.C. Herrera, AIP Conf. Proc. 57, p.302

Rechester, A.B. and White, R. B., 1980, Phys. Rev. Lett. 44, 1586

Rimmer, R., 1974, J. Diff. Eqns 29, 329

Robinson, R.C., 1970, Am. J. Math. 102, 562

Shenker, S.J. and Kadanoff, L.P., 1982, J. Stat. Phys. 27. 631

Schmidt, G and Bialek, J., 1982, Physica 5D, 397

Widom, M and Kadanoff, L.P., 1982, Physica 5D, 287

Wightman, A.S., 1981, in Perspectuves in Statistical Physics, ed. H.J. Raveche,p.343(North-Holland, Amsterdam)

면적보존 본드기에서 어터갈림 현상과 불변곡선에서의 임계현상

김 상윤

요약 : 일반적으로 면적이 보존되는 본드기의 위상공간속에서 주기궤도들, 준주기궤도들 그리고 난잡한 궤도들이 공존하면서 서로 영향을 미치고 있다. 우리는 이 3 종류의 궤도들 중에서 주기궤도와 준주기궤도에 관련된 2 개의 현상을 공부했다.

첫 번째 현상은 '덫'의 역할을 하는 섬들이 무한히 포개진 구조이다. 우리는 n(n=3,4,5,6) 갈림 현상의 집적점에서 모든 세대의 섬들이 존재하며, 점근적으로 자체상사적 구조를 갖고 있음을 보였다. 또한 그 숙적거동이 n 이 짝수일 때는 주기가 1인 그리고 n 이 홀수일 때는 주기가 2인 거동을 보였다. 게다가, 집적점 부근에서는 역학변수와 함께 매개변수도 적당한 숙적을로 숙적하면 주기궤도들의 형태가 또한 자체상사적 거동을 보인다.

또한, 이 점근적인 자체상사적 구조를 간단한 재규격화 방법으로 공부했다. 이 방법으로 집적점, 갈림비, 숙적을 그리고 보편적인 유수값을 얻었다. 이 값들은 어터갈림 현상의 수열을 좇아가면서 얻은 값들과 잘 일치한다. 게다가, 어터갈림 현상의 보편적인 본드기를 얻었다. 그래서, 근사적으로 위의 점근적인 자체상사적 거동이 보편적 거동임을 보였다.

우리가 공부한 두번째 현상은 거칠은 섬동이 가해졌을 때 '목'의 역할을하는 불변곡선들의 붕괴이다. 우리가 공부한 C^2- 본드기에서 어떤 고상한 불변곡선이 임계 매개변수 값 이하에서는 존속함을 수치적으로 보였다. 그러므로, 그 불변곡선은 임계값 이하에서는 난잡한 궤도들에 대해서 완전한 장벽 역할을 한다. 또한 그 불변곡선의 임계현상은 해석 본드기에서의 임계현상과 수치적 오차 한도 안에서 같았다. 그러므로, 그것들은 같은 보편성 모임에 속한다고 볼 수 있다.